Air pollution and meteorology monitoring report. Deliverable 5.2. Project iSCAPE, Grant Agreement number: 689954

Air pollution and meteorology monitoring report

D5.2

08/2018

This project has received funding from the European Union's Horizon 2020 research and innovation programme under grant agreement No 689954.

Project Acronym and Name	iSCAPE - Improving the Smart Control of Air Pollution in Europe	
Grant Agreement Number	689954	
Document Type	Report	
Document version & WP No.	V0.3	WP5
Document Title	Air pollution and meteorology report	
Main authors	Silvana Di Sabatino (Lead UNIBO), Erika Brattich (UNIBO), Francesco Barbano (UNIBO), Salem Gharbia (UCD), Francesco Pilla (UCD), KV Abhijith (UoS), Prashant Kumar (UoS), Achim Drebs (FMI), Kirsti Jyhlä (FMI), Antti Mäkelä (FMI), Marco Deserti (ARPA-ER), Luca Torreggiani (ARPA-ER), Carla Barbieri (ARPA-ER)	
Partner in charge	UNIBO	
Contributing partners	UNIBO, ARPA-ER, UCD, UOS, FMI	
Release date	30/08/2018	

Document Control Page	
Short Description	*This report documents good quality meteorological and air pollution data obtained as result of the experimental field campaigns carried out in the different iSCAPE cities, namely Bologna, Dublin, Guildford and Vantaa. We recall that these cities are those with a focus on "physical" interventions. The data obtained so far were carefully checked for their quality and their usage is twofold. From one hand measured data will be used for the validation of the model simulations run as part of other WPs (e.g. WP4 and WP6) and, on the other hand, they will provide the scientific basis to*

	establish the efficacy of different PCSs including low boundary walls and green infrastructure (trees and hedges), in each city.		
Review status	**Action**	**Person**	**Date**
	Quality Check	*Coordination Team*	
	Internal Review	*Muhammad Adnan (UH)* *Giuseppe Forino (T6)*	20/08/2018 14/08/2018
Distribution	Public		

Revision history			
Version	**Date**	**Modified by**	**Comments**
V0.1	07/08/2018	Silvana Di Sabatino, Erika Brattich, Francesco Barbano, Salem Gharbia, Francesco Pilla, KV Abhijith, Prashant Kumar, Achim Drebs Luca Torreggiani, Carla Barbieri	Complete first draft to be sent for internal revisions
V0.2	21/08/2018	Francesco Barbano, Erika Brattich	Report reviewed after first internal revision
V0.3	24/08/2018	Erika Brattich, Francesco Barbano, Silvana Di Sabatino	Report reviewed after second internal revision
V0.4	30/08/2018	Erika Brattich, Francesco Barbano, Silvana Di Sabatino	Final version

Statement of originality:

This deliverable contains original unpublished work except where clearly indicated otherwise. Acknowledgement of previously published material and of the work of others has been made through appropriate citation, quotation or both.

Table of Contents

Table of Contents

1 Executive Summary ..... - 10 -

2 Introduction ..... - 10 -

3 Methodology for air pollution and meteorology monitoring ..... - 12 -

3.1 Bologna ..... - 14 -

3.1.1 Site description ..... - 14 -

3.1.2 Instrumental setup ..... - 16 -

3.1.3 Experimental protocol and quality check ..... - 18 -

3.2 Dublin ..... - 22 -

3.2.1 Site description ..... - 22 -

3.2.2 Instrumental setup ..... - 23 -

3.2.3 Experimental protocol and quality check ..... - 25 -

3.3 Guildford ..... - 25 -

3.3.1 Site description ..... - 26 -

3.3.2 Instrumental setup ..... - 29 -

3.3.3 Experimental protocol and quality check ..... - 30 -

3.4 Vantaa ..... - 32 -

3.4.1 Site description ..... - 33 -

3.4.2 Instrumental setup ..... - 34 -

3.4.3 Experimental protocol and quality check ..... - 36 -

4 Environmental impact data ..... - 38 -

4.1 Bologna ..... - 38 -

4.1.1 Meteorological and turbulence variables ..... - 38 -

4.1.2 Air pollution ..... - 44 -

4.1.3 UHI study at neighborhood scale ..... - 55 -

4.2 Dublin ..... - 57 -

4.2.1 Meteorology and air pollution: statistical analysis ..... - 57 -

4.2.2 Meteorology and air pollution: preliminary results ..... - 61 -

4.3 Guildford ..... - 63 -

4.3.1 Air pollution ..... - 63 -

4.3.2 Influence of wind direction on air pollution ..... - 65 -

4.4 Vantaa ..... - 68 -

4.4.1 Meteorological data ..... - 68 -

4.4.2 Air pollution ..... - 70 -

5. Conclusions ..... - 71 -

6. References / Bibliography ..... - 73 -

Appendix Technical specifications for the instruments ..... - 76 -

List of Tables

TABLE 1. OVERVIEW OF THE PCSS EVALUATED, AND OF THE METEOROLOGICAL AND AIR POLLUTION POLLUTANTS VARIABLES MONITORED WITHIN THE MONITORING CAMPAIGNS SETUP IN THE FOUR ISCAPE CITIES. ..... - 13 -
TABLE 2: DETAILS ON AIR POLLUTION POLLUTANTS AND TIME RESOLUTION OF MEASUREMENTS AT THE TWO MOBILE LABORATORIES LOCATED IN THE TWO STREET CANYONS AND AT FIXED AIR POLLUTION MONITORING STATIONS WITHIN THE TWO EXPERIMENTAL FIELD CAMPAIGNS. ..... - 19 -
TABLE 3: DETAILS OF THE SIX MONITORING LOCATIONS IN GUILDFORD, UK. LAI IS MEASURED BY HAND HELD CEPTOMETER ACCU-PAR LP80. ..... - 28 -
TABLE 4: DESCRIPTIVE STATISTICS AND SIGNIFICANT DIFFERENCES OF METEOROLOGICAL VARIABLES (WS = WIND SPEED; T = TEMPERATURE) MEASURED WITHIN THE SUMMER EXPERIMENTAL CAMPAIGN IN BOLOGNA. FOR EACH VARIABLE, EQUAL LETTERS IN LAST COLUMN INDICATE THE ABSENCE OF SIGNIFICANT DIFFERENCES. - 39 -
TABLE 5: SAME AS TABLE 4 BUT FOR THE WINTER CAMPAIGN. ..... - 39 -
TABLE 6: DESCRIPTIVE STATISTICS AND SIGNIFICANT DIFFERENCES OF AIR POLLUTION POLLUTANTS MEASURED WITHIN THE SUMMER EXPERIMENTAL CAMPAIGN IN BOLOGNA. PARTICULATE MATTER AND BTX LEVELS ARE COMPARED ALSO AGAINST VALUES MEASURED AT THE ARPA-ER FIXED AIR POLLUTION STATIONS, SAMPLING WITH THE SAME TIME RESOLUTION, WHILE OTHER AIR POLLUTION PARAMETERS WERE SAMPLED AT HIGH TIME RESOLUTION ONLY AT THE TWO URBAN STREET CANYONS. FOR EACH VARIABLE, EQUAL LETTERS IN LAST COLUMN INDICATE THE ABSENCE OF SIGNIFICANT DIFFERENCES. ..... - 45 -
TABLE 7: SAME AS TABLE 6 BUT FOR THE WINTER CAMPAIGN. ..... - 47 -
TABLE 8: DISTRIBUTION OF PARTICLE MASS CONCENTRATIONS AMONG THE DIFFERENT SIZE RANGES OF THE OPTICAL PARTICLE COUNTER AT THE TWO STREET CANYONS IN BOLOGNA. ..... - 52 -

LIST OF FIGURES

FIGURE 1: SCHEMATIC FLOW DIAGRAM OF THE CONNECTIONS BETWEEN THIS REPORT/TASK AND OTHER TASKS IN THE SAME AND IN OTHER ISCAPE WPS. ..... - 12 -
FIGURE 2: MEASUREMENT SITES FOR AIR POLLUTION AND METEOROLOGICAL VARIABLES WITHIN THE TWO INTENSIVE EXPERIMENTAL FIELD CAMPAIGNS IN BOLOGNA. ..... - 14 -
FIGURE 3: STREET VIEWS AND DETAILS (W = WIDTH, H = HEIGHT, A = ORIENTATION ANGLE OF THE STREET CANYON) OF THE TWO STREET CANYONS IN BOLOGNA. ..... - 15 -
FIGURE 4: THE TWO ARPA-ER VANS USED FOR AIR POLLUTION AND METEOROLOGY MONITORING IN MARCONI (LEFT) AND LAURA BASSI STS. (RIGHT). ..... - 16 -
FIGURE 5: THE MET ONE OPTICAL PARTICLE COUNTER INSTALLED IN LAURA BASSI ST. WITHIN THE BOLOGNA WINTER EXPERIMENTAL CAMPAIGN (LEFT) AND THE AETHLABS MICROAETH AE51. ..... - 17 -
FIGURE 6: THE VAISALA CEILOMETER CL31 FOR THE MEASUREMENT OF BOUNDARY LAYER HEIGHT IN BOLOGNA CITY CENTRE. ..... - 18 -
FIGURE 7: DETAILS OF THE THREE INSTRUMENTED HEIGHT LEVELS AT GROUND LEVEL, INSIDE THE CANYON AND ABOVE THE CANYON IN MARCONI ST. ..... - 19 -
FIGURE 8: DETAILS OF THE THREE INSTRUMENTED HEIGHT LEVELS AT GROUND LEVEL, INSIDE THE CANYON AND ABOVE THE CANYON IN LAURA BASSI ST. ..... - 20 -
FIGURE 9: (A) EXPERIMENTAL SITE ON PEARSE STREET IN DUBLIN, IRELAND (B) MAP OF THE EXPERIMENTAL MONITORING SITE IN DUBLIN (SOURCE: GOOGLE MAPS). ..... - 23 -
FIGURE 10: TELEDYNE CHEMILUMINESCENT NO/NO_2/NO_x ANALYZER USED IN DUBLIN EXPERIMENTAL CAMPAIGN. - 24 -
FIGURE 11: WIND VANE TO MONITOR WIND SPEED AND DIRECTION IN DUBLIN. ..... - 25 -
FIGURE 12: MAP AND PICTURE OF THE SIX MONITORING LOCATIONS IN GUILDFORD, UK. 1. ALDERSHOT-HEDGE (H_{CB}), 2. STOKE PARK-HEDGE (H_{IB}), 3. ALDERSHOT-TREE (T_{CB}), 4. SUTHERLAND-TREE (T_{IB}), 5. SUTHERLAND- VEGETATION BARRIER (TH_{IB}), 6. SHALFORD-VEGETATION BARRIER (TH_{CB}). ..... - 27 -
FIGURE 13: SCHEMATIC REPRESENTATIONS OF THE SIX MONITORING LOCATIONS ALONG WITH THE TYPE OF VEGETATION AND ROAD DETAILS IN GUILDFORD, UK. THE ORANGE CIRCLE AND BLACK RING DENOTE MEASUREMENT POINT BEHIND AND IN FRONT OF THE VEGETATION BARRIER, RESPECTIVELY. ..... - 29 -
FIGURE 14: INSTRUMENTS ARE MOUNTED ON TRIPOD AND KEPT CLOSE TO EACH OTHER DURING INTER-CALIBRATION. IN THE FIGURE, 1) GRIMM AEROSOL SPECTROMETER, 2) PTRAK 8525, 3) QTRAK 7575, 4) MICROAETH AE51, 5) WEATHER STATION KESTREL 4500. ..... - 31 -

FIGURE 15: SCATTERPLOTS OF ONE INSTRUMENT VS. THE OTHER MEASURING SAME POLLUTANT. A) PM_1 MEASUREMENTS BY GRIMM 11-C ON X AXIS AND GRIMM 107 ON Y AXIS, B) $PM_{2.5}$ BY GRIMM 11-C ON X AXIS AND GRIMM 107 ON Y AXIS, C) PM_{10} BY GRIMM 11-C ON X AXIS AND GRIMM 107 ON Y AXIS, D) BC MEASUREMENTS BY MICROAETH AE51, E) PNC MEASUREMENTS BY P-TRAK ..... - 32 -
FIGURE 16: THE ISCAPE – VANTAA MONITORING STATIONS ON A MAP: 1 = MALMINIITTY, 2 = HEUREKA, 3 = HELSINKI-VANTAA AIRPORT (METEOROLOGICAL REFERENCE STATION)..... - 33 -
FIGURE 17: AERIAL VIEW OF THE TWO MONITORING STATIONS: MALMINIITTY (LEFT) AND HEUREKA (RIGHT). RED DOTS INDICATE THE LOCATIONS OF THE INSTRUMENTS, GREEN DOT INDICATES THE LOCATION OF THE HSY AIR POLLUTION MONITORING STATION (SOURCE: GOOGLE MAPS)..... - 33 -
FIGURE 18: THE ISCAPE MALMINIITTY MONITORING STATION INSTRUMENTAL SETUP (FROM LEFT TO RIGHT): KIPP&ZONEN, CNR 4 NET-RADIATION METER; VAISALA WEATHER SENSOR WXT536; FMI STANDARD EQUIPMENT FOR AIR TEMPERATURE AND HUMIDITY MEASUREMENTS (ALL PHOTOS BY ACHIM DREBS) ..... - 34 -
FIGURE 19: THE ISCAPE HEUREKA MONITORING STATION INSTRUMENTAL SETUP (FROM LEFT TO RIGHT): FMI STANDARD EQUIPMENT FOR AIR TEMPERATURE AND HUMIDITY MEASUREMENTS; THE FMI MOUNTING TEAM AND ISCAPE RESEARCHERS AT THE TIME OF THE INSTALLATION; THE OBSERVATION MAST WITH THE KIPP&ZONEN, CNR 4 NET-RADIATION METER AND VAISALA WEATHER SENSOR WXT536 AT 10 M HEIGHT (ALL PHOTOS BY ACHIM DREBS)..... - 35 -
FIGURE 20: THE HELSINKI REGION ENVIRONMENTAL SERVICES AUTHORITY (HSY) AIR POLLUTION AND ENVIRONMENTAL MONITORING STATION AT TIKKURILA, 150 METER NORTH OF THE SCIENCE CENTER HEUREKA, ATTENTION: NOT ALL SENSORS WERE MOUNTED AT THE TIME OF THIS PICTURE, SEE ALSO FIGURE 17; (ALL PHOTOS BY ACHIM DREBS, 2015) ..... - 35 -
FIGURE 21: HSY AIR POLLUTION STATION NETWORK ..... - 36 -
FIGURE 22: ISCAPE MALMINIITTY BUILT-UP AREA, LEFT 2-D MODEL, RIGHT 3-D MODEL, RED DOT: ISCAPE – MONITORING STATIONS (MODELS BY ACHIM DREBS AND ENVI-MET V4) ..... - 37 -
FIGURE 23: ISCAPE HEUREKA OPEN AREA, LEFT 2-D MODEL, RIGHT 3-D MODEL, RED DOT: ISCAPE – MONITORING STATIONS (MODELS BY ACHIM DREBS AND ENVI-MET V4). ..... - 37 -
FIGURE 24: BOXPLOTS DEPICTING THE FUNDAMENTAL STATISTICAL PARAMETERS FOR METEOROLOGICAL VARIABLES (WIND SPEED AND TEMPERATURE) OBSERVED WITHIN THE TWO STREET CANYONS DURING THE SUMMER AND WINTER EXPERIMENTAL CAMPAIGNS IN BOLOGNA. THE BOXES ENCLOSE THE 25-75TH PERCENTILE VALUES, THE WHISKERS REPRESENT THE 5-95TH PERCENTILE VALUES; THE HORIZONTAL LINE INSIDE THE BOX REPRESENTS THE MEDIAN, WHILE THE SQUARE REPRESENTS THE MEAN VALUE. ..... - 40 -
FIGURE 25: 1-HOUR AVERAGED WIND SPEED (TOP), WIND DIRECTION (MIDDLE), AND TEMPERATURE (BOTTOM). COLORS INDICATE THE DIFFERENT MEASUREMENT SITES: MARCONI ST. (YELLOW) AND LAURA BASSI ST. (GREEN), ASINELLI TOWER (PURPLE), SILVANI ST. (CYAN). SUMMER CAMPAIGN ON THE LEFT, WINTER ON THE RIGHT..... - 40 -
FIGURE 26: 1-HOUR AVERAGED TEMPERATURE IN THE STREET CANYON DURING SUMMER. ON THE LEFT: DATA COMPARISON BETWEEN STATIONS AT THE SAME LEVEL INSIDE THE CANYONS (RED LINE – MARCONI ST., BLUE LINE - LAURA BASSI ST.). ON THE RIGHT: VERTICAL STRUCTURE OF THE SIGNAL TIME SERIES IN EACH STREET CANYON (RED LINE – GROUND LEVEL, BLUE LINE – MID-CANYON LEVEL, GREEN LINE – ROOFTOP LEVEL). - 41 -
FIGURE 27: 1-HOUR AVERAGED TEMPERATURE IN THE STREET CANYON DURING WINTER. ON THE LEFT: DATA COMPARISON BETWEEN STATIONS AT THE SAME LEVEL INSIDE THE CANYONS (RED LINE – MARCONI ST., BLUE LINE - LAURA BASSI ST.). ON THE RIGHT: VERTICAL STRUCTURE OF THE SIGNAL TIME SERIES IN EACH STREET CANYON (RED LINE – GROUND LEVEL, BLUE LINE – MID-CANYON LEVEL, GREEN LINE – ROOFTOP LEVEL). - 42 -
FIGURE 28: 5-MINUTES AVERAGED KINEMATIC VERTICAL HEAT (ON THE LEFT) AND MOMENTUM (ON THE RIGHT) FLUXES FOR THE SUMMER CAMPAIGN COMPUTED AT ALL THREE LEVELS OF EACH CANYON (RED LINE – GROUND LEVEL, BLUE LINE – MID-CANYON LEVEL, GREEN LINE – ROOFTOP LEVEL)..... - 43 -
FIGURE 29: 5-MINUTES AVERAGED KINEMATIC VERTICAL HEAT (ON THE LEFT) AND MOMENTUM (ON THE RIGHT) FLUXES FOR THE WINTER CAMPAIGN COMPUTED AT ALL THREE LEVELS OF EACH CANYON (RED LINE – GROUND LEVEL, BLUE LINE – MID-CANYON LEVEL, GREEN LINE – ROOFTOP LEVEL). ..... - 44 -
FIGURE 30: BOXPLOTS DEPICTING THE FUNDAMENTAL STATISTICAL PARAMETERS FOR AIR POLLUTION CONCENTRATIONS OBSERVED WITHIN THE TWO STREET CANYONS IN BOLOGNA DURING THE SUMMER EXPERIMENTAL CAMPAIGN. THE BOXES ENCLOSE THE 25-75TH PERCENTILE VALUES, THE WHISKERS REPRESENT THE 5-95TH PERCENTILE VALUES; THE HORIZONTAL LINE INSIDE THE BOX REPRESENTS THE MEDIAN, WHILE THE SQUARE REPRESENTS THE MEAN VALUE. ..... - 48 -
FIGURE 31: SAME AS FIGURE 30 BUT FOR THE WINTER EXPERIMENTAL CAMPAIGN..... - 50 -

FIGURE 32: TIME SERIES OF DAILY AVERAGES OF PARTICLE MASS CONCENTRATIONS (PM_{10} AND $PM_{2.5}$) AS MEASURED BY THE ARPA-ER INSTRUMENTATION DURING THE WINTER EXPERIMENTAL CAMPAIGN IN BOLOGNA. ..... - 51 -
FIGURE 33: TIME SERIES OF DAILY AVERAGES OF PARTICLE MASS CONCENTRATIONS (PM_{10} AND $PM_{2.5}$) AS MEASURED BY THE ARPA-ER INSTRUMENTATION AND AS ESTIMATED FROM PARTICLE COUNTS IN THE TWO STREET CANYONS IN BOLOGNA (MARCONI ST. UPPER PANELS; LAURA BASSI ST. LOWER PANELS). ..... - 52 -
FIGURE 34: DAILY NO_2 AVERAGES OBTAINED DURING DIFFERENT WEEKS OF THE BOLOGNA SUMMER AND WINTER EXPERIMENTAL CAMPAIGNS AT THE DIFFERENT MEASUREMENT SITES..... - 53 -
FIGURE 35: MEAN DIURNAL PATTERN OF NO_x AS SUM OF NO AND NO_2 COMPONENTS AT THE DIFFERENT MEASUREMENT SITES IN BOLOGNA (THE TWO STREET CANYONS AND THE ARPA-ER URBAN TRAFFIC STATION) DURING THE SUMMER (UPPER) AND WINTER (LOWER) EXPERIMENTAL CAMPAIGNS. ..... - 54 -
FIGURE 36: EXAMPLE OF PRIMARY NO AND CO CONCENTRATIONS OBSERVED WITH A 1-MIN TIME RESOLUTION IN THE 2 STREET CANYONS IN BOLOGNA ON 30/01/2018. ..... - 55 -
FIGURE 37: WIND ROSE PLOT FOR WIND SPEED AND DIRECTION OBSERVED AT SILVANI ST. ARPA-ER METEOROLOGICAL STATION WITHIN THE SUMMER AND WINTER INTENSIVE THERMOGRAPHIC CAMPAIGNS IN BOLOGNA (22-23/08/2017 AND 08-09/02/2018). ..... - 56 -
FIGURE 38: TEMPERATURE EVOLUTION WITHIN THE DAY OF THE SUMMER INTENSIVE THERMOGRAPHIC CAMPAIGN IN BOLOGNA (22-23/08/2017), MEASURED BY THE THERMO-HYGROMETERS, THE ARPA-ER INSTRUMENTATION IN ONE URBAN (SILVANI ST.) AND ONE RURAL METEOROLOGICAL STATION (MEZZOLARA) AND OF BUILDING FAÇADES OF BUILDINGS LOCATED ON THE WEST AND EAST SIDE OF THE 2 STREET CANYONS (MARCONI ST. UPPER AND LAURA BASSI ST. LOWER) AS RETRIEVED FROM THE THERMAL IMAGES. ..... - 56 -
FIGURE 39: SAME AS FIGURE 38 BUT FOR THE DAY OF THE WINTER INTENSIVE THERMOGRAPHIC CAMPAIGN IN BOLOGNA (08-09/02/2018). ..... - 57 -
FIGURE 40: DISTRIBUTION PLOT OF WIND SPEED DATA ACCORDING TO THE DIFFERENT WIND DIRECTION CATEGORIES. ..... - 58 -
FIGURE 41: WIND ROSE PLOT FOR THE DUBLIN SITE. ..... - 59 -
FIGURE 42: MINIMUM, MAXIMUM AND AVERAGE WIND SPEED DATA. ..... - 59 -
FIGURE 43: DISTRIBUTION PLOT OF NO_x (PPB) IN FRONT (F) OF THE LBW. ..... - 60 -
FIGURE 44: DISTRIBUTION PLOT OF NO_x (PPB) BEHIND (B) THE LBW. ..... - 60 -
FIGURE 45: TIME SERIES PLOT FOR THE NO_x CONCENTRATIONS (PPB) RECORDED ON BOTH SIDES OF THE LBW.... - 61 -
FIGURE 46: NO_x CONCENTRATION (PPB) IN (F) & (B) OF THE LBW PER WIND DIRECTION. ..... - 62 -
FIGURE 47: MEDIAN NO_x (PPB) REDUCTION BEHIND LBW. ..... - 62 -
FIGURE 48: STANDARD DEVIATION OF NO_x (PPB) REDUCTION BEHIND LBW. ..... - 63 -
FIGURE 49: BOXPLOTS OF POLLUTANT CONCENTRATION BEHIND (RED) AND CLEAR/IN FRONT (GREEN) MEASUREMENT POINTS AT THE SIX MONITORING SITES IN GUILDFORD, UK: A) PNC, B) $PM_{2.5}$, C) BC, D) PM_1, E) PM_{10}. TABLE WITH PERCENTAGE CONCENTRATION REDUCTION AT BEHIND LOCATION IN ALL SITES..... - 64 -
FIGURE 50: WIND ROSE DIAGRAM FOR EACH SITE WITH WIND DIRECTION CLASSIFICATION IN GUILDFORD, UK. COLOR CODES: BLUE-CROSS ROAD WINDS, YELLOW- ALONG ROAD, AND GREEN –CROSS VEGETATION. .. - 66 -
FIGURE 53: COMPARISON OF DAILY AIR TEMPERATURE AVERAGES (T), HIGHEST AIR TEMPERATURES (TMAX), AND LOWEST AIR TEMPERATURES (TMIN) OF THE STATIONS MALMINIITTY, HEUREKA, AND HELSINKI-VANTAA AIRPORT (AIRPORT) FOR THE PERIOD JULY 14TH - 26TH 2018. ..... - 68 -
FIGURE 52: 1-MINUTE AVERAGE OF SOLAR INCOMING SHORTWAVE RADIATION (BLUE) AND REFLECTED SHORTWAVE RADIATION (RED) AT ISCAPE MONITORING STATION MALMINIITTY (LEFT) AND HEUREKA (RIGHT) FOR THE PERIOD JULY 14TH - 26TH 2018 ..... - 69 -
FIGURE 53: MEAN WIND SPEED (LEFT) AND DAILY MAXIMUM WIND SPEED (RIGHT) AT ISCAPE MONITORING STATION MALMINIITTY (BLUE) AND HEUREKA (RED) FOR THE PERIOD MAY 1ST - JULY 26TH 2018 ..... - 69 -
FIGURE 54: RESULTS FROM THE HSY AIR POLLUTION NETWORK MONITORING STATIONS, LEFT: WEEKLY $PM_{2.5}$ MEASUREMENTS FROM 12 AIR POLLUTION STATIONS (HSY AND LOHJA), JULY 16TH - 22ND 2018; RIGHT: DETAIL OF 24-HOUR $PM_{2.5}$ MEASUREMENTS FROM 7 STATIONS IN THE METROPOLITAN AREA, JULY, 25TH 2018 (SOURCE: HSY, 2018) ..... - 70 -
FIGURE 55: RESULTS FROM THE HSY AIR POLLUTION NETWORK MONITORING, LEFT: WEEKLY NITROGEN DIOXIDE MEASUREMENTS FROM 12 AIR POLLUTION STATIONS (HSY AND LOHJA), JULY 16TH - 22ND 2018; RIGHT: DETAIL OF 24-HOUR NITROGEN DIOXIDE MEASUREMENTS FROM 8 STATIONS IN THE LARGER METROPOLITAN AREA, JULY 25TH 2018 (SOURCE: HSY, 2018) ..... - 70 -

List of abbreviations

AGL: Above Ground Level
ARPA-ER: Emilia Romagna Environmental Protection Agency
BC: Black Carbon
BTEX: Benzene, Toluene, Ethylbenzene, Xylenes
CB: Clear area and Behind
CFD: Computational Fluid Dynamics
CO: Carbon Monoxide
D: Deliverable
FIR: Far Infrared Radiation
FMI: Finnish Meteorological Institute
GHG: Greenhouse Gas
GI: Green Infrastructure
H: Height
H_{CB}: Hedge only in clear vs behind
H_{IB}: Hedge only in clear vs in-front
HSY: Helsinki Region Environmental Services Authority
IB: In front and Behind
L: Length
LAI: Leaf Area Index
LBW: Low Boundary Wall
LTZ: Low Traffic Zone
NO: Nitric Oxide
NO_2: Nitrogen Dioxide
NOx: Nitrogen Oxides
O_3: Ozone
ONA: Optimised Noise-reduction Averaging
PCS: Passive Control System
PM: Particulate Matter
PM_1: Particulate Matter with aerodynamic diameter less or equal to 1 µm
$PM_{2.5}$: Particulate Matter with aerodynamic diameter less or equal to 2.5 µm
PM_{10}: Particulate Matter with aerodynamic diameter less or equal to 10 µm

PNC: Particle Number Concentration
SO_2: Sulphur Dioxide
T: Temperature
T_{CB}: Tree only in clear vs behind
T_{IB}: Tree only in clear vs in-front
TH_{CB}: Tree with Hedge case in clear vs behind
TH_{IB}: Tree with Hedge case in clear vs in-front
TMAX: Highest air temperatures
TMIN: Lowest air temperatures
UHI: Urban Heat Island
UPI: Urban Pollution Island
W: Width
WHO: World Health Organization
WP: Work Package
WS: Wind Speed

1 Executive Summary

This report documents good quality meteorological and air pollution data obtained as result of the experimental field campaigns carried out in the different iSCAPE cities, namely Bologna, Dublin, Guildford and Vantaa. We recall that these cities are those with a focus on “physical” interventions, or rather on the evaluation of the impacts of Passive Control Systems (PCSs) on air pollution mitigation through the analysis of environmental data gathered during different monitoring campaigns, as described in D3.3. Other iSCAPE cities focused instead on behavioral interventions (Hasselt) and infrastructural solutions (Bottrop). The data obtained so far were carefully checked for their quality and their usage is twofold. From one hand measured data will be used for the validation of the model simulations run as part of other WPs (e.g. WP4 and WP6) and, on the other hand, they will provide the scientific basis to establish the efficacy of different PCSs including low boundary walls and green infrastructure (trees and hedges), in each city. Specifically, regarding this last goal, preliminary results show a strong dependency of the impact of the different PCSs on the local morphology of the analyzed urban environment and the local meteorological conditions impacts, leading to both mitigation and deterioration effects of air pollution. It is worth to recall that this is a preliminary version of the report which will be updated later by the end of the project when all the monitoring activities will be completed, and further analyses of the results will be carried out meanwhile.

The instrumental setup and protocols, along with the description of the experimental sites, already presented in D3.3, are here summarized and updated.

This report also provides some preliminary results about the efficacy of the different PCSs in contrasting/reducing air pollution and/or reducing the UHI (Urban Heat Island) effect at urban level, especially in the city of Bologna, where as noted in D1.4 and thoroughly studied in D6.1, the UHI phenomenon is large and show very strong diurnal variations. To this end, and for the purpose of detailing and analyzing the UHI phenomenon at the street/neighborhood scale, within the experimental campaigns conducted in Bologna, two intensive thermographic campaigns were performed, and this report presents the preliminary results obtained, which show well the efficacy of trees as regards the thermal comfort within the urban environment. This fulfils the objective of detailing air pollution levels and meteorological conditions in the target cities, as measured within the different pilots.

2 Introduction

Air pollution continues to pose an important global problem with diverse and substantial public health implications. The WHO (World Health Organization) currently estimates that 4.2 million deaths, 25% of heart diseases and 43% of all lung diseases every year result from exposure to ambient (outdoor) air pollution; in addition, air pollution levels remain at dangerously high levels in many parts of the world, with 91% of world’s population living in places where air pollution exceeds WHO guideline limits (WHO, 2018). According to the 2018 Environmental Performance Index (https://epi.envirocenter.yale.edu/), poor air pollution is the greatest environmental threat to public health; diseases related to airborne pollutants contributed to 65% of all life-years lost to environmentally related deaths and disabilities in 2016 (Friedrich, 2018).

Challenges to maintaining and improving air pollution include population growth, more people living in urban areas where exposure to traffic-related pollutants tends to be higher, and growing demand for energy and transportation. In the recent decades, indeed, rapid urbanization, one of the biggest social transformations of modern times, has deeply affected the environment, and in

particular air pollution, ecosystems, land use, biogeochemical cycles, water pollution, solid waste management, and the climate (Bai et al., 2017).

It is also well known that meteorological factors have an important effect on the amount of pollution in the atmosphere. In fact, serious pollution episodes in the urban and suburban environment are often not directly caused by sudden increases in pollutants emissions but by unfavourable meteorological conditions, for example limiting the ability of the atmosphere to disperse pollutants and transport them to other areas (Latini et al., 2002). This aspect becomes fairly important especially in regions (e.g., the Po Valley, but also the Ruhr region) characterized by a high density of anthropogenic emissions and by the frequent occurrence of stagnant meteorological conditions (Thunis et al., 2009). The observed temporal pattern of air pollutants is thus derived from a combination of various factors, among which atmospheric and hydrological processes (e.g., through the action of wet removal which is the main removal mechanism especially for particle-related pollution), human activities, long-range transport, natural emissions and extreme events (Bigi et al., 2012).

Various studies have indeed already investigated the impacts and links of local meteorological parameters (e.g., wind speed and direction, relative humidity, rainfall, and temperature) with air pollution pollutants (e.g., Niu et al., 2018; Shi et al., 2017; Yassin et al., 2018; Wang et al., 2018). To a first approximation, since air movements influence the fate of air pollutants, any study on air pollution should also include a study of the local weather patterns. Meteorological data, in fact, may help to: 1) identify the source of pollutants; 2) predict air pollution levels such as inversions and high-pollutant concentration days; 3) simulate and predict air pollution. In addition, since UHI and UPI (Urban Pollution Island), two major problems of the urban environment which are becoming more serious with rapid urbanization, can interact with each other, they should be studied concurrently for a better urban environment (Li et al., 2018).

Within the iSCAPE project, various experimental campaigns have been setup in different target cities to monitor air pollution and meteorological variables, both to obtain experimental data to be used for the calibration and validation of simulations conducted at neighborhood/city scale as part of WP6 as well as to analyze the potential of different PCSs (Passive Control Systems) including low boundary walls (Dublin), and green infrastructure (trees and hedges, monitored within the pilots in Bologna, Guildford and Vantaa), for reducing air pollution and/or improving urban thermal comfort (Gallagher et al., 2015).

In particular, this report is the output of Task 5.2, which involves the monitoring of the interventions deployed as part of WP3 and WP4 in order to optimize them. In particular, the monitoring stations installed as part of WP3 and WP5 collected environmental data to be used as input and feedback for the simulations run as part of WP4 and WP6. Figure 1 presents an overview of all the activities interconnected with the present report/task, in the same WP as well as in other iSCAPE WPs.

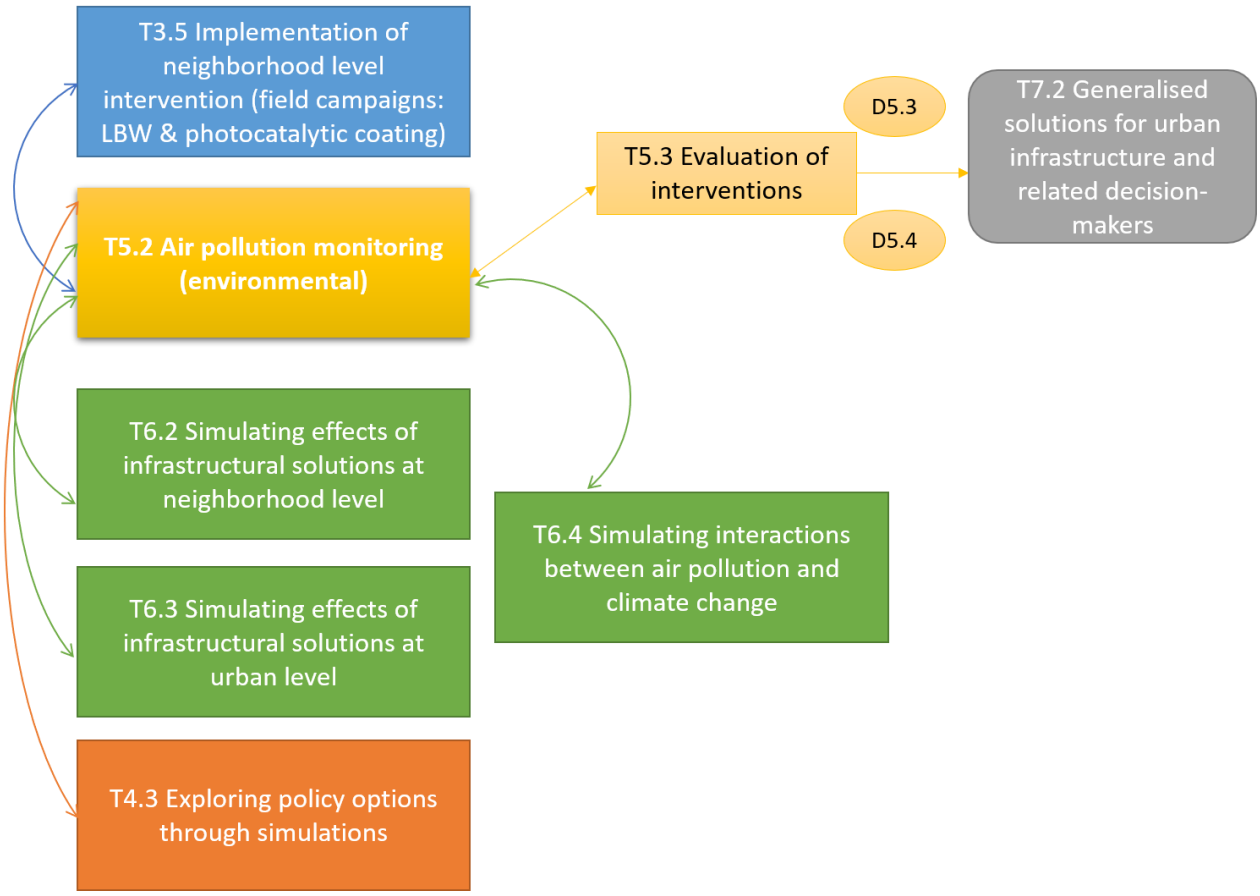

Figure 1: Schematic flow diagram of the connections between this report/task and other tasks in the same and in other iSCAPE WPs.

As such, this report intends to document good quality meteorological and air pollution data obtained so far at the monitoring stations set in the different iSCAPE cities. In addition, preliminary results obtained about the efficacy of various PCSs in contrasting air pollution and improving urban thermal comfort are also presented here. The structure of the report is as follows: first, the methodology, instrumental setup and experimental protocol adopted within the different monitoring stations is described in Section 4; Section 5 presents the environmental data collected within the experimental campaigns at the 4 pilots. Finally, preliminary conclusions are drawn.

3 Methodology for air pollution and meteorology monitoring

This section is dedicated to the methodology description. All the field campaigns required by DoA and already introduced in D3.3 are extensively presented and described. Despite the final goal of all the monitoring campaigns is the same, i.e. to obtain the data for the validation of simulations conducted as part of other WPs and specifically the assessment of the efficacy of the different PCSs in contrasting air pollution and climate change, each city has a stand-alone and different campaign where in particular a different physical intervention is studied. For the sake of presenting the results of each single intervention in the most homogeneous and general manner, a precise description of monitoring sites, instrumentations and protocols is essential.

Site description is a multiscale geographical and morphological issue. The region where the pilot city is located helps to settle the background conditions both related to atmospheric circulation and air pollution, and to identify which could be the best intervention in the geographical area (a detailed description of the cities geography and morphology, as well as air pollution and recent climatology was previously reported in D6.1). Physical features specific of each experimental site are also described to address the topological conditions where each field campaign is performed.

Instrumental setup is needed to set the quantities of interest, depending on the goal on the campaign. The result is that different variables were measured in each site according to the specific challenge being addressed. As such, the experimental campaigns and instrumental setups deployed at the various sites are not always directly comparable, nevertheless the variety and the data volume acquired will allow us to draw more general understanding of mitigation strategies in sites located in different geographical zones.

In conclusion, the experimental protocol and quality check are crucial aspects for the reliability of the measured data. The protocol identifies how the instrumentation is used, both in terms of performance and location in the site. The quality check is also crucial: all the instrumentations must be calibrated before the beginning of the campaign and the reliability of collected data must be ensured before subsequent analyses.

Table 1 presents an overview of the PCSs evaluated within the different monitoring campaigns, and of the collected meteorological and air pollution pollutants at the four iSCAPE cities, which will be described in detail in the following sections.

City	PCSs	Meteorological variables	Air pollution pollutants
Bologna	Green infrastructure	wind speed, wind direction, high-frequency 3-d wind field (including turbulence), air temperature, relative air humidity, four-energy radiation components, atmospheric pressure	NO_x, NO, NO_2, CO, SO_2, O_3, PM_{10}, $PM_{2.5}$, BTX, CO_2 and H_2O fluxes; PNC and BC (only during the winter campaign),
Dublin	Low Boundary Walls	wind speed, wind direction	NO_x, NO, NO_2
Guildford	Vegetation	air temperature, relative air humidity, wind speed, wind direction	PM_1, $PM_{2.5}$, PM_{10}, PNC, BC, CO
Vantaa	Green infrastructure embedded on high stores buildings	wind speed, wind direction, air temperature, relative air humidity, four-energy radiation components, atmospheric pressure, rain intensity	NO_x, NO, NO_2, PM_{10}, $PM_{2.5}$, BC

Table 1. Overview of the PCSs evaluated, and of the meteorological and air pollution pollutants variables monitored within the monitoring campaigns setup in the four iSCAPE cities.

3.1 Bologna

Due to its location within the Po Valley, Bologna is a well-known hotspot in terms of air pollution and climate change. Green infrastructures[1] can offer a mitigating solution to both problems, but their implementation must be carefully defined. Seeking this goal, air pollution and meteorological variables were monitored during two intensive experimental field campaigns carried out in two different urban areas. In the following subsections, we describe the measurement sites, the instrumental setup, and the experimental protocol adopted.

3.1.1 Site description

In this study, we carried out two intensive experimental field campaigns, one in summer (10/08/2017-24/09/2017) and one in winter (16/01/2018-14/02/2018), to monitor both air pollution and meteorological variables in two parallel urban street canyons, Marconi and Laura Bassi Sts. (Figure 2).

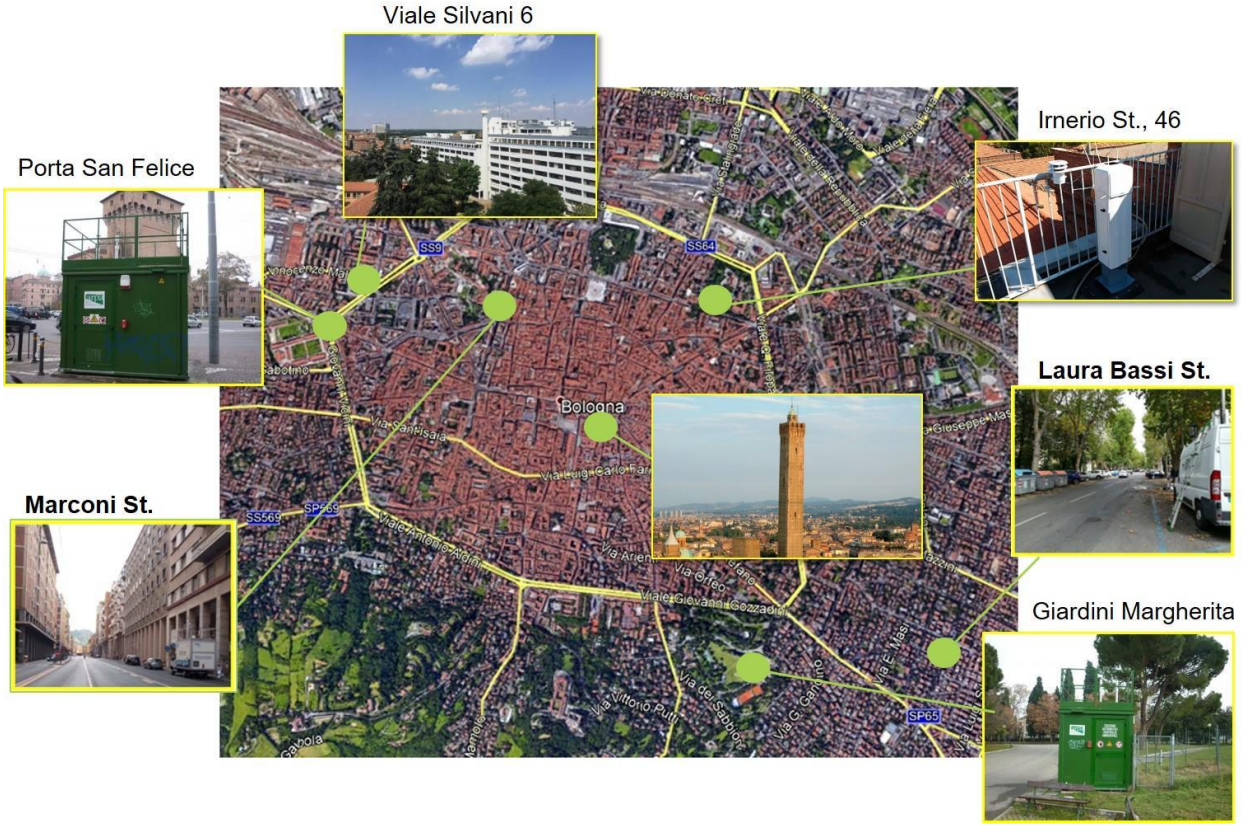

Figure 2: Measurement sites for air pollution and meteorological variables within the two intensive experimental field campaigns in Bologna.

[1] In this report, the wide concept of green infrastructures for Bologna refers to the evaluation of the effect of trees in street canyons. The impact of other green infrastructures elements, such as green roofs and green façades will be evaluated by means of numerical simulations carried out in WP6 using the data gathered within the monitoring campaigns herein described.

The Figure also depicts other air pollution and meteorological stations in the city, used for supporting measurements of ancillary variables and/or for comparison with data measured in the two experimental sites. In particular, Asinelli Tower and Silvani St. are two ARPA-ER (Emilia Romagna Regional Environmental Protection Agency) meteorological stations: more precisely, Asinelli Tower is a synoptic meteorological station (100 m height), while Silvani St. is an urban meteorological station in the city center (30 m height), respectively. Porta San Felice and Giardini Margherita are two ARPA-ER air pollution monitoring stations, characterized as urban traffic and urban background, respectively. Finally, at Irnerio St., on the roof of the Department of Physics and Astronomy of the University of Bologna, additional supporting measurements of boundary layer height were carried out, which will be described in detail in the following paragraphs.

Since the primary aim of the Bologna experimental campaigns was to evaluate the impact of trees in street canyons on air flow and pollution levels, the two canyons were chosen to have a similar N-S configuration and similar traffic volumes, but with a major difference in the presence of vegetation: in fact, while Marconi St. is a main business road located in the historical city center, almost free of vegetation and highly packed buildings encompassing a four-lines street, Laura Bassi St. is located in a residential area in the outskirts of Bologna, characterized by small houses and apartments, wide frontal distances and by the presence of a tree line of deciduous trees on both sides of the street (Figure 3).

Figure 3: Street views and details (W = width, H = height, α = orientation angle of the street canyon) of the two street canyons in Bologna.

Both streets are characterized by similar intense traffic rates, and as such are classified as trafficked urban street canyons.

3.1.2 Instrumental setup

In this section, we describe all the equipment and instruments used for the two experimental campaigns for air pollution and meteorology monitoring in Bologna.

Two ARPA-ER mobile laboratories (Figure 4), i.e., vans equipped for air pollution and meteorological measurements were deployed in each measurement site.

Figure 4: The two ARPA-ER vans used for air pollution and meteorology monitoring in Marconi (left) and Laura Bassi Sts. (right).

Mobile laboratories were equipped for continuous measurements of air pollution pollutants such as nitrogen dioxides (NO_x), carbon monoxide (CO), sulphur dioxide (SO_2), ozone (O_3), and particulate matter (PM_{10} and $PM_{2.5}$). The ARPA-ER van located in Marconi St. was further equipped for the measurements of BTX (benzene, toluene, ethylbenzene and xylenes). Technical specifications for the instrumentation used onboard the ARPA-ER for air pollution measurements are available in the Appendix of D3.3.

Owing to the importance of particle pollution especially during the cold season, within the winter experimental campaign two further instruments for the measurements of particle size distribution and of black carbon concentrations were added to the standard air pollution measurements. In particular, two Met One Model 212 Ambient Particulate Counters (Figure 5) were deployed to size and count particles in eight digital bins, with a minimum sensitivity of 0.3 µm. Such instruments use light scatter technology with a laser-diode based optical sensor to detect, size, and count particles. The detected information is output as particles per size range. Black Carbon (BC) concentrations were monitored through the use of two real-time pocket-sized BC aerosol monitors, the AethLabs microAeth AE51 (Figure 5). This instrument is a high sensitivity, miniature, portable instrument designed for measuring the optically-absorbing BC component of aerosol particles. BC aerosol, often called soot, is an operationally defined term for describing carbon as measured by light absorption. BC is emitted by incomplete combustion processes: as such, in an urban street canyon, it is mostly emitted by anthropogenic activities (combustion engines and residential heating). Due to its ability to absorb visible and infrared radiation and to darken surfaces (specifically, snow and ice), BC concentrations play an important role in the radiative balance of the earth system through its direct effect of heating the lower atmosphere and indirect effect of affecting cloud properties (Ramanathan and Carmichael, 2008). However, unlike long-lived GHG such as CO_2, BC has a short residence time (1-2 weeks), so it tends to have a more regional than global impact, particularly close to its emission sources. There is enough evidence that BC may also have adverse impacts on human health (Janssen et al., 2012).

The microAeth AE51 draws an air sample through a 3 mm diameter portion of filter media. Optical transmission through the 'Sensing' spot is measured by a stabilized 880 nm LED light source and photo-diode detector. The gradual accumulation of optically-absorbing particles leads to a gradual increase in the absorbance of the spot, measured relative to an adjacent 'Reference' portion of the filter once per timebase period. The increment during each timebase is then converted to a mass concentration of BC expressed in nanograms per cubic meter (ng/m^3) using the known optical absorbance of BC material.

Technical specifications of the optical particle counter and of the microaethalometer used in the winter campaign are reported in the Appendix.

Figure 5: The Met One Optical Particle Counter installed in Laura Bassi St. within the Bologna winter experimental campaign (left) and the AethLabs microAeth AE51.

ARPA-ER mobile laboratories are also equipped with instruments for measuring basic meteorological variables such as: cup anemometer and wind vane for wind speed and direction measurements; barometer for the measurement of atmospheric pressure; thermohygrometers for temperature and relative humidity measurements.

In addition, traffic counts were available by means of inductive loops from the Bologna Municipality.

Due to the need of fast, high-precision and high temporal resolution measurements of the three components of wind velocity (*u, v, w*), air temperature, relative humidity, and pressure, the instrumentation onboard the ARPA-ER mobile laboratories were further instrumented with:

- GILL Windmaster sonic anemometer for rapid response measurements of the 3-d wind field; data obtained from such instruments allows the estimation of a range of turbulence parameters and fluxes, using eddy covariance methods, in addition to obtaining the mean horizontal wind.
- HCS2S3 Rotronic temperature and relative humidity probe for accurate temperature and relative humidity measurements.

- Vaisala Barometer PTB110 for accurate barometric pressure measurements at room temperature and for general environmental pressure monitoring over a wide temperature range.

Additional measurements of the energy balance between incoming short-wave and long-wave Far Infrared Radiation (FIR) versus surface-reflected shortwave and outgoing long-wave radiation and of CO_2 densities in turbulent air structures were performed through CNR4 net radiometer (Kipp & Zonen) and LI-COR LI-7500 DS instruments, respectively. In particular, the use of open path CO_2/H_20 gas analyzers provide the determination of CO_2 and water vapor fluxes, when coupled with sonic anemometers air turbulence data and by means of eddy correlation techniques. Further information, as well as technical specifications, for all these instruments are available in D3.3.

Within both winter and summer experimental campaign, high-performance thermal imaging cameras were used to quantify thermal characteristics of various physical elements on urban streets (building façades, asphalt, etc.) and their temporal variations. To this aim, two high-performance FLIR T620 ThermalCAMs, with uncooled microbolometer, 640 x 480 pixels resolution and an image acquisition frequency of 50-60 Hz were used.

Finally, a Vaisala Ceilometer CL31 (Figure 6) was installed on the roof of the Department of Physics and Astronomy (Irnerio St., 46: see Figure 2) for measurements of boundary layer height. The specific locations allowed to characterize the urban atmospheric structure for the two investigated sites.

Technical specifications of the two thermal cameras and of the Vaisala Ceilometer are available in the Appendix.

Figure 6: The Vaisala Ceilometer CL31 for the measurement of boundary layer height in Bologna city centre.

3.1.3 Experimental protocol and quality check

During both winter and summer experimental campaign, one ARPA-ER mobile laboratory was located in each street canyon. The following Table reports information on the measurements and the time resolution of the ARPA-ER instrumentations located in the two street canyons and in the two fixed air pollution stations used for comparison.

Time resolution										
	Daily		Hourly					Minute		
	PM_{10}	$PM_{2.5}$	NO_x	CO	O_3	SO_2	BTX	NO_x	CO	O_3
Marconi St.	✓	✓	✓	✓	✓	✓	✓	✓	✓	✓
Laura Bassi St.	✓	✓	✓	✓	✓	✓		✓	✓	✓
Porta S. Felice	✓	✓	✓	✓			✓			
Giardini Margherita	✓	✓	✓		✓					

Table 2: Details on air pollution pollutants and time resolution of measurements at the two mobile laboratories located in the two street canyons and at fixed air pollution monitoring stations within the two experimental field campaigns.

Both street canyons were equipped with high frequency meteorological instrumentation at three different height levels in and above the canyon (Figure 7 and Figure 8), i.e. at ground level (on the roof of the ARPA-ER van), at mid-level inside the canyon (on the banisters of a balcony at the second floor) and above the canyon on the rooftop on the highest building. The installation heights are different in the street canyon due to different possible locations. In Marconi St. ground level instrumentations are set at 4 m (AGL), mid-canyon level is set at 8 m (AGL) and the rooftop is located at 35 m (AGL). In Laura Bassi St. the respective heights are 3 m, 9 m and 20 m (AGL).

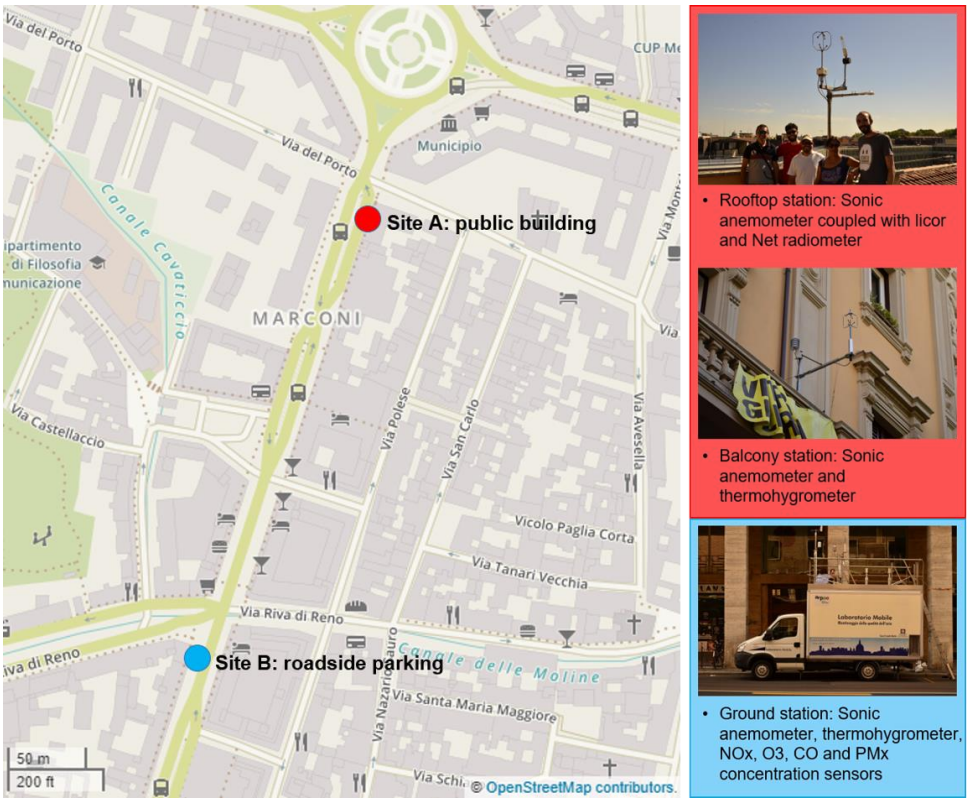

Figure 7: Details of the three instrumented height levels at ground level, inside the canyon and above the canyon in Marconi St.

Figure 8: Details of the three instrumented height levels at ground level, inside the canyon and above the canyon in Laura Bassi St.

In particular, all sonic anemometers were setup to collect measurements with a 50 ms time resolution, to allow for a high-resolution determination of turbulent features, such as momentum and sensible heat fluxes; thermo-hygrometers and net radiometers acquired measurements at 1 sec and 1 min time basis respectively; finally, the coupling of the LI-COR on the rooftop station in Marconi St. enabled the estimation of CO_2 and H_2O fluxes at a 100 ms rate.

During the winter experimental campaign, the optical particle counter and the micro-aethalometer were setup on the roof of the ARPA-ER vans, with a 1 min time resolution; this allows to directly compare the patterns of sized particle counts and BC concentrations with that of the other air pollution pollutants collected nearby and with the same time resolution. Prior to their displacement in field, one instrument of each pair was calibrated by the manufacturer, and the correct functioning of the two pairs was checked simultaneously collecting measurements for one-day (24 h) in a controlled environment. Results indicate good agreement between each pair of instruments (coefficient of determination ranging between 0.86 and 0.99), while the derived bias with respect to the calibrated instrument (i.e. from the regression equation in the scatter plot) was used to correct measurements collected during the winter experimental campaign. Loading effects of aethalometer data were corrected using the procedure of Virkkula et al. (2007) while attenuation generated by instrumental noise was post-processed through the Optimized Noise-reduction Averaging algorithm (ONA; Hagler et al., 2011).

During summer, the collection of simultaneous measurements using the same experimental setup in the two street canyons allowed for a direct comparison between them, characterized by a different presence of vegetation. In addition, measurements were collected both during the month

of August, when traffic in Bologna is largely decreased, and in the month of September, when people come back from holidays and traffic volumes are back to normal levels. Instead, the winter campaign was characterized by a reduced impact of vegetation due to the fall of leaves and by the occurrence of frequent stagnant conditions deeply affecting pollution levels.

As indicated previously, supporting measurements of hourly averaged meteorological variables (and in particular, temperature, wind speed and wind direction) were collected at ARPA-ER fixed meteorological stations (Silvani St. and Asinelli Tower): within the campaigns, these measurements were used to assess synoptic features of the incident flows.

The ceilometer was installed during the summer experimental campaign on the roof of the Department of Physics and Astronomy of the University of Bologna in order to estimate the urban boundary layer height especially during events of special interest.

Fast sampled raw high-resolution measurements from sonic anemometers were transformed into high quality clean data by first eliminating all the spikes and after using the procedure suggested by McMillen (1988). The despiking procedure assumes a Gaussian distribution inside a stationary set of data (30 minutes interval in the data series). Values falling outside 3 standard deviations from the mean are rejected. Despiked wind components are then rotated to align the reference system to the canyon direction, so that *u* is the cross-canyon, *v* is the along-canyon and *w* is the vertical wind component, respectively. The McMillen method consists in: (1) 'detrending' (by use of running mean removal), (2) calculation of the entire stress tensor (which allows a three-dimensional coordinate rotation to be performed on the covariances), (3) software-adjustable timing delays for each instrument channel. Once data have been despiked and rotated according to the canyon orientation, both mean flow and turbulent quantities are computed at the three levels inside and above the canyons. To ensure a general robustness of the analysis, without losing small scales processes, all quantities have been averaged in time over a 5 minutes period.

Data self-consistence of each instrumentation type is ensured by a former laboratory test comparison between them to ensure the validity of the calibration. Moreover, the same test is also performed in a real but controlled environment. After the campaign, a final quality check is performed by comparing equivalent quantities measured at approximatively the same location by different instrumentations. For example, thermo-hygrometers data taken with ARPA-ER sensors were compared with the analogous collected by the supplementary one installed at the same level. The same procedure was carried out for all the other quantities with double independent measurements at the same level.

During both the winter and summer experimental field campaigns, two intensive thermographic campaigns with the two thermal cameras were performed in the two street canyon areas. The aim of these campaigns was to analyze temperature distribution of building façades and ground surfaces in the two streets, in order to collect and analyse data for the UHI effect at neighborhood and city scale levels. Images were simultaneously collected by an operator on foot at the two sites during a 24-hour acquisition with regular intervals of 2 hours (total of 12 acquisitions in 24 hours at each site). During both campaigns, the days for the so-called UHI experiment (intensive thermographic campaigns) were selected according to the weather forecast to have a clear sky, calm wind, day (22-23/08/2017 during the summer campaign, and 08-09/02/2018 during the winter campaign).This choice allowed to collect images at 12:00 (close to the maximum surface temperature), 14:00, 16:00 (close to the maximum air temperature), 18:00, 20:00, 22:00 (close to maximum UHI intensity). Analyzed buildings were selected on the basis of the homogeneity of construction material and the absence of obstacles (balconies, eave, etc.), metal or glass. Several shots or portions of the same building façade at several different heights were taken in order to maintain a similar resolution for all images. Finally, measurements of ground surfaces were also collected.

Data collected within the experimental campaigns were subjected to a thorough statistical analysis; statistical differences between the measurements collected in the two canyons and at other ARPA-ER fixed stations were evaluated by means of Kruskall-Wallis test with p = 0.05 significance level.

3.2 Dublin

Low-Boundary walls (LBWs) can provide a solution to enhance localized dispersion and improving air pollution in distinct street canyons settings.

Within iSCAPE, Dublin city in Ireland has been chosen as the location for examining LBWs in the built environment. LBWs are a type of physical PCSs and have been shown to effectively impact on air flow and pollutant dispersion in low-rise street canyons (Gallagher et al., 2012, Gallagher et al., 2013, King et al., 2009, McNabola et al., 2008, McNabola et al., 2009). Therefore, Dublin provides an experimental setup and location to examine the implications of the LBW on personal exposure to air pollution as a type of PCS.

This report explores the potential of using LBWs as an effective intervention to reduce the personal exposure to air pollution in the built environment through a real-world field experiment.

The report provides results relating to the effects of the LBWs on the dispersion of NO_x gases based on different sets of wind directions in a street canyon geometry.

3.2.1 Site description

A comprehensive air pollution monitoring campaign was implemented in Dublin. This four-week campaign was implemented in 2018 based on two weeks of winter monitoring (March 2018) and the other two weeks of monitoring during summer (July 2018). This campaign takes place on Pearse Street, which is located in the city center (Figure 9). This street canyon is characterized by a high traffic volume. Pearse Street has 4 lanes all going in the same direction with a total width of 16 m and it has a North-South alignment. An LBW 18 m long and 1m high has been installed along the edge of the footpath on one side of the street, see Figure 9.

Two monitoring points have been installed on the LBW, one at each side of the wall, Front side (F) and Backside (B).

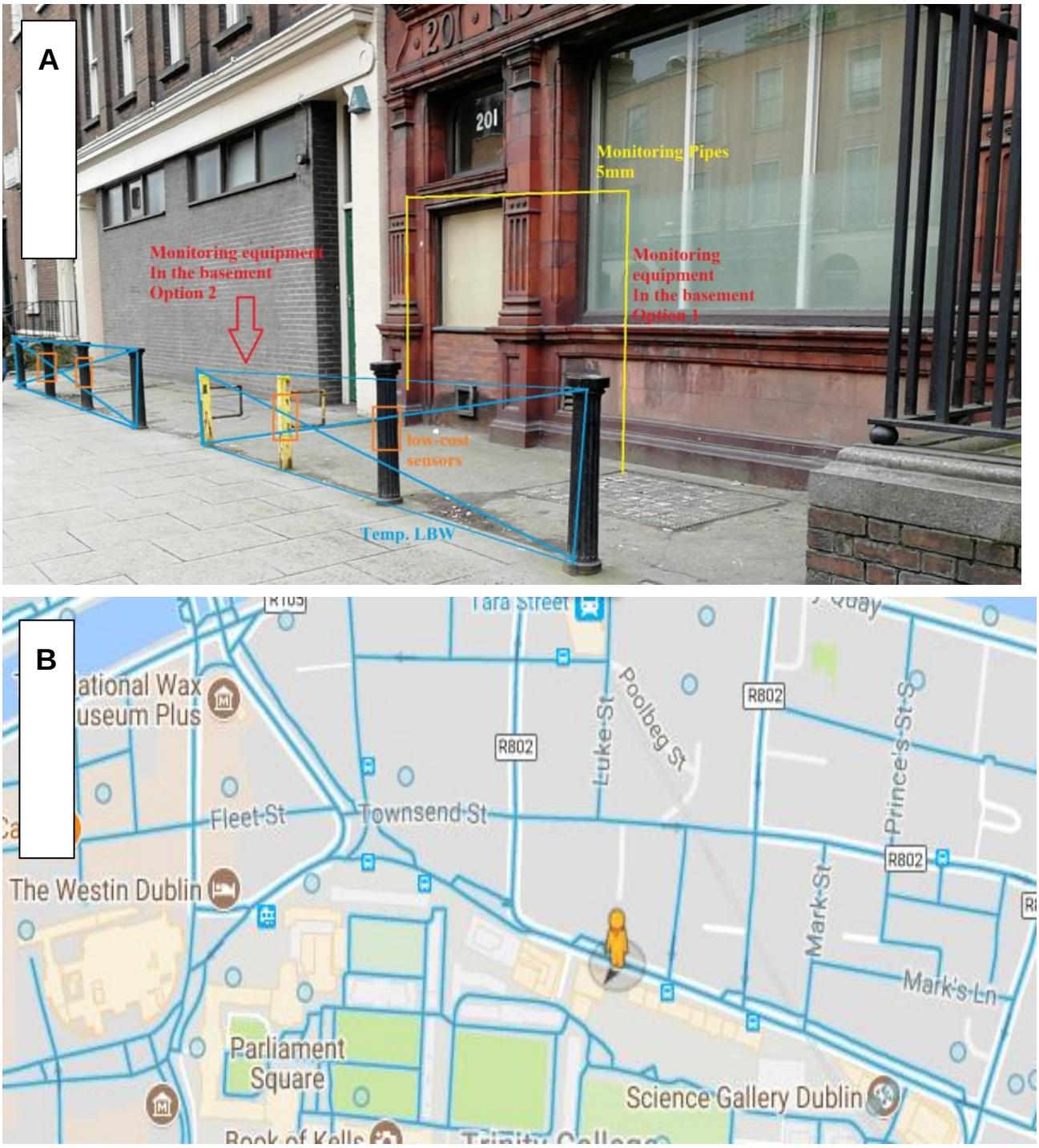

Figure 9: (A) Experimental site on Pearse Street in Dublin, Ireland (B) Map of the experimental monitoring site in Dublin (source: Google Maps).

3.2.2 Instrumental setup

Two Teledyne Chemiluminescent NO/NO_2/NO_x Analyzers (Model 200E and 200EU) (Figure 10) have been used to monitor the NO_x gases in the two monitoring points (F) and (B) (the two sides

of the LBW). A wind vane (Cabled Vantage Pro2™ with Standard Radiation Shield) was installed on the rooftop of the adjacent building to monitor the wind speed and wind direction (Figure 11).

Data presented in this report were collected from the fortnight period during working hours (08:00 to 19:00) and 5 days per week.

Data were collected using the following equipment and time resolution:

- $NO/NO_2/NO_x$ concentrations (ppm) (5-minute averaged values) from the NO_x analyzer (N2CNC1-AVG, NXCNC1-AVG and NoCNC1-AVG).
- Wind Speed and wind direction (5-minute averaged values).

Figure 10: Teledyne Chemiluminescent $NO/NO_2/NO_x$ Analyzer used in Dublin experimental campaign.

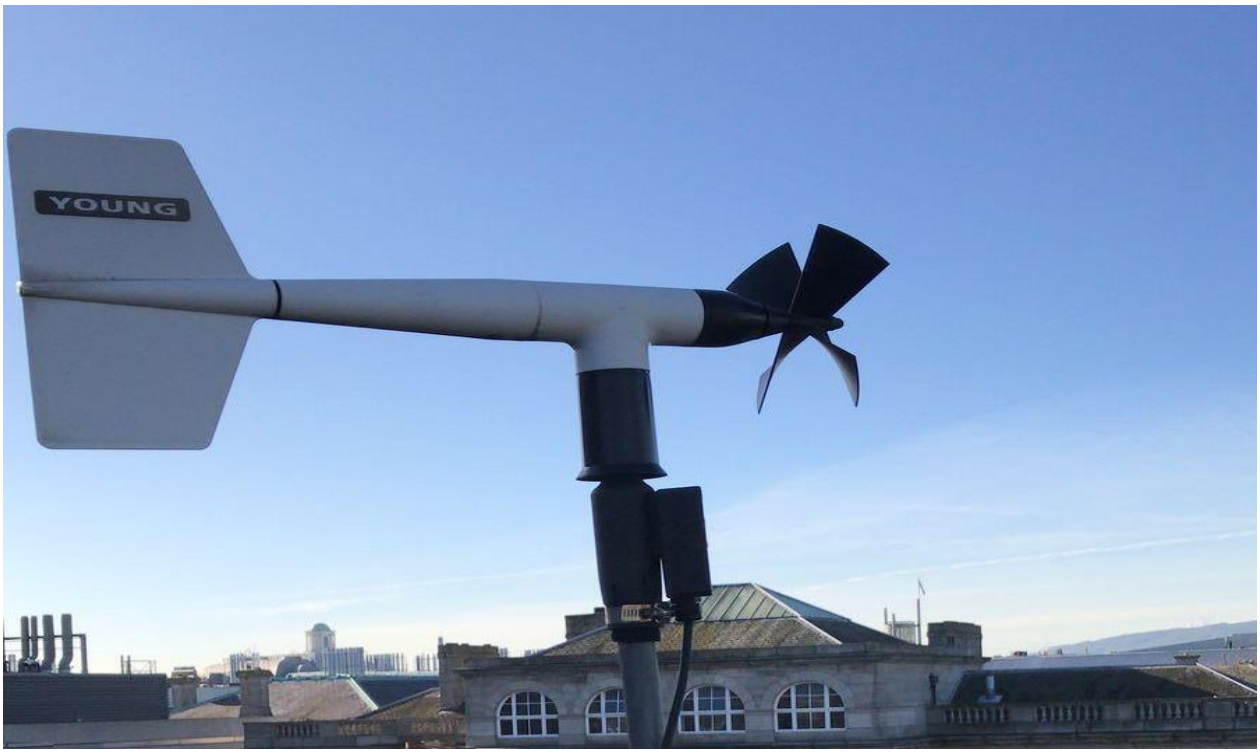

Figure 11: Wind vane to monitor wind speed and direction in Dublin.

3.2.3 Experimental protocol and quality check

The Pearse Street monitoring site has a bright area (without any disturbance to air flow) adjacent to the LBW.

The campaign is designed to be conducted in two fortnight experiments one in winter 2018 (whose results are presented in this report) and another one in summer 2018, which is currently being implemented, collecting a total batch of 30 days' data. The complete set of data would be analyzed, and results will be presented in the updated D5.2 report by the end of the project.

The field measurement is started and ended around 08.00 and 18.00 (local time) each day, respectively. This enables to collect 8 to 10 hours of data every day. Inter-calibration between each set of instruments is achieved by running instruments side by side for 20 to 30 min prior beginning and after finishing the measurements.

3.2 Guildford

Despite the most critical conditions for air pollution exacerbation are represented by enclosed environments, also open road pollutant dispersion can be influenced by PCSs.

Due to its green residential and small business area, Guildford is the perfect urban environment to test the mitigation effects of different green infrastructures in disperse pollutant concentrations related to open road traffic emissions.

3.3.1 Site description

Being the focus in Guildford the evaluation of green infrastructure, the experimental campaigns focused in addressing three vegetation configurations: (i) trees, (ii) hedges, and (iii) mixed vegetation barrier with trees and shrubs. The aim of the campaign was to evaluate the air pollution reduction potentials of these three types of vegetation. Monitoring was carried out identifying 30 days of not-rainy conditions during the period 05/05/2017-15/09/2017, with the objective to conduct measurements in 3 complete days per week. Monitoring locations were selected based on the type of green infrastructure present near the highways. As detailed in Table 3, six sites were identified near major roads of Guildford town. On Table 3 the Leaf area index (LAI – a dimensionless metric of leaf area per unit ground area m^2/m^2) is also reported to classify the sites on a key parameter identifying the vegetation types. Guildford town is a highly populated area in Guildford Borough, which is a part of Surrey County (Surrey-i, 2015). Guildford Borough has a population of 137,183 (Surrey-i, 2015). The most popular mode of transportation is the car that includes about 72% of trips to work and 42% of commute to school (Al-Dabbous and Kumar, 2014). A map of monitoring locations is provided in Figure 12. In order to assess the impact of distance of green infrastructure from the road, we have selected two sites for each vegetation type. One of them is close to the traffic (≤1 m) and the other is away from the road (≥2 m). Figure 13 shows a schematic diagram of the monitoring sites. All monitoring sites had one sampling point behind the vegetation barrier. In half of the sites one measurement point was located at a clear area next to vegetation, equidistant from the road, and a second sampling point was behind the barrier (Figure 12, sites A, C, and E): in these cases, where the green infrastructure was close to the street (distance from edge of road <1 m) leaving no space for placing instruments, an abbreviation of “CB” is added to the site name (Table 3 and Figure 12). The remaining sites had the second measurement location in front of the vegetation barrier (Figure 12, sites B, D, and F). The combination of sampling points is thus specified in site names by an abbreviation of “CB – clear area and behind” and “IB- in front and behind”. In particular, the measurement sites include Aldershot-Hedge (Hedge only-H_{CB}) and Aldershot-Tree (Tree only-T_{CB}) sites that are along the same road, approximately 200m away from each other (Figure 12, sites A and C). Green infrastructure on Aldershot sites is close to the traffic emission. These sites are situated in a residential area with double story houses on either side of a two lanes road. Similarly, Sutherland-Tree (Tree only-T_{IB}) site and Sutherland-vegetation barrier (Tree with hedges -TH_{CB}) site are 100 m apart from each other and these are next to a recreational park near a two lanes road (Figure 12, sites 4 and 5). Vegetation in Sutherland sites is away from traffic emissions. Stoke road-Hedge site (Hedge only-H_{IB}) is near a children’s play area adjacent to a two lanes street and the hedge is away from the traffic emission (Figure 12, site 2). The vegetation barrier site at Shalford (Tree with hedges –TH_{IB}) is next to a public park and a busy two lanes traffic road is close to the barrier. Average traffic volume and direction of roads at each site were counted and are provided in Table 3. Dimensions of green infrastructure, distance from the edge of road to monitoring point, and width of lanes are depicted in Figure 12. Here, we are aiming to quantify the pollutant reduction potentials of different vegetation by comparing the concentration levels of clear area/ in front of vegetation and behind vegetation. Moreover, the statistical analysis of data collected during the campaign can give some insights on the impact of meteorology and vegetation characteristics on pollutant removal.

Figure 12: Map and picture of the six monitoring locations in Guildford, UK. 1. Aldershot-Hedge (H_{CB}), 2. Stoke park-hedge (H_{IB}), 3. Aldershot-Tree (T_{CB}), 4. Sutherland-Tree (T_{IB}), 5. Sutherland- vegetation barrier (TH_{IB}), 6. Shalford-vegetation barrier (TH_{CB}).

Site Name with vegetation type	Name of the road, number of lanes, width and direction of the road	Average hourly Traffic volume per hour	Vegetation type (species) LAI	Distance from road	Vegetation barrier attributes L: Length W: Width H: Height
1. Aldershot-Hedge: H_{CB}	A323 2 lanes ~ 7m E-W	750	Hawthorn, Ivy LAI= 6.64 m^2/m^2	1m	L = 36m W = 1m H = 1.2m
2. Stoke park-Hedge: H_{IB}	A320 2 lanes ~7m	1200	Horn beam (*Fagus sylvatica*) or beach (*Carpinus betulus*) LAI=4.47 m^2/m^2	2m	L = 36m W = 1.2m H = 2m
3. Aldershot-Tree: T_{CB}	A323 2 lanes ~ 7m E-W	750	common lime (*Tilia* x *europaea)* LAI=4.25 m^2/m^2	1m	L = 40m W = 6m H = 10m
4. Sutherland-Tree: T_{IB}	A3100 2lanes ~7m NW-SE	1650	Acer, poplar, cherry birds' eye LAI=4.63 m^2/m^2	3m	L = 50m W = 9m H = 7m
5. Sutherland-Vegetation barrier: TH_{IB}	A3100 2 lanes ~7m NW-SE	1650	Hawthorn, ivy and common ash Trees: LAI=1.54m^2/m^2 overall LAI= 3.4 m^2	3m	L = 40m W = 7m H= 5m
6. Shalford-Vegetation barrier: TH_{CB}	A281 2 lanes ~ 7m N-S	1200	London plane, pine and hedge LAI= 4.07 m^2/m^2	1m	L = 66 m W = 3.5 m H = 4 m

Table 3: Details of the six monitoring locations in Guildford, UK. LAI is measured by hand held ceptometer Accu-PAR LP80.

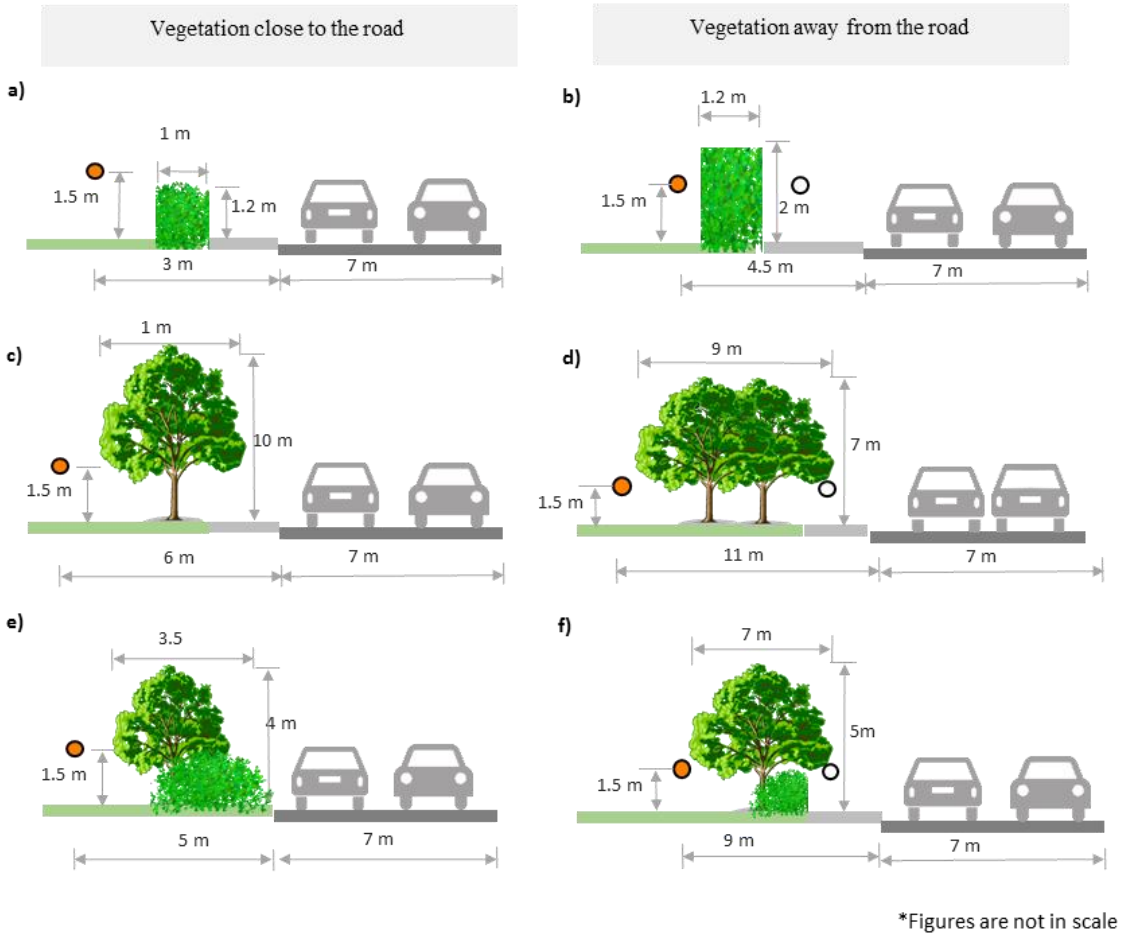

Figure 13: Schematic representations of the six monitoring locations along with the type of vegetation and road details in Guildford, UK. The orange circle and black ring denote measurement point behind and in front of the vegetation barrier, respectively.

3.3.2 Instrumental setup

In this work, we have monitored PM_1, $PM_{2.5}$, PM_{10}, particle number concentration (PNC), black carbon (BC) and carbon monoxide (CO). Two GRIMM aerosol monitors, model EDM 107 and 11-C measured PM_1, $PM_{2.5}$, and PM_{10}. The instrument provides particulate matter concentrations on 31 different channels at 6 seconds time resolution. In addition, particles collected on PTFE filters inside the GRIMM monitor can be used for chemical and morphological characterization. Two PTRAK 8525 (TSI Inc.) are employed to measure PNC in the size range of 0.2 to 1 µm. In this study, we set PTRAK to record PNC values every 6 seconds. BC concentrations were collected using a couple of MicroAeth AE51 (Aeth Labs) with time averaging period of 10 seconds. Attenuation generated due to instrumental optical and electronic noise is rectified by post processing the data with Optimized Noise-reduction Averaging algorithm (ONA; Hagler, et al. 2011). CO and CO_2 are monitored in ppm with two QTRAK 7575 (TSI Inc.) having time base of 6 seconds. Local meteorological conditions (air temperature, relative humidity and wind speed and direction) are logged by a portable weather station (Kestrel 4500) at 1-min resolution. All instrument data is averaged to 1 minute to match with the wind data. Traffic counting is performed by using the SMART Traffic Counter App developed by University of Wollongong, Australia. LAI

(LAI – a dimensionless metric of leaf area per unit ground area m^2/m^2) is estimated from changes photosynthetically active radiation passes through overlaying foliage by hand held ceptometer Accu-PAR LP80.

3.3.3 Experimental protocol and quality check

One set of instruments (including GRIMM, PTRAK, QTRAK, and MicroAeth) is mounted on a tripod stand at a typical breathing height of about 1.5 m. Three monitoring sites, namely A, C, and F, present a clear area (without any disturbance to air flow) adjacent to the green infrastructure. At the other sites, i.e., 2, 4, and E, the green intervention is continued leaving no clear area (without any vegetation) along the same road. Because of this, one of the instrument setups was placed in the clear area and the remaining one is positioned behind the green infrastructure on sites A, C, and F. Both tripods are located equidistant from the road. On the other hand, at sites B, D, and E, tripods are held in front and behind the vegetation. The portable weather station is always attached to the tripod in the clear area or in front of the vegetation. The campaign is designed to conduct 5 days of monitoring per site, making a total of 30 days. The field measurement is started and ended around 08.00 and 18.00 (local time), respectively. This enables to collect 8 to 10 hours of data every day. Inter calibration between each set of instruments is achieved by running instruments side by side for 20 to 30 min prior the beginning and after finishing the measurements as shown in Figure 14. No field measurements were carried out on rainy days. Traffic is counted in the first 20 minutes of an hour.

Figure 14: Instruments are mounted on tripod and kept close to each other during inter-calibration. In the figure, 1) GRIMM aerosol spectrometer, 2) PTRAK 8525, 3) QTRAK 7575, 4) MicroAeth AE51, 5) weather station Kestrel 4500.

Various air pollutants concentrations were monitored using two sets portable near reference instruments such as microAeth AE51 and AE51, GRIMM 107 and 11-C, and P-TRAK 8525. All instruments performed a calibration period. One set of instruments was new and recently calibrated, and these were taken as 'reference'. To assess the accuracy of pollutant concentrations estimates among similar instruments, we implemented the following quality control activity. Both sets of monitors were kept side by side for at least 30 minutes prior to and after finishing the air pollution measurements. Some of the days, this check was performed in the middle of monitoring. This co-location of instruments enabled the simultaneous collection of air pollution concentration data for more than 10% of total field measurement data available. This enabled inter comparison between two similar instruments and the finding of relative differences. Similar inter-comparison method was performed in previous studies (Lin et al. 2016; Brantley et al., 2014). All instruments sets performed well and obtained good agreement on estimating concentration levels (Figure 15). As shown in Figure 15, we obtained a minimum R^2 value of 0.85 for BC measurements by microAeths. GRIMMs showed an inter-relation in estimates with R^2 values of 0.87, 0.93, and 0.88 for PM_{10}, $PM_{2.5}$ and PM_1, respectively. The highest R^2 value of 0.97 was found between P-TRAKs. Notwithstanding the general good agreement, a slight underestimate by one of the instruments in all sets was identified. In order to remove this

discrepancy, we corrected data obtained from one of the instruments using the derived equation from the scatter plot. This relation accounts for various factors affecting pollutant estimates by monitors such as different field measurement conditions, various possible meteorological situations like high and low temperature and humidity. This quality control procedure ensured and validated the detection of pollutant concentration changes between the two monitoring points at each monitoring site.

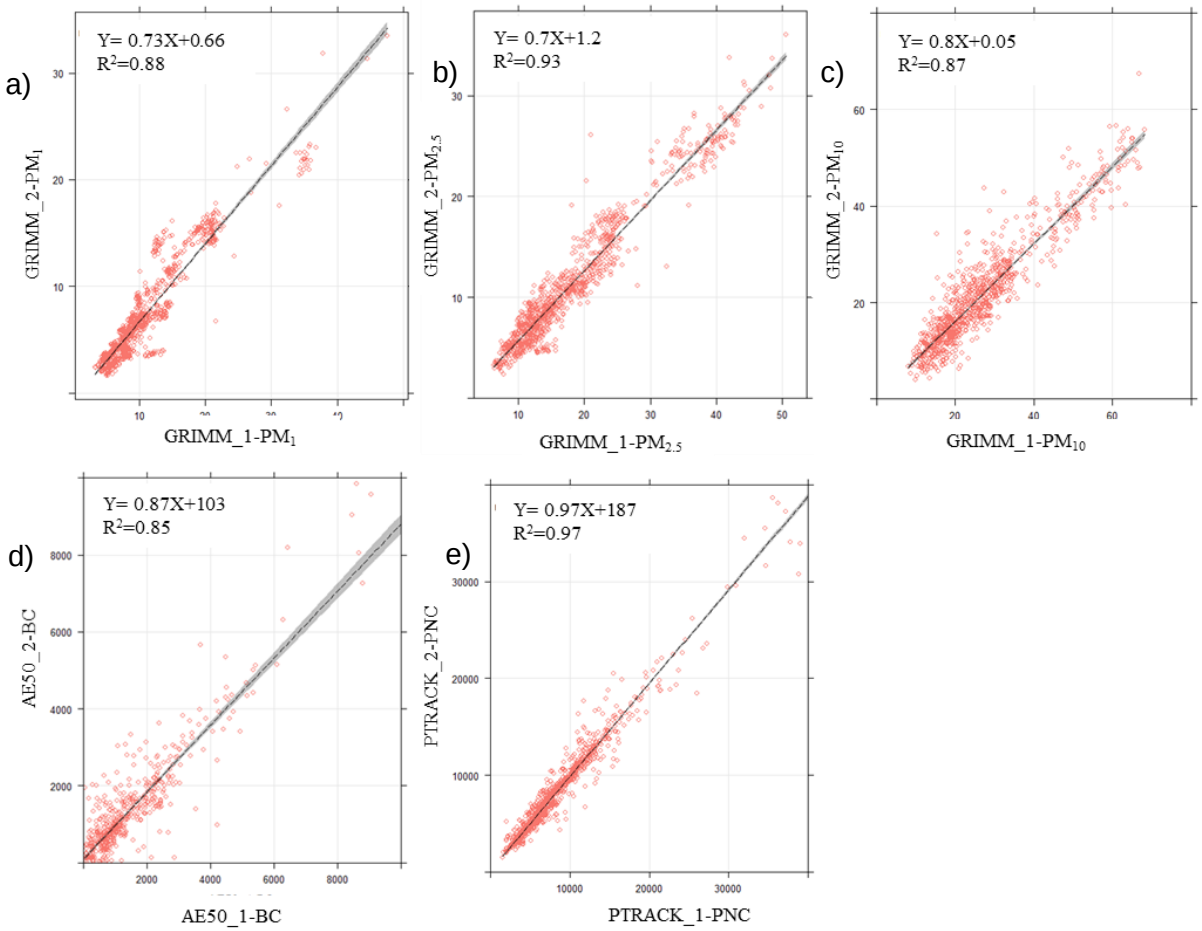

Figure 15: Scatterplots of one instrument vs. the other measuring same pollutant. a) PM_1 measurements by GRIMM 11-C on x axis and GRIMM 107 on y axis, b) $PM_{2.5}$ by GRIMM 11-C on x axis and GRIMM 107 on y axis, c) PM_{10} by GRIMM 11-C on x axis and GRIMM 107 on y axis, d) BC measurements by microAeth AE51, e) PNC measurements by P-TRAK

3.3 Vantaa

The development of green infrastructures embedded on high stores buildings can help both in terms of air pollution mitigation and thermal regulation, enhancing the citizen comfort. It could influence different sources of pollution not necessarily related with vehicular traffic, which is the main focus of the other cities campaigns. The city of Vantaa was chosen as test case due to the mutual presence of different pollutant sources such as the international airport and the location in the Metropolitan Area of Helsinki.

3.4.1 Site description

The Vantaa experimental setup consists of two sites in the proximity of each other. Figure 16 shows their location on a map. The first experiment site, Malminiitty, started the monitoring of meteorological variables in April 2018, and lies at the southwest edge of a conglomeration of 20 up to 8 stories high buildings. The site is surrounded by areas of detached houses. The PCS is located in a yard of four 6-storey houses.

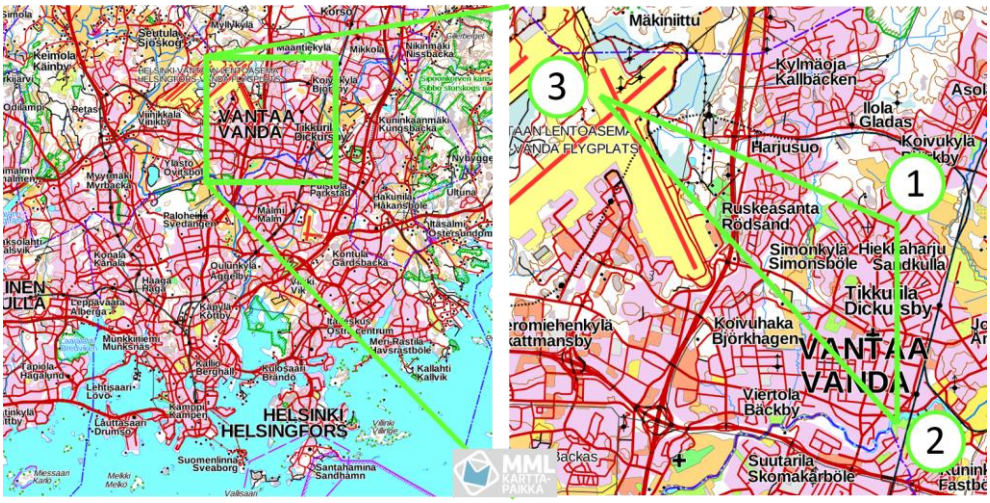

Figure 16: The iSCAPE – Vantaa monitoring stations on a map: 1 = Malminiitty, 2 = Heureka, 3 = Helsinki-Vantaa airport (meteorological reference station)

The courtyard consists of a 1000 square meter green area with a playground for children and 8 different trees and bushes. Some of the trees reach the top of the buildings. This experiment site represents a typical multi-story building Finnish neighborhood. The second site is located at the Finnish Science Center Heureka (https://www.heureka.fi/?lang=en) out-door area Galileo, mounted on a 20-meter-high mast, and there the monitoring of meteorological variables started in May 2017.

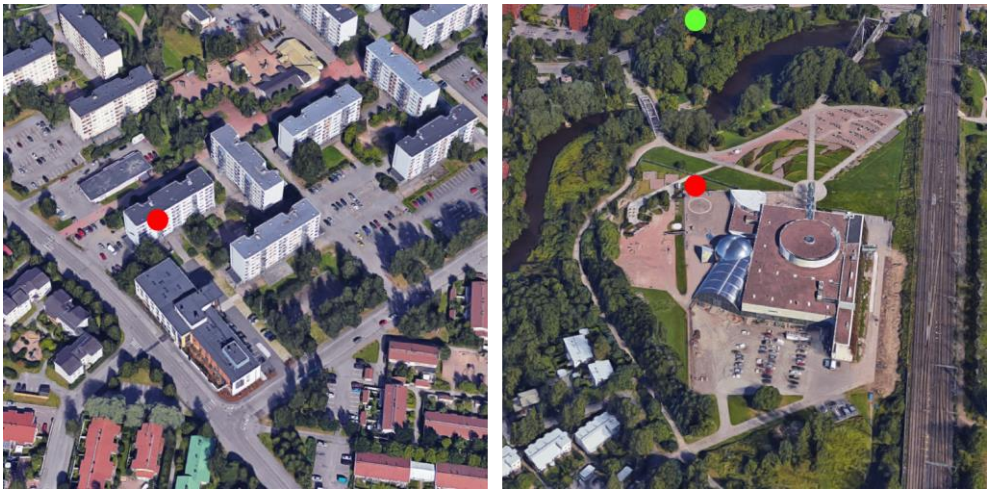

Figure 17: Aerial view of the two monitoring stations: Malminiitty (left) and Heureka (right). Red dots indicate the locations of the instruments, green dot indicates the location of the HSY air pollution monitoring station (source: Google Maps)

The immediate surroundings consist of sand and lawn. The river Kerava flows 50 meters in the north to west. On the riverbank and in the southwest of the experiment site there are deciduous and coniferous trees up to 15 meters height. Beyond the trees, in the southwest, there is an area of detached houses. The next stone multi-story buildings located in north to west are 120 to 150 meters away. The only disturbing building in the proximity is the science center building itself 20 meters to the southeast. Beyond this building lies the one of the Finnish main railroads. The experiment site can be considered as an open space park landscape functioning as PCS. The second experiment site is located 2.8 kilometers in the south of the Malminiitty monitoring station. Figure 17 shows the aerial views of both monitoring stations. The densely build-up area of Tikkurila, one of the two mail centers of the City of Vantaa, lies in between the two sites.

3.4.2 Instrumental setup

Both sites are equipped with the same instruments (Figure 18). A CNR4 Kipp&Zonen net-radiometer measures the four energy radiation components, the incoming short-wave radiation from the sun, the reflected short-wave radiation from buildings, the ground and other obstacles, the incoming long-wave radiation from the atmosphere, and the out-going long-wave radiation from buildings, the ground, and other obstacles. Wind speed and direction, rain intensity and duration, and air pressure are measured with a Vaisala WXT weather sensor (WXT536). Additionally, air temperature and humidity are measured with thermo-hygrometer sensors according to the standards of the Finnish Meteorological Institute (FMI).

Figure 18: The iSCAPE Malminiitty monitoring station instrumental setup (from left to right): Kipp&Zonen, CNR 4 net-radiation meter; Vaisala Weather sensor WXT536; FMI standard equipment for air temperature and humidity measurements (all photos by Achim Drebs)

All instruments are tested and approved for scientific use. At Malminiitty all instruments are mounted at the height of 20 meters on an edge of the outlying balcony to the southeast. The instruments are at least 2 meters away from the wall of the building (Figure 18). At the science center, the net-radiometer and the weather sensor are mounted according to World Meteorological Organization recommendation to the south at the height of 10 meters. Due to the uneven ground, air temperature and humidity are measured at the height of 3 meters (Figure 19). All instruments record their observations every second in real-time to the FMI database. The meteorological data is available for free upon request from the FMI.

Figure 19: The iSCAPE Heureka monitoring station instrumental setup (from left to right): FMI standard equipment for air temperature and humidity measurements; the FMI mounting team and iSCAPE researchers at the time of the installation; the observation mast with the Kipp&Zonen, CNR 4 net-radiation meter and Vaisala Weather sensor WXT536 at 10 m height (all photos by Achim Drebs)

To monitor the quality of the observation data the results were compared on a random basis with the observation of the nearest-by official synoptic weather station of the FMI located at the Helsinki-Vantaa airport. For the air pollution measurements, there is a near-by HSY (https://www.hsy.fi/en/residents/pages/default.aspx) official measuring station in Tikkurila, almost 150 meter close to the science center.

Figure 20: The Helsinki Region Environmental Services Authority (HSY) air pollution and environmental monitoring station at Tikkurila, 150 meter north of the science center Heureka, attention: not all sensors were mounted at the time of this picture, see also Figure 17; (all photos by Achim Drebs, 2015)

At this monitoring station, among others, the concentrations of nitrogen dioxide, particles of different sizes and black carbon are measured. The Tikkurila air pollution station belongs to a

network of seven permanent and four temporal stations in the Helsinki metropolitan area (Figure 21).

Figure 21: HSY air pollution station network

3.4.3 Experimental protocol and quality check

The use of the same instrumental setup at two experimental sites enabled for cross-comparison of the data collected at the two sites. As for the meteorological observations, it was assumed that the differences between the two sites in the overall averages were negligible. However, in the case of single meteorological parameters like different cloudiness, heavy rain, and strong wind conditions, the differences should be perceptible. All these events need to be cross-checked with the official FMI weather observations. Furthermore, the meteorological observations were compared with modelled results for selected areas in Heureka, Tikkurila, and Malminiitty.

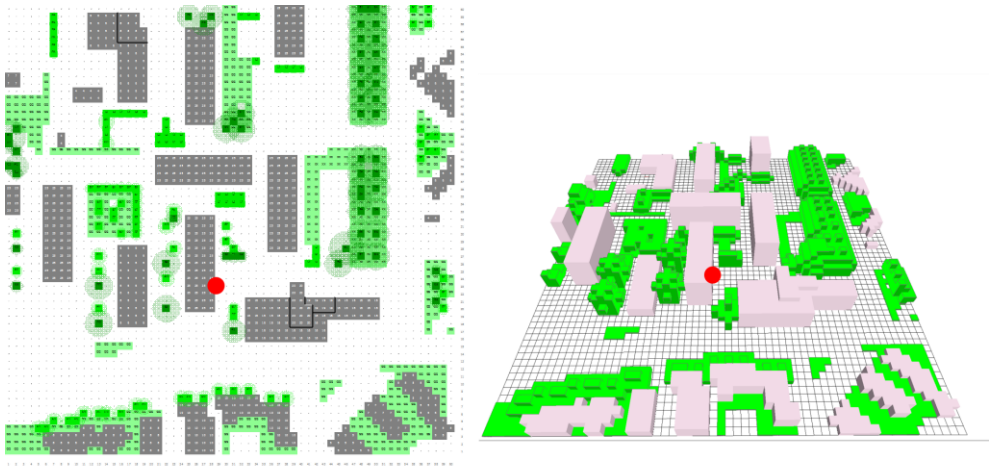

Figure 22: iSCAPE Malminiitty built-up area, left 2-D model, right 3-D model, red dot: iSCAPE – monitoring stations (models by Achim Drebs and ENVI-met v4)

The meteorological and air pollution data were used as an input into the ENVI-met simulation software (http://www.envi-met.com). ENVI-met v4 is a holistic three-dimensional non-hydro static model for simulations of surface-plant-air interactions with a horizontal resolution from 0.5 to 5 meters (Huttner and Bruse, 2009). Simulation runs were executed for the surroundings of the two iSCAPE - monitoring station Malminiitty (Figure 22) and Heureka (Figure 23).

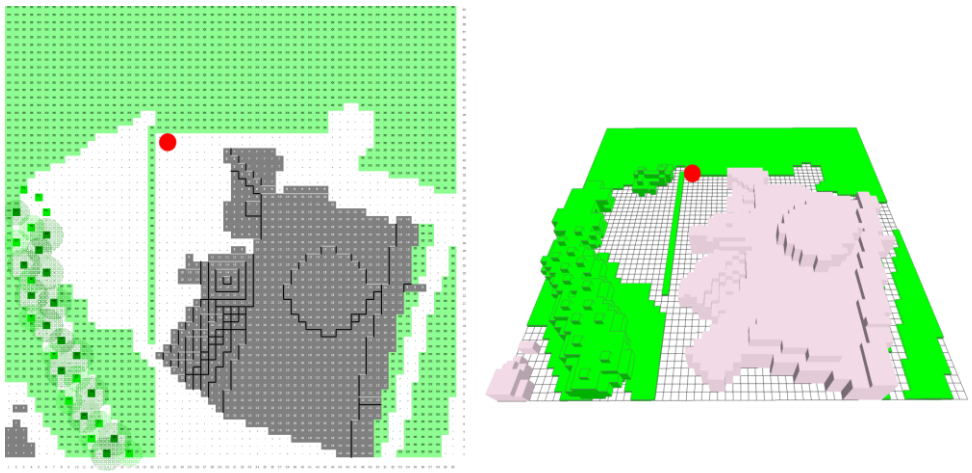

Figure 23: iSCAPE Heureka open area, left 2-D model, right 3-D model, red dot: iSCAPE – monitoring stations (models by Achim Drebs and ENVI-met v4).

During three Heureka summer camp weeks in July/August 2018 a thermal sensation questionnaire was carried out to find out about the children impressions of their environmental surroundings. One day during these weeks with more or less clear sky conditions was chosen for the questionnaire. The questionnaire was executed twice during this day. The data has not been analyzed yet; results will be presented in the updated version of this Deliverable.

4 Environmental impact data

Section 3 described the setup of the various campaigns within the project in terms of site description, instrumentations setup and protocol of usage, as well as the data quality check to ensure the reliability of results. All this information defines the baseline to understand the analysis of collected data under the monitoring campaigns reported in the current section. Air pollution data are strongly influenced by the environmental conditions: once the site morphology is set, the analysis of meteorological data is crucial to define transport and dispersion phenomena related to pollutant, as well as to identify the most suitable conditions where PCSs might have a mitigating impact. Therefore, in the current section, a detailed analysis of environmental (meteorological and air pollution) results obtained so far is reported and described for each pilot city.

4.2 Bologna

4.1.1 Meteorological and turbulence variables

Local scales atmospheric processes are the main forcing of pollutant dispersion in complex terrain. Thermal and inertial circulations dominate air flows when synoptic conditions are weak (commonly referred as geostrophic wind velocity U_g < 5 m/s). Under these conditions, local scales gradients are the key driver of air flow and the morphology of the terrain is fundamental in inducing these gradients or channeling the flow itself. In this context a city can be schematize as a heterogeneous array of buildings which interacts with the main atmospheric flows, directing them, driving the formation of stagnation zones, channeled flows, rotors, recirculation, wake motions. All these atmospheric phenomena present turbulent features, depending on how the flow interacts with obstacles, the morphology of the canopy and the spatial scale. Moreover, the thermal properties of city obstacles can induce heat gradient at different scales: thermal gradient can be generated between different areas of the same city depending on the neighborhood type, the presence of parks or densely built-up areas; in turn, thermal gradients can develop also inside the same street following the different insolation of buildings at each side during the day.

Inside a street canyon, thermal circulation induced by differential insolation during the day, and inertial circulation driven by air entrainment from flow overpassing the canyon and horizontal cross sections, are the only conditions to break stagnation during no-synoptic conditions (which is the focus of the current analysis since this is the most common situation developing in the Po Valley). As a consequence, after a general statistical framework and an overview of the whole campaigns, in the following, only short period analysis is reported when concerning meteorological variables.

The following Tables present the descriptive statistics for meteorological variables (wind speed and temperature, while the comparison for relative humidity is not presented for the whole campaigns due to problems with the ARPA-ER instrumentation in Laura Bassi St.) collected at the two urban street canyons during the two experimental campaigns, along with statistical differences between the two sites.

	site	Num cases	mean	Std. dev	min	max	sig diff
ws ($m\ s^{-1}$)	Marconi St.	41119	1.2	0.8	0.2	5.8	a
	Laura Bassi St.	35309	0.4	0.2	0.1	2.5	b
T (°C)	Marconi St.	53908	22.1	4.8	12.7	35.4	a
	Laura Bassi St.	54763	21.6	5.4	11.8	38.5	b

Table 4: Descriptive statistics and significant differences of meteorological variables (ws = wind speed; T = temperature) measured within the summer experimental campaign in Bologna. For each variable, equal letters in last column indicate the absence of significant differences.

	site	Num cases	mean	Std. dev	min	max	sig diff
ws ($m\ s^{-1}$)	Marconi St.	38705	0.9	0.6	0.2	5.7	a
	Laura Bassi St.	35118	0.4	0.3	0.1	3.3	b
T (°C)	Marconi St.	43189	6.7	2.5	0.7	14	a
	Laura Bassi St.	41639	5.9	3.1	-0.7	16	b

Table 5: Same as Table 4 but for the winter campaign.

The Tables show very clearly that at Laura Bassi St. winds were lower than at Marconi St. during both experimental campaigns. This observation can be closely linked with the presence of vegetation. The comparison for temperature shows more limited differences especially in summer, while in winter lower temperatures are observed in Laura Bassi St.; however, temperatures will be analyzed with more details in the following.

The following boxplots make even clearer the result of the comparison between the two canyons as regards meteorological variables.

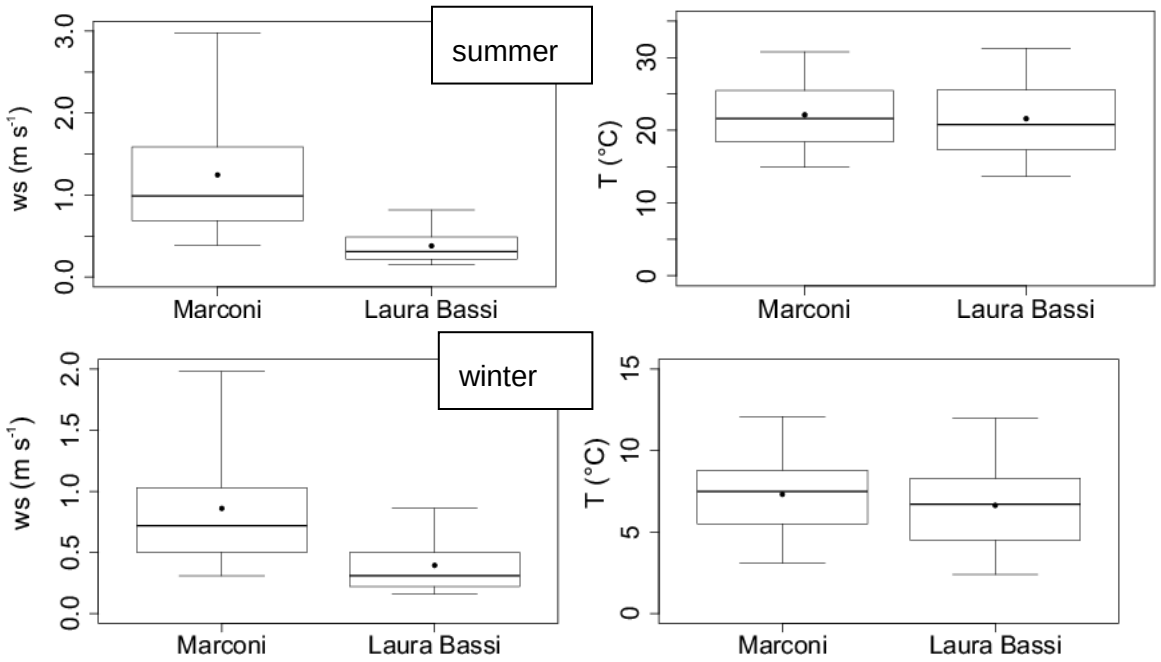

Figure 24: Boxplots depicting the fundamental statistical parameters for meteorological variables (wind speed and temperature) observed within the two street canyons during the summer and winter experimental campaigns in Bologna. The boxes enclose the 25-75th percentile values, the whiskers represent the 5-95th percentile values; the horizontal line inside the box represents the median, while the square represents the mean value.

To understand flow and turbulence behaviors inside the canyon it is crucial to know how the mean flow behaves above the canyon. For the purpose of illustrating features of meteorology during summer and winter campaigns, a few consecutive days were selected and are discussed in the following. Figure 25 shows the main atmospheric properties descending from a synoptic scale down to the rooftop level measurements inside the urban boundary layer.

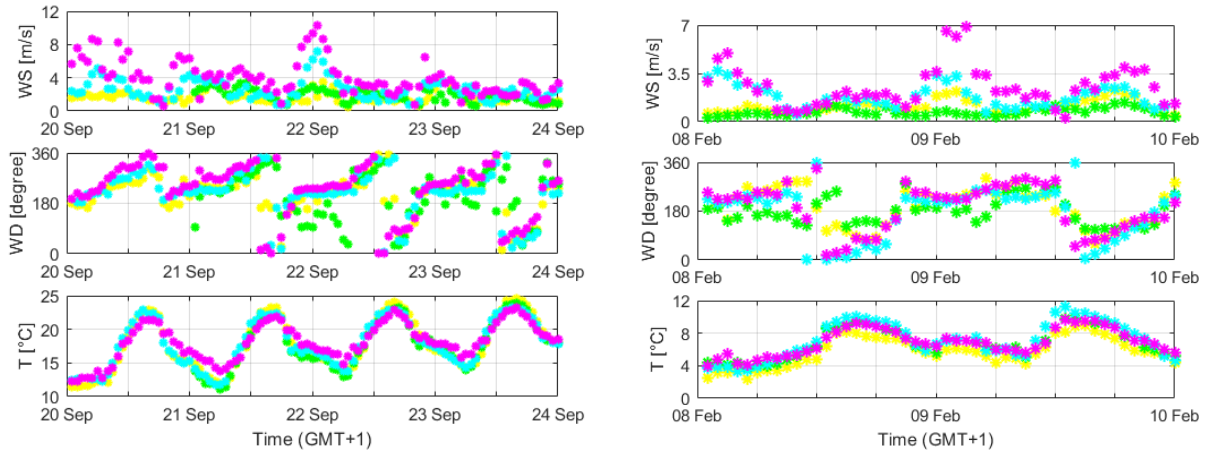

Figure 25: 1-hour averaged wind speed (top), wind direction (middle), and temperature (bottom). Colors indicate the different measurement sites: Marconi St. (yellow) and Laura Bassi St. (green), Asinelli Tower (purple), Silvani St. (cyan). Summer campaign on the left, winter on the right.

During summer, temperature signals show a typical diurnal behavior, reaching maximum values around 15:00-16:00 and a strong nighttime inversion (up to 5 °C between the tower and the rooftop levels). Wind velocity is quite flat in time, apart from the intense maximum during late evening early night on September 22nd, whose nature could depend on low-level jet behavior of the boundary layer flow or induced by an over imposed passage of a synoptic wind. Finally, wind directions are typical of a thermal circulation developing at the valley scale. They show a well-defined katabatic flow along the canyon direction during the nighttime and a continuous wind rotation during daytime, with a predominance of anabatic conditions.

Winter conditions are almost similar to the summer ones as for wind velocity and directions. On the other hand, the temperature is almost homogeneous at the rooftop level of the city, with flattened differences with respect to those depicted during summertime. These observations are caused by multiple reasons: first of all, during winter boundary layer stable or neutral conditions are predominant with respect to the convective one. Therefore, horizontal advection of atmospheric quantities, especially scalars, is such that the city scale presents a homogeneous pattern, with reduced differences between different neighborhoods. Moreover, the impact of trees on air temperature is weaker than during summer since vegetation is leafless and the shadow effect is only provided by branches and trunks. Definitively, considering only the atmospheric heat storage and release above the canopy layer, a vegetated street behaves similarly to a green area only during summertime, while during wintertime no differences with a central urban area have been detected.

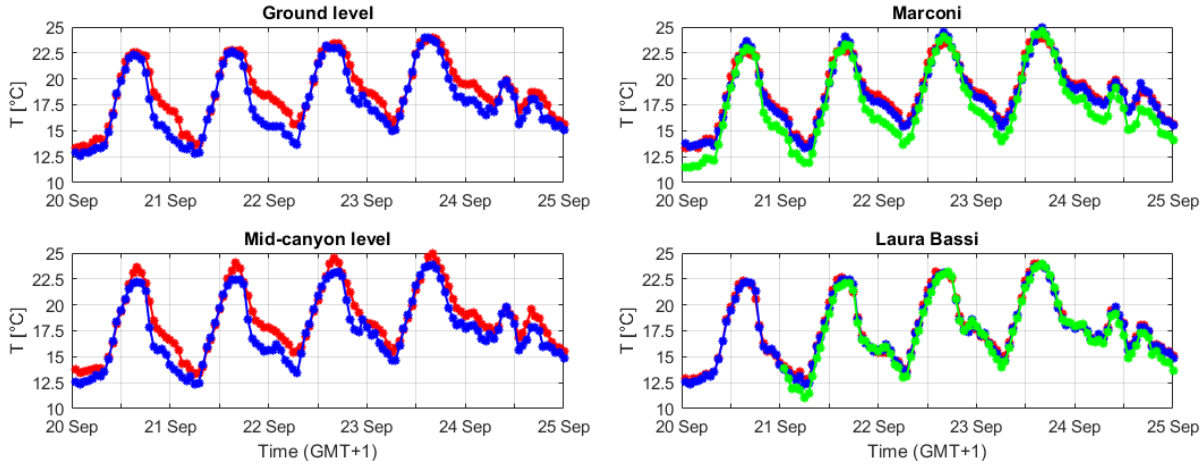

Figure 26: 1-hour averaged temperature in the street canyon during summer. On the left: data comparison between stations at the same level inside the canyons (red line – Marconi St., blue line - Laura Bassi St.). On the right: vertical structure of the signal time series in each street canyon (red line – ground level, blue line – mid-canyon level, green line – rooftop level).

As expected, temperatures inside the canyons are homogeneous since mixing conditions are dominant in a closed environment like these. During summertime, the strong heating generates a vertical mixing whose vertical extension is enough to include the rooftop level of each canyon, which in turn is well coupled with the temperatures inside them. During night the coupling weakens in Marconi St. since the heat release of the building let the in-canyon temperature preserve higher values with respect to the rooftop where, especially in clear sky conditions, thermal radiation is lost directly into the free atmosphere (Figure 26 on the right). This phenomenon enhances the thermal discomfort at pedestrian levels in the very core of the city center due to the heat trapping

produced by the canopy morphology. On the other hand, Laura Bassi St. shows a full homogeneity during the whole period, without distinctions during day or night times. The reason could be attributed to the morphology of the neighborhood. Being a residential area mostly composed by single and isolated houses or buildings, the canyon is not as occluded to lateral air entrainment as Marconi St. Moreover, the canyon aspect ratio is greater than 1 (meaning a wider than higher canyon), therefore mass, momentum and energy exchanges between the canopy and the atmosphere above are more efficient with respect to Marconi St., increasing the mixing layer. Another factor that can impact on the temperature profile is the vegetation. During daytime, the shadowing effect of the tree-crowns reduces the heat storage of the street and the buildings; this effect cannot be observed during the day, when solar heating is the main factor which impacts on the temperature at city scale. During night instead, the building heat release is less intense due to the reduced storage during the sunny hours. Moreover, thermal trapping is also inhibited by the favorable aspect ratio of the street, and by the evapotranspiration processes of the vegetated compounds (trees and front yards above all). The result is a thermal homogeneity in the whole canyon.

During winter the homogeneity within the canyons is preserved, but at the rooftop levels the signal is decoupled, especially in Marconi St. (Figure 27 on the right). In fact, despite the lower temperatures typical of the winter season, the heat storage and release processes by the buildings and the stagnation or recirculation of air within the canyon preserve the mixed condition already observed during summer. On the other hand, the strength of convective processes is less effective and does not directly involve the boundary layer above the canopy, where thermal stratification plays a role in regulating air temperature. In this condition, signals above and within the canyon show a similar shape and gradient (at least during daytime) but a bias arises since the thermal forcing of the buildings is limited (or stronger) inside the canyon.

Nevertheless, Laura Bassi St. maintains a clear homogeneity in the signals inside and above the canyon. This feature is probably due to the different location of the sensor with respect to the summer campaign. While during summer the rooftop station was located on one of the tallest building of the street while for logistic reasons during winter the sensor location was moved to a below mean building height edifice. Therefore, it is likely that the rooftop level in Laura Bassi St. behaved more like one in-canyon station during winter.

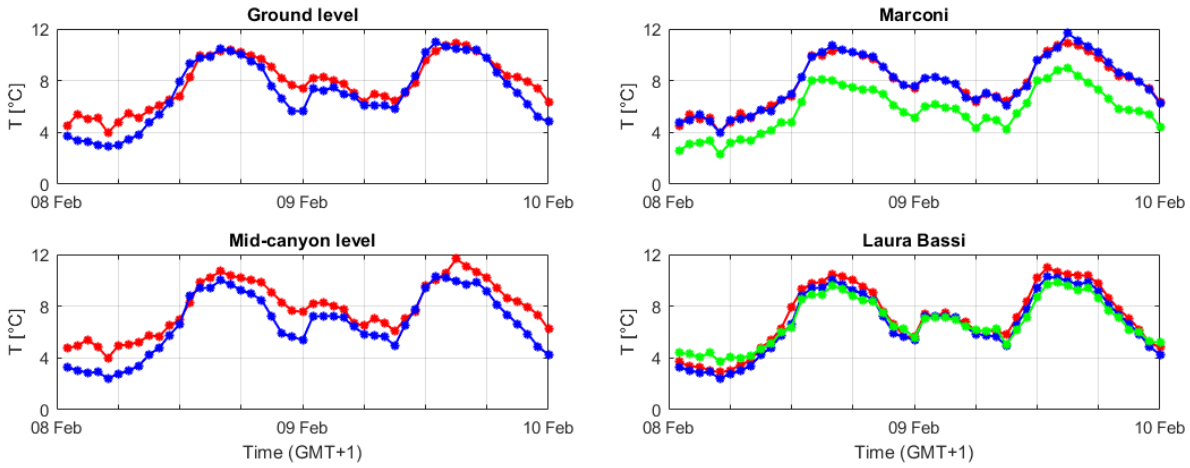

Figure 27: 1-hour averaged temperature in the street canyon during winter. On the left: data comparison between stations at the same level inside the canyons (red line – Marconi St., blue line - Laura Bassi St.). On the right: vertical structure of the signal time series in each street canyon (red line – ground level, blue line – mid-canyon level, green line – rooftop level).

Differences between the two canyons are also observed during both seasons (Figure 26 and Figure 27 on the left). During summer daytimes the effect of the solar radiation dominates the signals in both canyons: the time gradient of temperature from sunrise to sunset is almost the same in all the four stations, neutralizing the geometric and vegetative differences of the canyons. During nighttime, the same differences play a key role in determining a within-the-city UHI effect with a maximum intensity of about 2 °C. This phenomenon will be extensively analyzed in the following in a dedicated paragraph, where the buildings thermal forcing on air temperature and thermal circulation is also assessed.

During winter, solar radiation is not strong enough to drive daytime temperature homogeneity and canyon signals show quite different shapes and tendency across various heights. Temperature maxima are equal in both canyons, but local features strongly affect the signals. The thermal forcing of the buildings, strengthened by residential heating, smooths the signals much more at Marconi St. than at Laura Bassi St., which shows the more efficient effect of building packaging than of the shadowing of crownless trees. Nighttime UHI effect is still present with similar intensities to the summer season. In conclusion, the thermal properties of a neighborhood are strongly affected by its morphology, the canyon geometry and the vegetation amount within it.

Vertical kinematic fluxes are the main quantities governing the local dynamics and energetic behavior of circulation within a street canyon, both in presence or in absence of vegetation. Especially in the absence of synoptic conditions, they are also responsible for the exchanges between the canopy and the atmosphere above, regulating the inflow of fresh air and the outflow of the polluted one. They are therefore the main vehicle for pollutant transport and removal from a street canyon (Salizzoni et al., 2011). The major regulator of air exchanges is the fluxes behavior at rooftop levels, driving the circulation within the canopy, which in turn is affected by the geometry of the canyon and the presence of obstacles. In particular, momentum fluxes are responsible for inducing and sustaining the inertial circulation within the canyon while the heat fluxes have an impact on the thermal aspects and induced dynamics. In a real environment, both aspects contribute to the local transport of pollutants (Dallman et al., 2014).

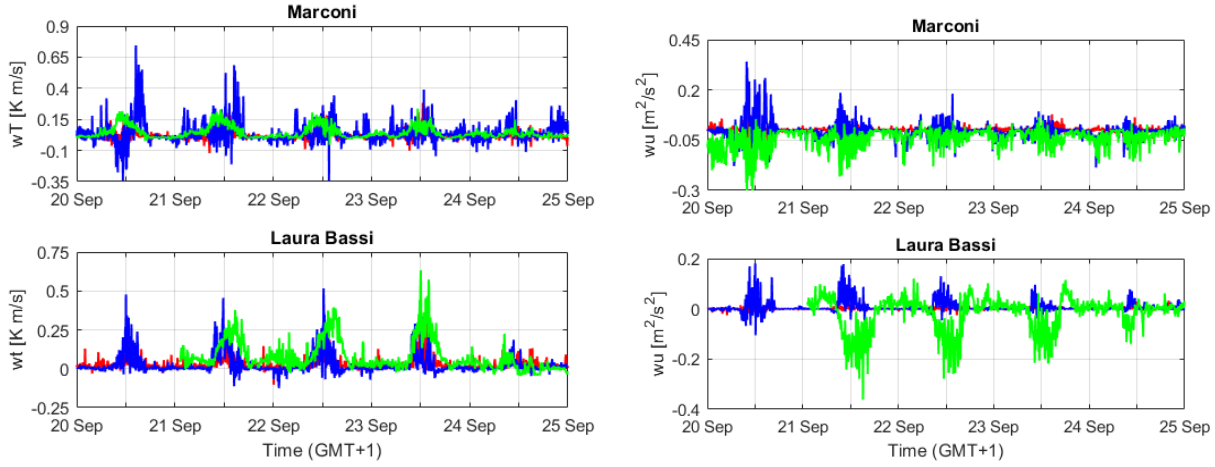

Figure 28: 5-minutes averaged kinematic vertical heat (on the left) and momentum (on the right) fluxes for the summer campaign computed at all three levels of each canyon (red line – ground level, blue line – mid-canyon level, green line – rooftop level).

Figure 28 and Figure 29 show the behavior of mechanical and thermal fluxes in and above the studied canyons. In general, fluxes are stronger at rooftop levels than inside the canyons since

they drive the turbulent structures. Inside the canyons, instead, the vicinity to the buildings can impact on measurements by adding extra turbulence: in particular, mechanical turbulence increases due to the façade drag, while the thermal forcing enhances the heat generated turbulence.

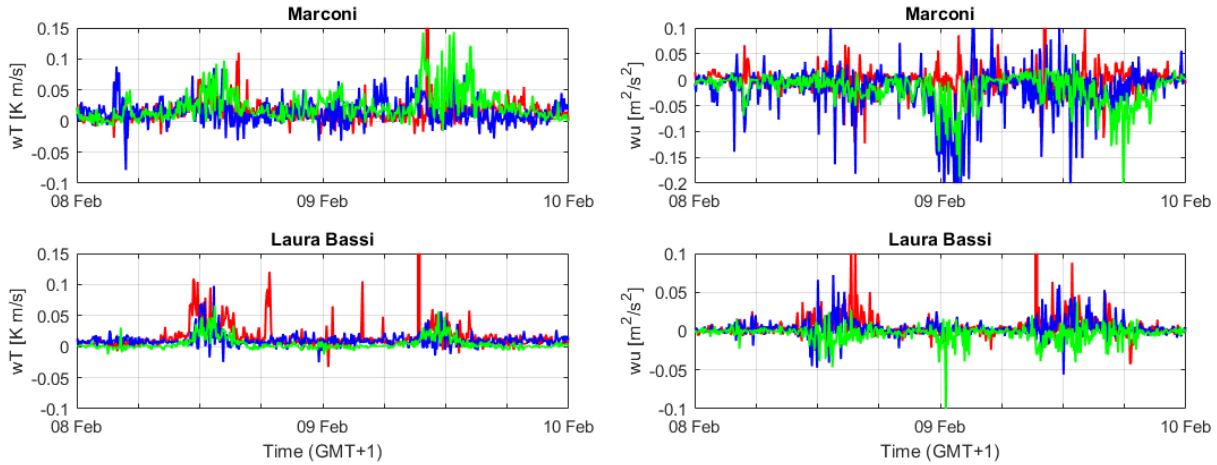

Figure 29: 5-minutes averaged kinematic vertical heat (on the left) and momentum (on the right) fluxes for the winter campaign computed at all three levels of each canyon (red line – ground level, blue line – mid-canyon level, green line – rooftop level).

Again, a general homogeneous structure appears within the canyon also in terms of fluxes. The major seasonal and between canyons differences concern the intensities of the turbulence, both considering thermal and mechanical factors. Seasonal differences are trivial: the more is the energy gained by the atmosphere and the more is the intensity of the turbulence. Slight differences arise also comparing the two canyons. During daytime, the streets behave similarly both in terms of momentum and heat fluxes. The main differences appear during night when Marconi St. benefits from additional turbulence sources, again mainly related to the thermal forcing of facades.

4.1.2 Air pollution

The following Table presents the descriptive statistics for air pollution levels measured at the two urban street canyons during the two experimental campaigns, along with statistical differences between the two sites.

	site	Num cases	mean	Std. dev	min	max	sig diff
NO_x ($\mu g\ m^{-3}$)	Marconi St.	53908	98	95	2.6	1210	a
	Laura Bassi St.	54766	40	38	6.2	768	b
NO ($\mu g\ m^{-3}$)	Marconi St.	53908	29	42	0.3	642	a
	Laura Bassi St.	54701	10	15	0.8	383	b
NO_2 ($\mu g\ m^{-3}$)	Marconi St.	53908	53	38	0.0	526	a
	Laura Bassi St.	54765	25	17	0.5	263	b
NO_2/NO	Marconi St.	53046	0.4	0.3	0.0	28	a
	Laura Bassi St.	53884	0.3	0.2	0.0	8	b
CO ($mg\ m^{-3}$)	Marconi St.	53046	0.4	0.3	0.0	28	a
	Laura Bassi St.	53884	0.3	0.2	0.0	7.5	b
O_3 ($\mu g\ m^{-3}$)	Marconi St.	52919	52	30	2.3	799	a
	Laura Bassi St.	54280	57	33	0.0	168	b
PM_{10} ($\mu g\ m^{-3}$)	Marconi St.	36	19	7	5.0	33	a
	Laura Bassi St.	46	16	6	5.0	28	ab
	Porta S. Felice	47	16	6	4.0	29	b
	Giardini Margherita	44	14	5	2.0	29	b
$PM_{2.5}$ ($\mu g\ m^{-3}$)	Marconi St.	38	8.7	2.8	3.0	14	a
	Laura Bassi St.	46	8.9	3.9	2.0	18	a
	Porta S. Felice	49	8.8	2.9	3.0	17	a
	Giardini Margherita	42	8.9	4.4	1.0	17	a
$PM_{10}/PM_{2.5}$	Marconi St.	35	2.2	0.5	1.3	3.4	a
	Laura Bassi St.	46	2.0	0.6	1.1	3.7	a
	Porta S. Felice	47	1.8	0.3	1.3	2.4	a
	Giardini Margherita	40	2.1	1.3	1.0	7.0	a
Benz ($\mu g\ m^{-3}$)	Marconi St.	871	1.1	0.9	0.2	6.2	a
	Porta S. Felice	1042	0.8	0.5	0.1	4.2	b
Tol ($\mu g\ m^{-3}$)	Marconi St.	866	6.7	6.7	0.9	102	a
	Porta S. Felice	1039	3.2	2.7	0.4	29	b
EthylBenz ($\mu g\ m^{-3}$)	Marconi St.	866	1.1	0.9	0.2	6.2	a
	San Felice	1039	0.5	0.4	0.1	4.0	b
Xyl ($\mu g\ m^{-3}$)	Marconi St.	866	6.0	4.9	0.9	33	a
	Porta S. Felice	1032	1.6	1.2	0.1	15	b

Table 6: Descriptive statistics and significant differences of air pollution pollutants measured within the summer experimental campaign in Bologna. Particulate matter and BTX levels are compared also against values measured at the ARPA-ER fixed air pollution stations, sampling with the same time resolution, while other air pollution parameters were sampled at high time resolution only at the two urban street canyons. For each variable, equal letters in last column indicate the absence of significant differences.

	site	Num cases	Mean	Std. dev	min	max	sig diff
NO_x ($\mu g\ m^{-3}$)	Marconi St.	42147	184	132	10	1730	a
	Laura Bassi St.	42728	135	91	10	814	b
NO ($\mu g\ m^{-3}$)	Marconi St.	42147	76	70	0.6	1129	a
	Laura Bassi St.	42728	54	52	2.1	453	b
NO_2 ($\mu g\ m^{-3}$)	Marconi St.	42147	68	32	0.0	593	a
	Laura Bassi St.	42728	52	16	6.5	170	b
NO_2/NO	Marconi St.	42147	2.1	3.0	0.0	51	a
	Laura Bassi St.	42728	1.8	1.4	0.1	11	b
CO ($mg\ m^{-3}$)	Marconi St.	42169	0.9	0.4	0.1	14	a
	Laura Bassi St.	42992	0.9	0.5	0.2	12	b
O_3 ($\mu g\ m^{-3}$)	Marconi St.	42373	11	12	0.4	67	a
	Laura Bassi St.	43734	11	14	0.0	77	b
p0.3* (counts m^{-3})*	Marconi St.	28556	1.8E+08	1.3E+08	2.0E+06	5.8E+08	a
	Laura Bassi St.	26433	2.0E+08	1.4E+08	2.7E+06	5.6E+08	b
p0.5 (counts m^{-3})*	Marconi St.	28556	2.4E+07	2.9E+07	3.8E+05	1.6E+08	a
	Laura Bassi St.	26433	2.9E+07	3.6E+07	7.4E+05	2.0E+08	b
p0.7 (counts m^{-3})*	Marconi St.	28556	4.3E+06	6.2E+06	1.3E+05	4.5E+07	a
	Laura Bassi St.	26433	5.9E+06	9.4E+06	2.3E+05	6.7E+07	b
p1 (counts m^{-3})*	Marconi St.	28556	1.0E+06	1.4E+06	4.2E+04	1.4E+07	a
	Laura Bassi St.	26433	1.6E+06	2.7E+06	9.8E+04	3.2E+07	b
p2 (counts m^{-3})*	Marconi St.	28556	2.4E+05	2.7E+05	5.0E+03	7.3E+06	a
	Laura Bassi St.	26433	3.1E+05	4.3E+05	2.2E+04	8.3E+06	b
p3 (counts m^{-3})*	Marconi St.	28556	8.2E+04	9.5E+04	0.0E+00	4.4E+06	a
	Laura Bassi St.	26433	1.2E+05	3.2E+05	4.9E+03	9.1E+06	b
p5 (counts m^{-3})*	Marconi St.	28556	2.2E+04	3.8E+04	0.0E+00	2.1E+06	a
	Laura Bassi St.	26433	5.1E+04	2.5E+05	1.3E+03	7.2E+06	b
p10 (counts m^{-3})*	Marconi St.	28556	3445	15723	0.0	658274	a
	Laura Bassi St.	26433	12537	93694	0.0	3194331	b
BC ($ng\ m^{-3}$)**	Marconi St.	13515	10974	9999	74	224334	a
	Laura Bassi St.	12340	2418	1407	1.0	11531	b
PM_{10} ($\mu g\ m^{-3}$)	Marconi St.	30	44	22	4.0	105	a
	Laura Bassi St.	30	34	18	4.0	82	ab
	Porta S. Felice	30	36	20	2.0	90	ab
	Giardini Margherita	25	30	22	0.0	87	b
$PM_{2.5}$ ($\mu g\ m^{-3}$)	Marconi St.	30	26	16	2.0	67	a
	Laura Bassi St.	30	23	14	3.0	60	a
	Porta S. Felice	30	25	14	1.0	60	a
	Giardini Margherita	28	26	16	0.0	69	a

$PM_{10}/PM_{2.5}$	Marconi St.	30	1.9	0.8	1.4	5.3	a
	Laura Bassi St.	30	1.6	0.4	1.1	3.0	b
	Porta S. Felice	30	1.5	0.2	1.1	2.0	bc
	Giardini Margherita	22	1.3	0.3	0.9	2.2	c
Benz ($\mu g\ m^{-3}$)	Marconi St.	732	2.4	1.1	0.4	7.2	a
	Porta S. Felice	692	2.0	0.9	0.3	6.2	b
Tol ($\mu g\ m^{-3}$)	Marconi St.	731	8.0	4.9	0.7	32	a
	Porta S. Felice	693	5.1	3.3	0.4	28	b
EthylBenz ($\mu g\ m^{-3}$)	Marconi St.	731	1.4	0.9	0.1	6.0	a
	Porta S. Felice	692	0.9	0.6	0.1	4.6	b
Xyl ($\mu g\ m^{-3}$)	Marconi St.	732	7.4	4.9	0.0	32	a
	Porta S. Felice	611	2.4	1.4	0.3	12	b

** The comparison refers to data acquired over the 25/01-14/02/2018 period*

*** The comparison refers data acquired over the 25/01-02/02/2018 period*

Table 7: Same as Table 6 but for the winter campaign.

The comparison shows that both during summer and during winter the concentration of most pollutants are significantly different in the two street canyons: in particular, while primary and traffic generated pollutants show significantly higher concentrations at Marconi St., secondary pollutants (i.e., not directly emitted to the air but resulting from reactions of precursor gases, such as O_3, but also secondary particulate matter), present either non-significantly different values, which is the case for PM_{10} and $PM_{2.5}$, either higher values at Laura Bassi St., which is the case of ozone and sized particle counts. The higher concentrations of primary and traffic-generated pollutants (NO_x, CO, BC) is mainly linked to the very high traffic rates observed at Marconi St., while the absence of significant differences for PM_{10} and $PM_{2.5}$ might depend on the reduced time resolution (daily) of measurements. Finally, the higher concentrations of secondary pollutants at Laura Bassi St. are attributed to the reduced reaction rates due to the reduced concentration of primary pollutants in this street canyon: in both street canyons the high NO_2 concentrations typical of urban areas tend to produce O_3 under warm and sunny conditions from NO_2 but, similarly to rural areas, the reduced NO concentrations in Laura Bassi St. inhibits O_3 degradation. The reason of the higher sized particles number, both fine as well as coarse, observed at Laura Bassi St. is still under investigation, even though we speculate that it might depend on different PM sources other than traffic active at the two measurement sites.

Similar observations hold observing the boxplots depicting the main statistical parameters of frequency distributions for air pollution levels registered within the summer and winter experimental campaigns, which are reported in Figure 30-31.

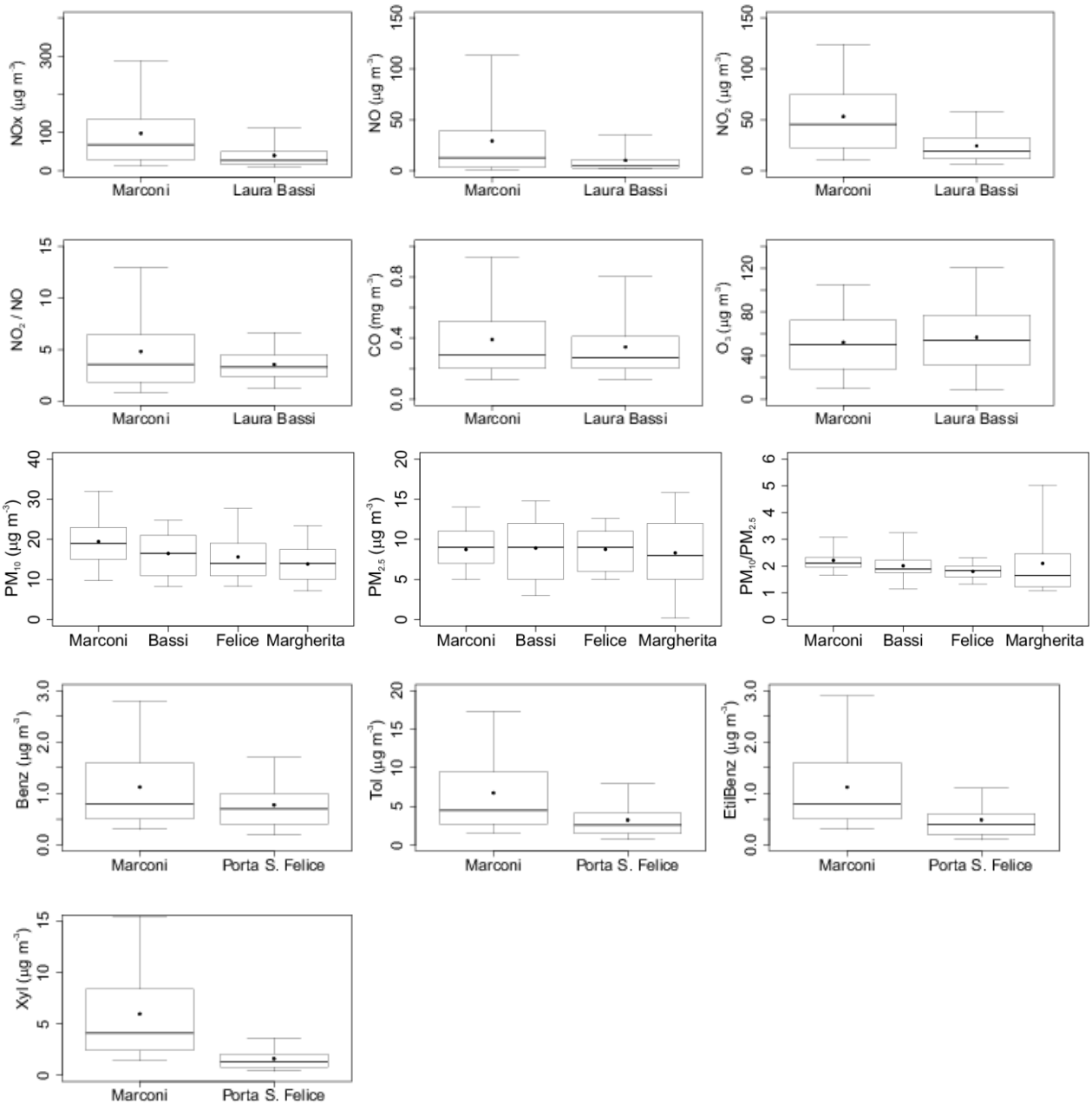

Figure 30: Boxplots depicting the fundamental statistical parameters for air pollution concentrations observed within the two street canyons in Bologna during the summer experimental campaign. The boxes enclose the 25-75th percentile values, the whiskers represent the 5-95th percentile values; the horizontal line inside the box represents the median, while the square represents the mean value.

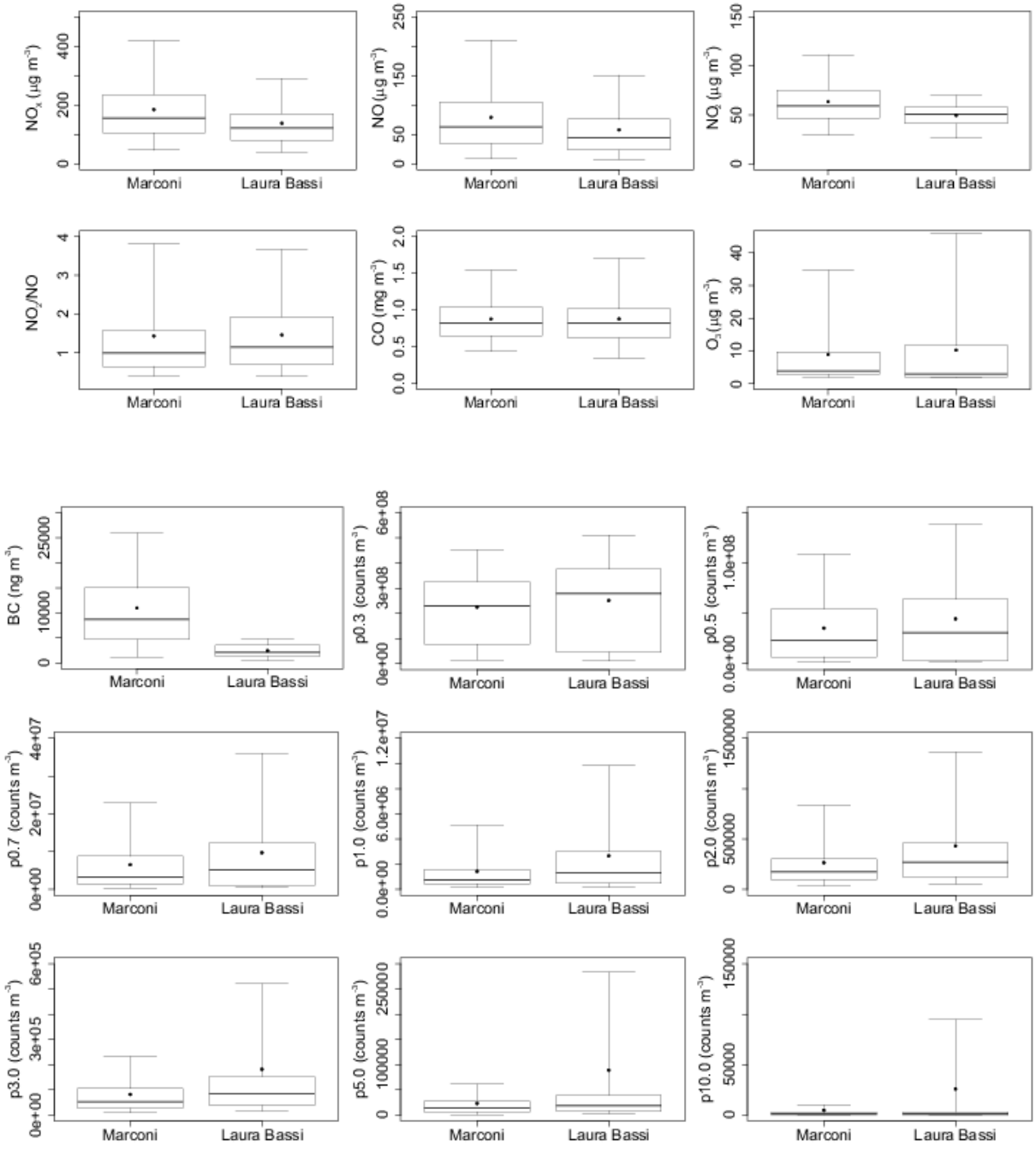
NOx (µg m-3)
NO (µg m-3)
NO2 (µg m-3)
NO2/NO
CO (mg m-3)
O3 (µg m-3)
BC (ng m-3)
p0.3 (counts m-3)
p0.5 (counts m-3)
p0.7 (counts m-3)
p1.0 (counts m-3)
p2.0 (counts m-3)
p3.0 (counts m-3)
p5.0 (counts m-3)
p10.0 (counts m-3)
Marconi
Laura Bassi

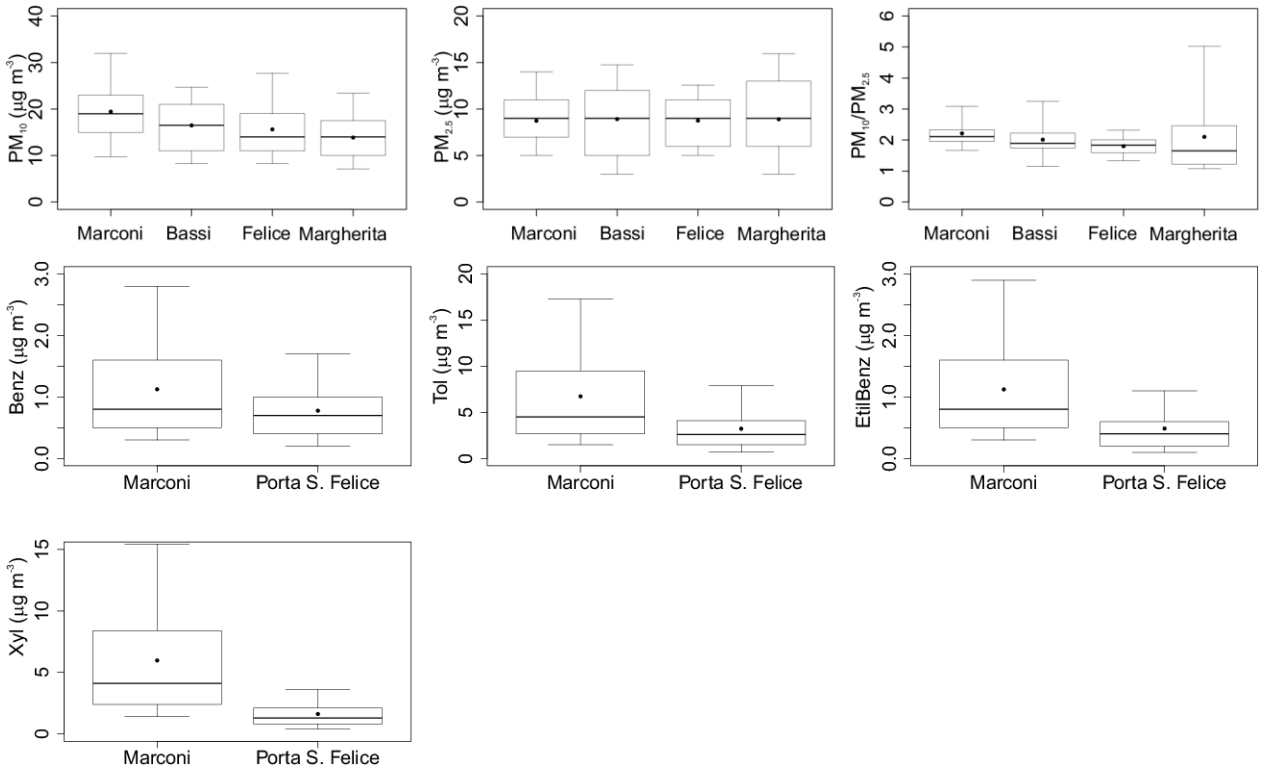

Figure 31: Same as Figure 30 but for the winter experimental campaign.

At Marconi St., PM_{10} concentration is on average 25% higher than that recorded at the other ARPA-ER air pollution stations, especially during winter; on the contrary, $PM_{2.5}$ concentration does not present significant differences between the 4 sampling sites.

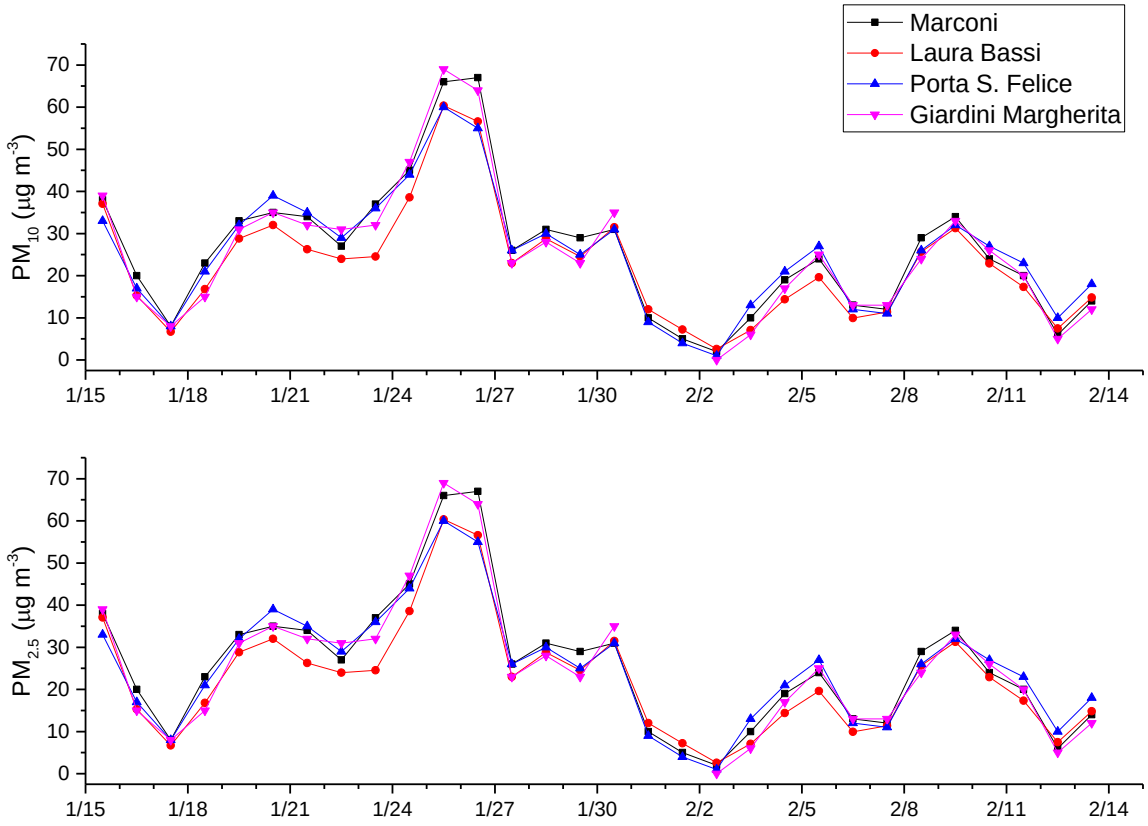

Figure 32: Time series of daily averages of particle mass concentrations (PM_{10} and $PM_{2.5}$) as measured by the ARPA-ER instrumentation during the winter experimental campaign in Bologna.

The reduced PM_{10} and $PM_{2.5}$ concentrations at all measurement sites from 30th January are due to wet removal of particles, in agreement with the frequent rain and snow conditions of this period.

In order to get insights into particle pollution, particle counts were converted to particle mass concentrations (PM_{10} and $PM_{2.5}$) through the algorithm developed by Tittarelli et al. (2008), i.e. assuming the particles to be spherical (Wittmack, 2002) and having a density of 1.65 g cm^{-3} as suggested by Tuch et al. (2000) and Weijers et al. (2004). Practically, the following equation was applied:

$$m(d_p) = \frac{4}{3}\pi d_p^3 \rho_p n(d_p)$$

where ρ_p is the particle density and d_p is the mean particle diameter.

The following Figures report the comparison between PM_{10} and $PM_{2.5}$ as measured from ARPA-ER instrumentation and as estimated from particle counts in the two street canyons.

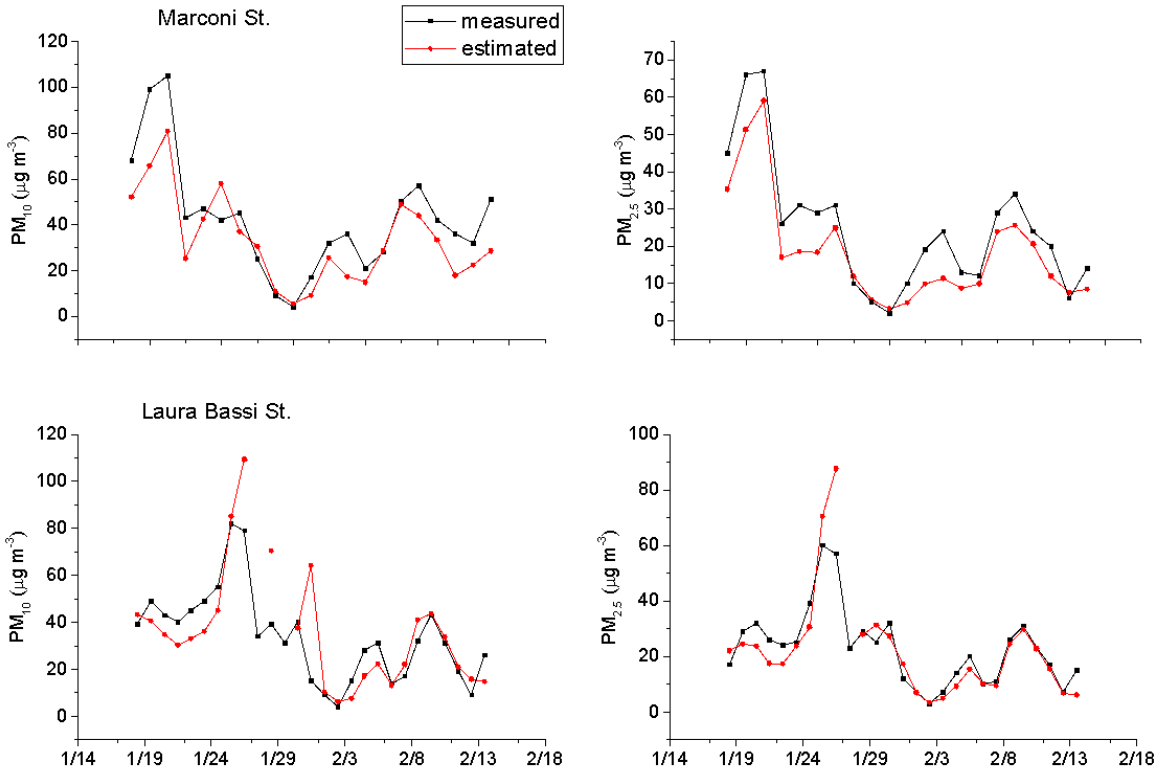

Figure 33: Time series of daily averages of particle mass concentrations (PM_{10} and $PM_{2.5}$) as measured by the ARPA-ER instrumentation and as estimated from particle counts in the two street canyons in Bologna (Marconi St. upper panels; Laura Bassi St. lower panels).

The comparison yields very good agreement especially for Marconi St. (R^2 =0.91 and 0.94 for PM_{10} and $PM_{2.5}$, respectively), while at Laura Bassi St. the comparison shows a partial overestimation in particular for PM_{10} (R^2 = 0.6 and 0.86 for PM_{10} and $PM_{2.5}$, respectively): this can be attributed to errors in particle counts especially for larger particle sizes as well as to a different particle density (due to the presence of different particle sources) in this street canyon. Notwithstanding this partial overestimation, this check suggests the general validity of the algorithm and the use of particle counts collected with high time resolution to understand the difference between the two street canyons about particulate matter.

As from the Table below, at both street canyons, most of the mass was contributed by the smaller particles (first channel) and the larger particles, while particles in the intermediate sizes contributed less.

Diameter (μm)	**0.3-0.5**	**0.5-0.7**	**0.7-1.0**	**1.0-2.0**	**2.0-3.0**	**3.0-5.0**	**5.0-10.0**
Marconi St.	29	10	5.2	7.6	9.5	14	25
Laura Bassi St.	26	9	5.2	8.5	9.1	14	28

Table 8: Distribution of particle mass concentrations among the different size ranges of the optical particle counter at the two street canyons in Bologna.

The following Figures present a snapshot on NO_2 daily averages collected within particular weeks during the summer and winter experimental campaigns.

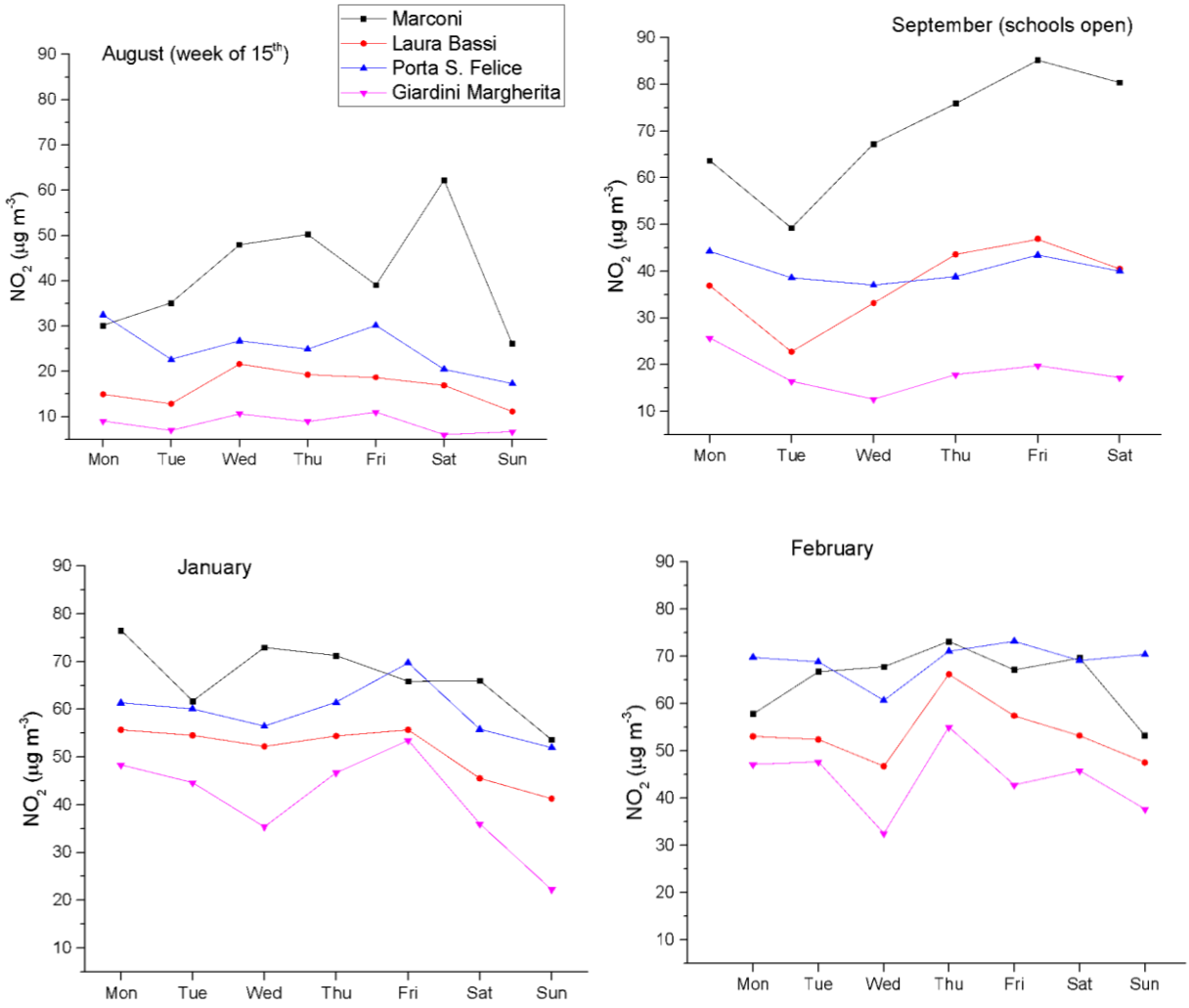

Figure 34: Daily NO_2 averages obtained during different weeks of the Bologna summer and winter experimental campaigns at the different measurement sites.

The plots show that except for the 15th August week, when concentrations were low due to the fact that most of the people were on vacation during that period, NO_2 concentrations obtained in Marconi St. during the summer period are comparable to those measured during the winter campaign. In fact, while during winter the reduced boundary layer height tends to homogenize concentrations observed all over the different measurement sites, during summer the canyon effect is instead very evident in particular for NO_2 in Marconi St.

The following plots (Figure 35) show very clearly that the primary pollutant NO during summer was evident only at Marconi St., while at the other two remaining traffic sites the concentration of this pollutant was rather low. This could be attributed to the canyon effect, which is more pronounced at Marconi than at Laura Bassi St., also a canyon as described earlier.

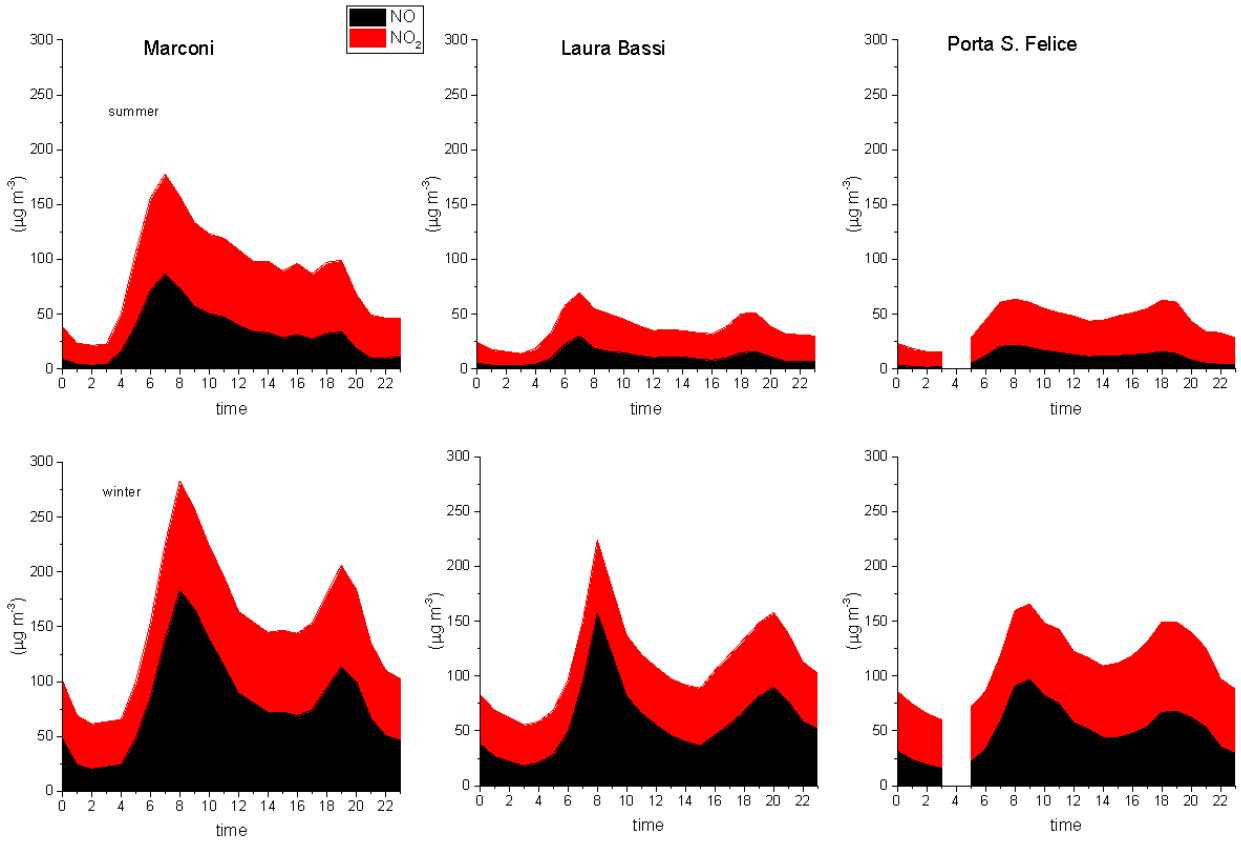

Figure 35: Mean diurmal pattern of NO_x as sum of NO and NO_2 components at the different measurement sites in Bologna (the two street canyons and the ARPA-ER urban traffic station) during the summer (upper) and winter (lower) experimental campaigns.

Finally, when observing primary pollutants concentrations at the 2 street canyons with 1-min time resolution (Figure 36), it is clear that:

- NO levels are very variable mostly during the morning;
- the peak in primary pollutants is more evident at Laura Bassi St. at times when there is a long line at the traffic light.

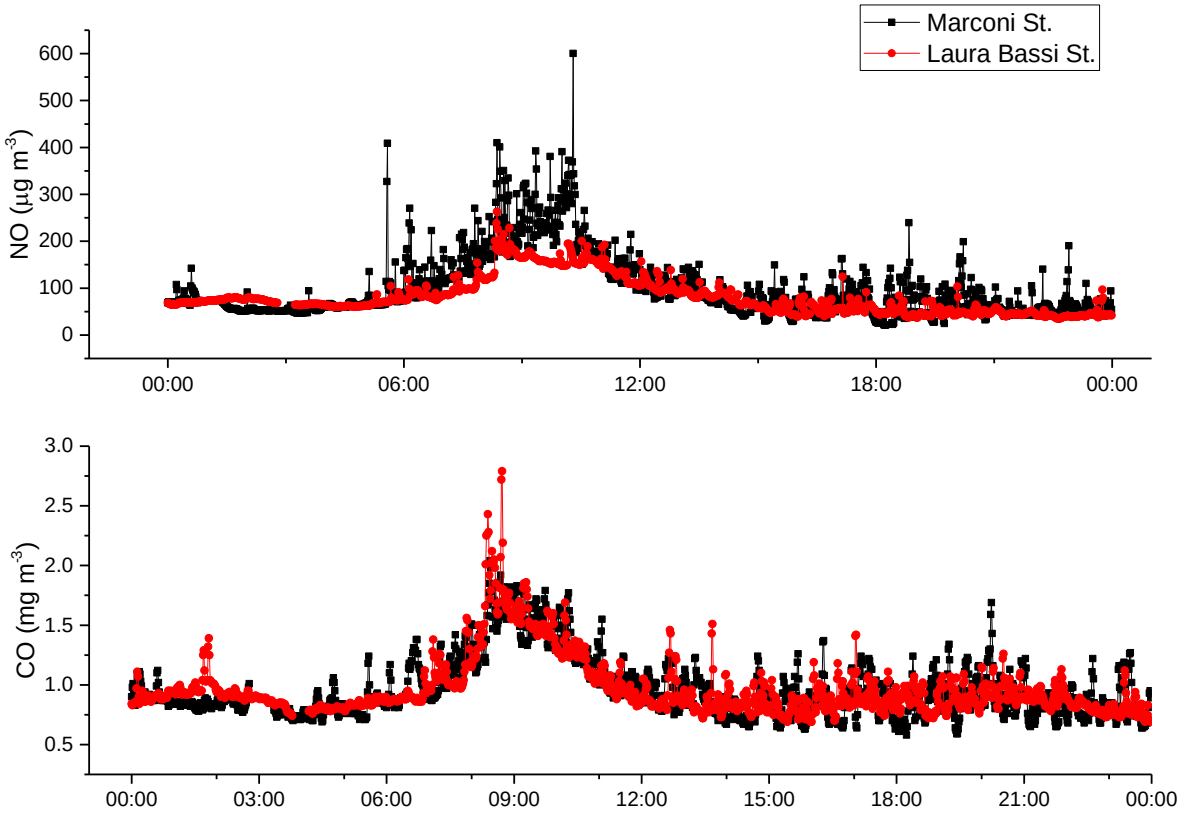

Figure 36: Example of primary NO and CO concentrations observed with a 1-min time resolution in the 2 street canyons in Bologna on 30/01/2018.

In conclusion, even though the differences between the two experimental sites was connected not only to the different presence of vegetation but also to the different traffic volumes and vehicle types typically travelling in the two street canyons, due to the fast variability of pollutants directly connected to the variability of the traffic source, in order to analyze the impact of the green infrastructure on air pollution, an algorithm was developed to normalize the concentrations observed at the two street canyons. The normalization takes into account the geometry (canyon aspect ratio, i.e., ratio of canyon height over canyon width), the wind speed observed above the canyons (bulk velocity) and the traffic emissions, as obtained and estimated by the traffic counts at the two sites.

4.1.3 UHI study at neighborhood scale

In the following, we analyze with details the temperature data gathered during the two summer and winter intensive thermographic campaigns. As reported in the previous section, the day for the UHI experiment was selected according to the weather forecast conditions to have a clear-sky, calm wind, day. Figure 37 represents the wind rose plot for wind speed and wind direction measurements collected within the summer and winter thermographic campaigns.

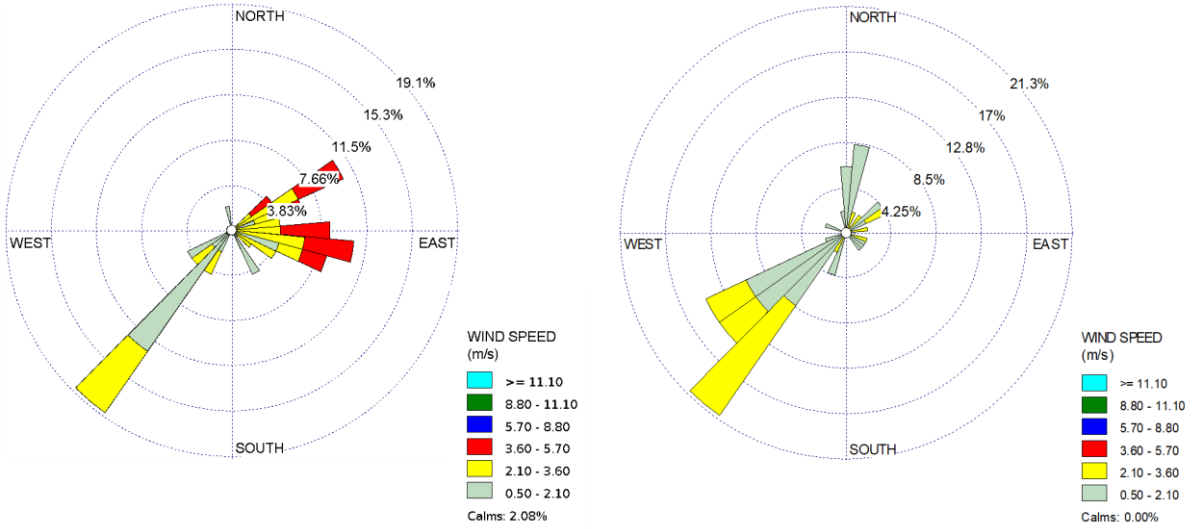

Figure 37: Wind rose plot for wind speed and direction observed at Silvani St. ARPA-ER meteorological station within the summer and winter intensive thermographic campaigns in Bologna (22-23/08/2017 and 08-09/02/2018).

Figure 38 and Figure 39 represent the evolution of temperature measured in the two street canyons with the thermo-hygrometers, that measured by the ARPA-ER fixed meteorological stations (one urban, Silvani St., and one rural, Mezzolara), and the temperature of building façades along the West and East side of the two canyons as retrieved from the thermal images collected during the campaigns.

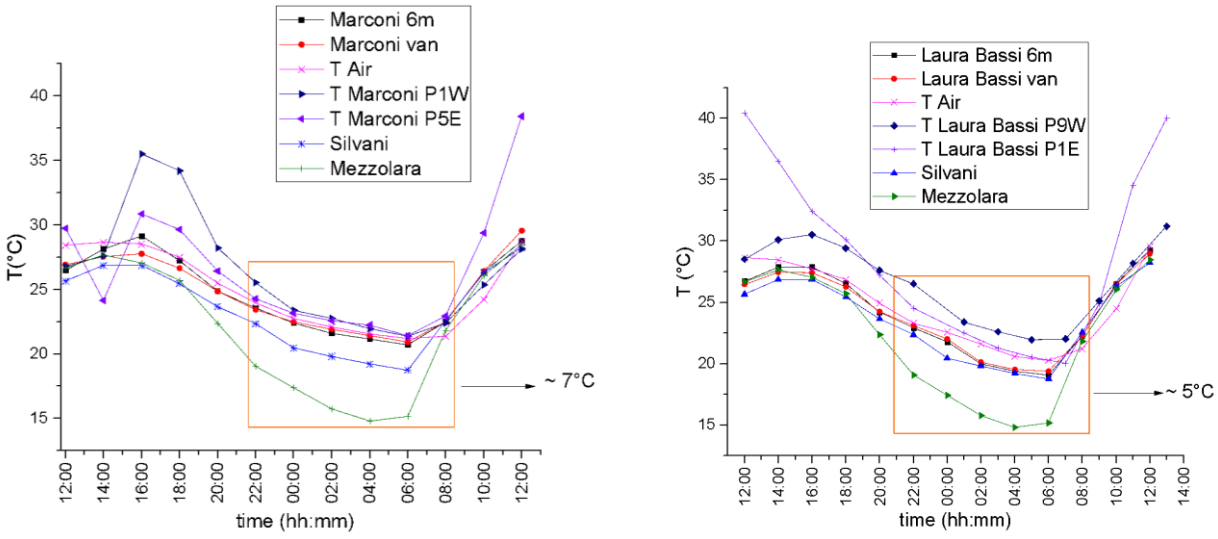

Figure 38: Temperature evolution within the day of the summer intensive thermographic campaign in Bologna (22-23/08/2017), measured by the thermo-hygrometers, the ARPA-ER instrumentation in one urban (Silvani St.) and one rural meteorological station (Mezzolara) and of building façades of buildings located on the West and East side of the 2 street canyons (Marconi St. upper and Laura Bassi St. lower) as retrieved from the thermal images.

The plots show very clearly the UHI effect, i.e., the effect of overheating of cities with respect to the countryside. The effect is reduced at Laura Bassi St. with respect to Marconi St., both due to the presence of vegetation as well as being located further from the city centre in a residential area in the outskirts of Bologna where the presence of small houses and apartments favor heat exchange and urban thermal comfort with respect to the highly packaged buildings typical of the historical city centre where Marconi St. lies. In addition, the plots also show that during night both street canyons are isothermal, i.e., there is no temperature difference between the building façades on the two sides of the streets nor with the temperature of the air in the street canyon, while during the day, depending on the position of the Sun, one side is hotter than the other one: this effect is visible at both street canyons but it is more evident at Marconi St. During winter, similar UHI effects are observed at both sites, with urban-rural differences of about 6°C at both sites: this mainly depends on the absence of the shadowing effect of the trees, reducing the effect to that caused by the different building packaging only. Further, the isothermal conditions within the canyons are no more observed during night, because of residential heating causing differences between building façades and air temperatures. In particular, the plots show an enhancement in both air and building temperatures in Bologna during night from 22:00 until 02:00, which is not observed in Mezzolara and cause increased UHI effect at night: the reason of this observation is still not completely clear, however, it might be related to the presence of clouds in Bologna (cloud cover during night was noted during the thermographic campaign) but not in Mezzolara. This will be further explored in the updated version of this Deliverable.

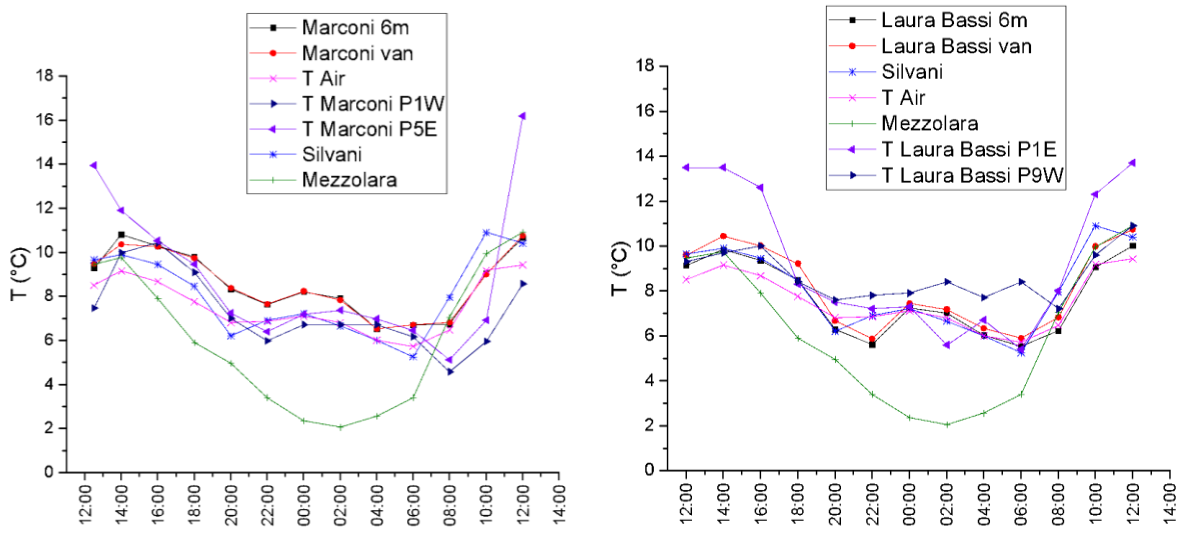

Figure 39: Same as Figure 38 but for the day of the winter intensive thermographic campaign in Bologna (08-09/02/2018).

4.2 Dublin

4.2.1 Meteorology and air pollution: statistical analysis

This section presents some preliminary statistical analyses of collected data within the winter experimental campaign with the experimental setup previously described. Figure 40 presents the normal distribution plots for the wind speed data categorized by wind direction groups; the figure illustrates that different wind directions are characterized by different values distribution and magnitudes for wind speed. The wind rose plot represented in Figure 41 shows more properly that

even though the east and south-east are the dominant wind directions in the sampling site the west component is also important, while S and N directions are very rare: this is mainly because of the street canyon orientation as illustrated in the site description. As such, the local wind rose is very different from the local climatological one (see D6.1 Figure 18), characterized by dominant strong west and south-west winds, which clearly depends from the different nature of the two sampling sites (i.e., being Pearse Street an urban site in a street canyon, while data described in D6.1 were collected at the Dublin airport).

Figure 42 shows the time series for the collected maximum, minimum and average wind speeds (m/s): as can be observed, the values fluctuate by time and there are many peak values to be considered and further investigated.

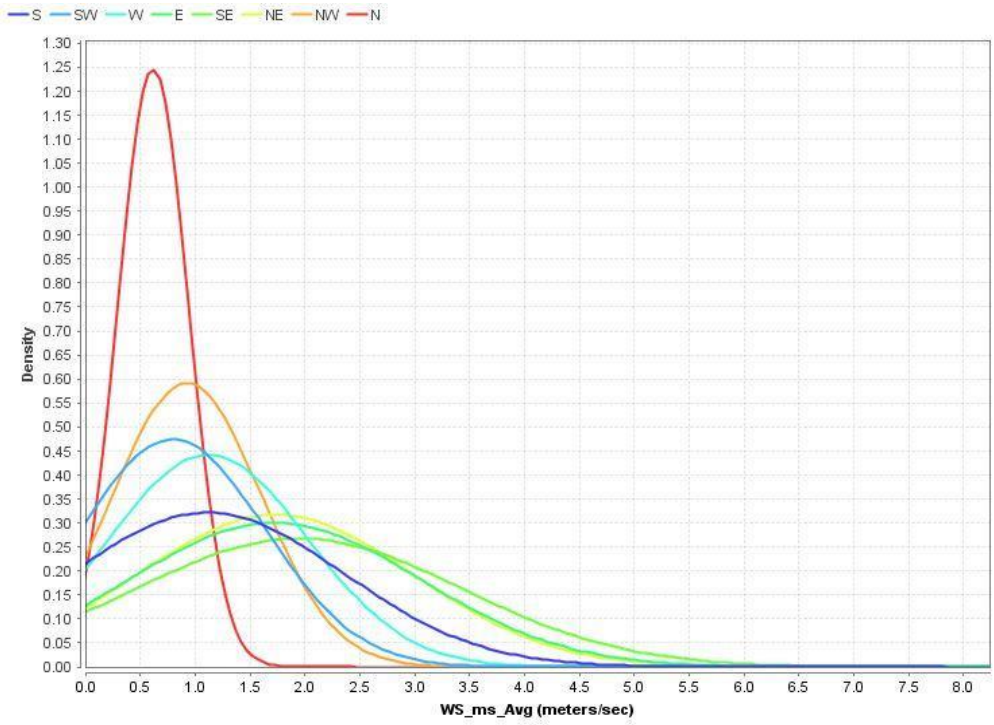

Figure 40: Distribution plot of wind speed data according to the different wind direction categories.

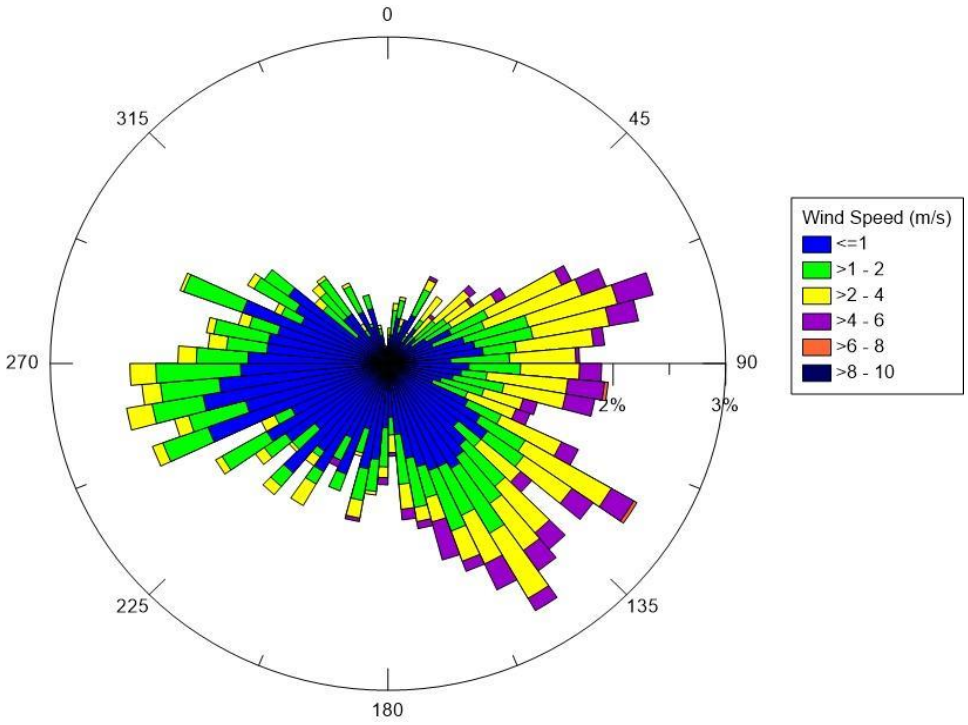

Figure 41: Wind rose plot for the Dublin site.

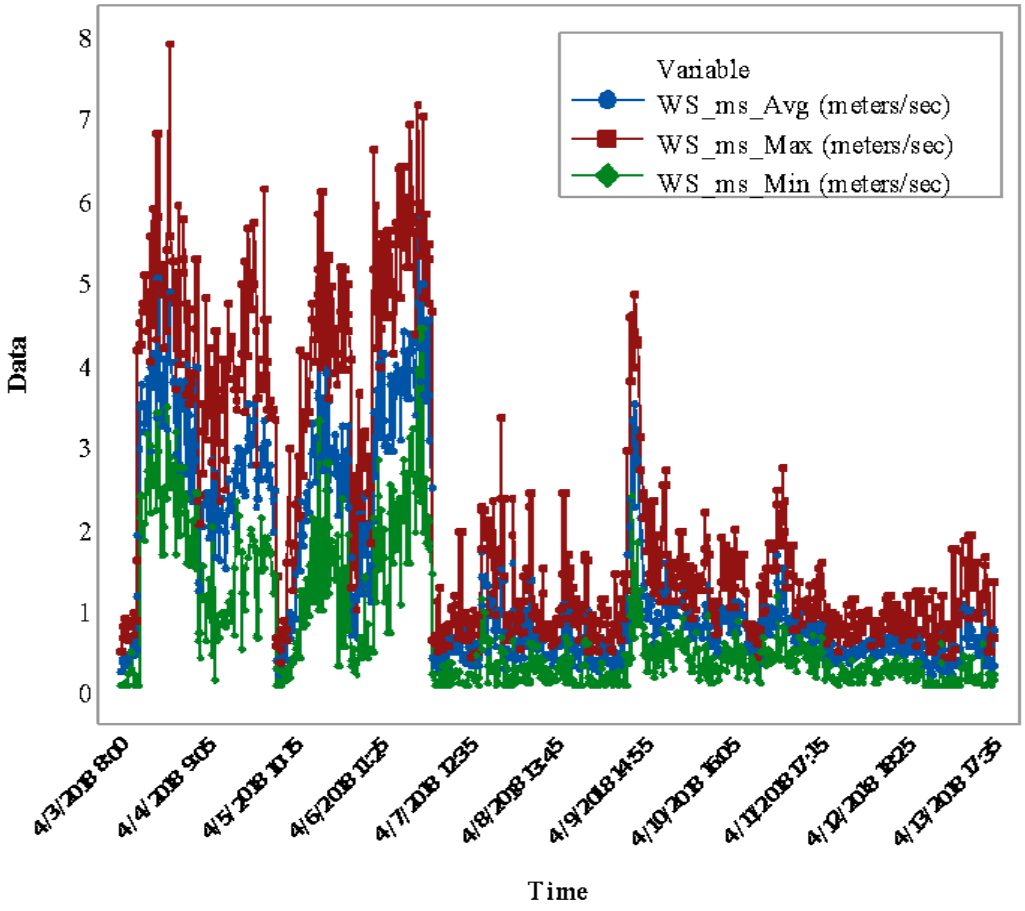

Figure 42: Minimum, maximum and average wind speed data.

Figure 43 and Figure 44 show the normal distribution curves for the NO_x concentrations in front of the LBW and behind the LBW, respectively. The normal distributions demonstrate that wind direction produces significant effects on the distribution of NO_x concentrations. In particular, the highest concentrations are observed in correspondence with the South-East direction, while the lowest concentrations are connected with East directions.

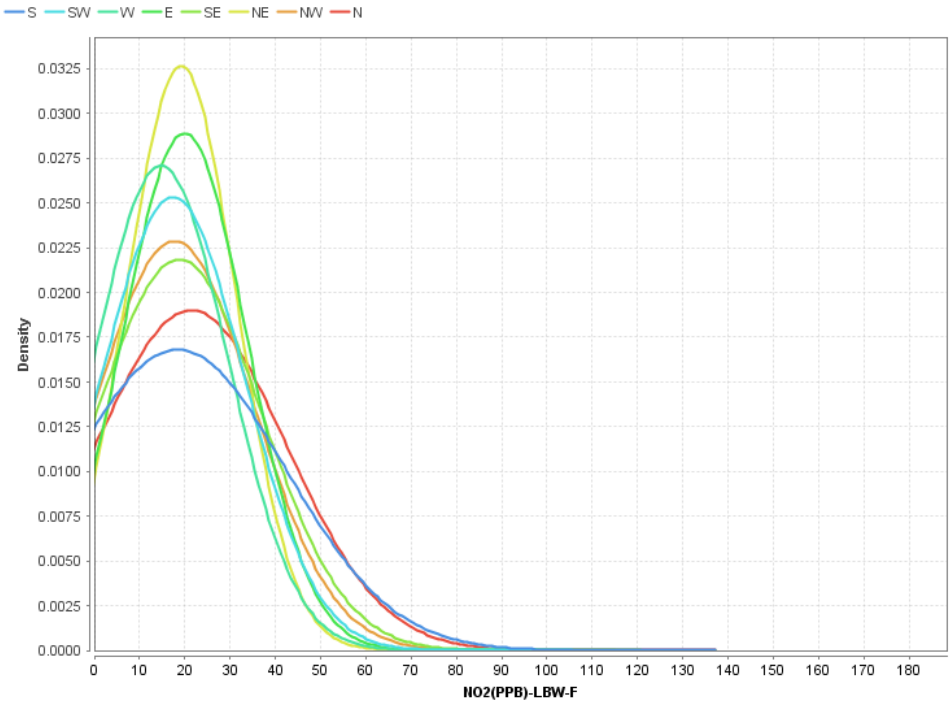

Figure 43: Distribution plot of NO_x (ppb) in front (F) of the LBW.

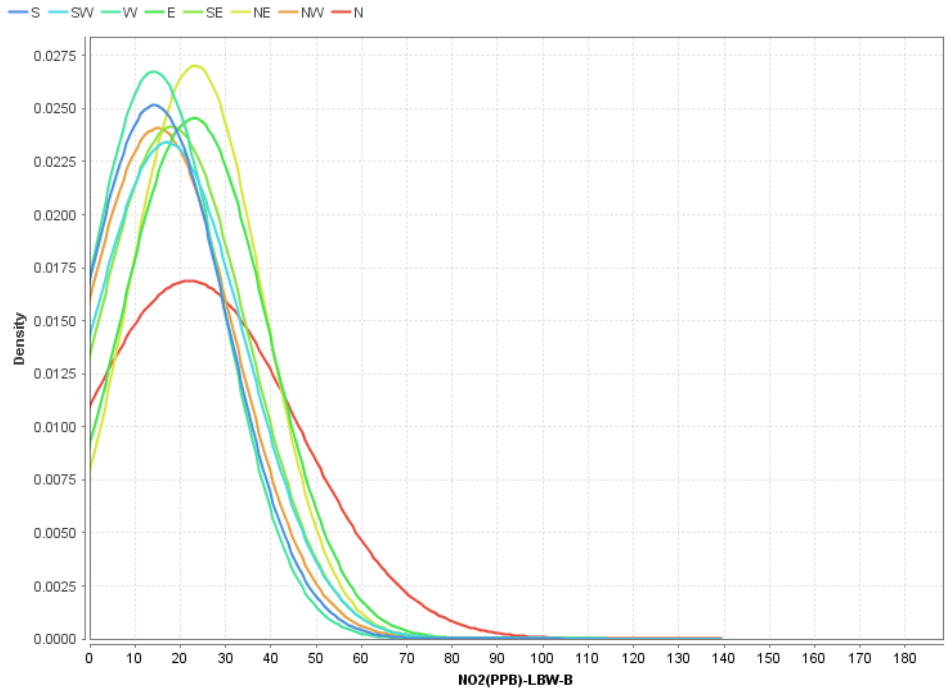

Figure 44: Distribution plot of NO_x (ppb) behind (B) the LBW.

Figure 45 further provides a multi-scale time series plot for the NO_x concentrations recorded in front of the LBW (red line) and behind the LBW (blue line). As such, Figure 45 shows that, in general, the NO_x concentrations are higher in front of the LBW than behind it, which demonstrates the potential to use LBWs as a passive control system to control air pollution in the built environment.

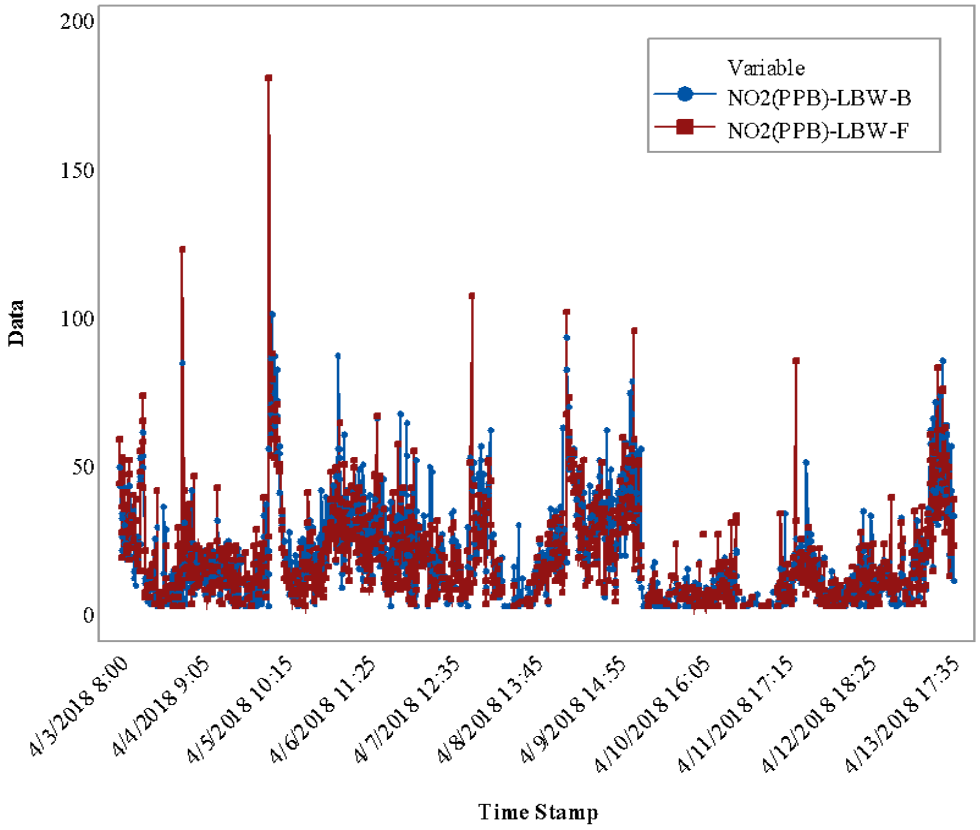

Figure 45: Time series plot for the NO_x concentrations (ppb) recorded on both sides of the LBW.

4.2.2 Meteorology and air pollution: preliminary results

This section presents the preliminary results and an outlook from the Dublin LBW field experiment. Figure 46 shows the distribution of the calculated reduction in the NO_x concentration between the front of the LBW and the back of it, which can be very different depending on the different wind directions categories.

Figure 46 and Figure 47 show that LBW may also produce negative effects in some occasions. Figure 46 and Figure 47 clearly demonstrate that LBWs, in the current experimental setup, work for most of the wind direction categories except for the East, North-east and North directions.

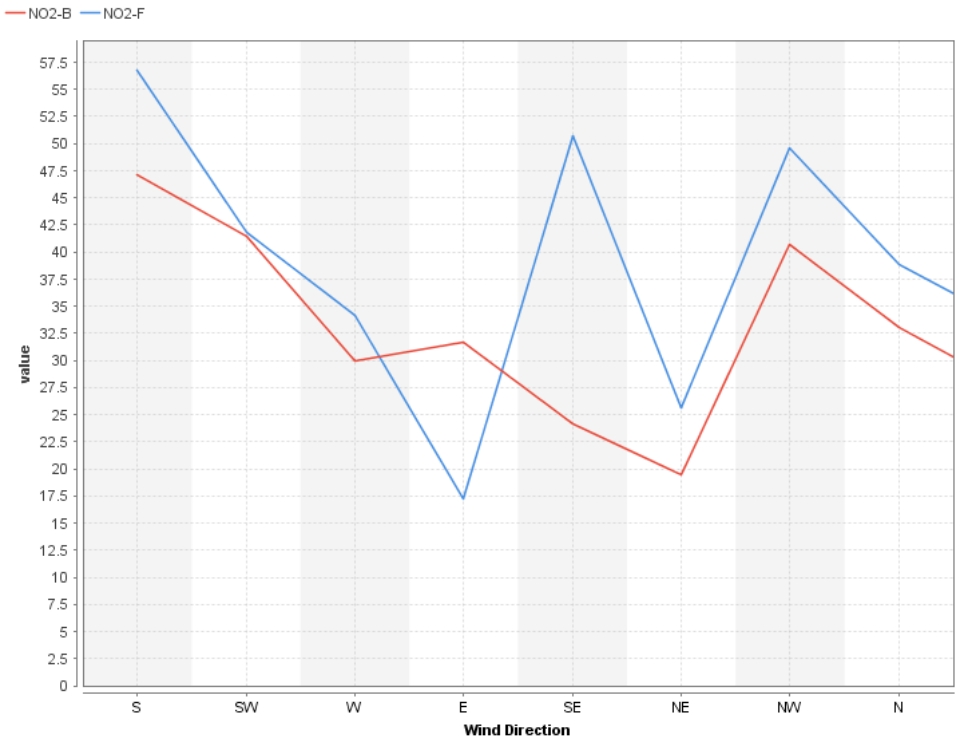

Figure 46: NO_x concentration (ppb) in (F) & (B) of the LBW per wind direction.

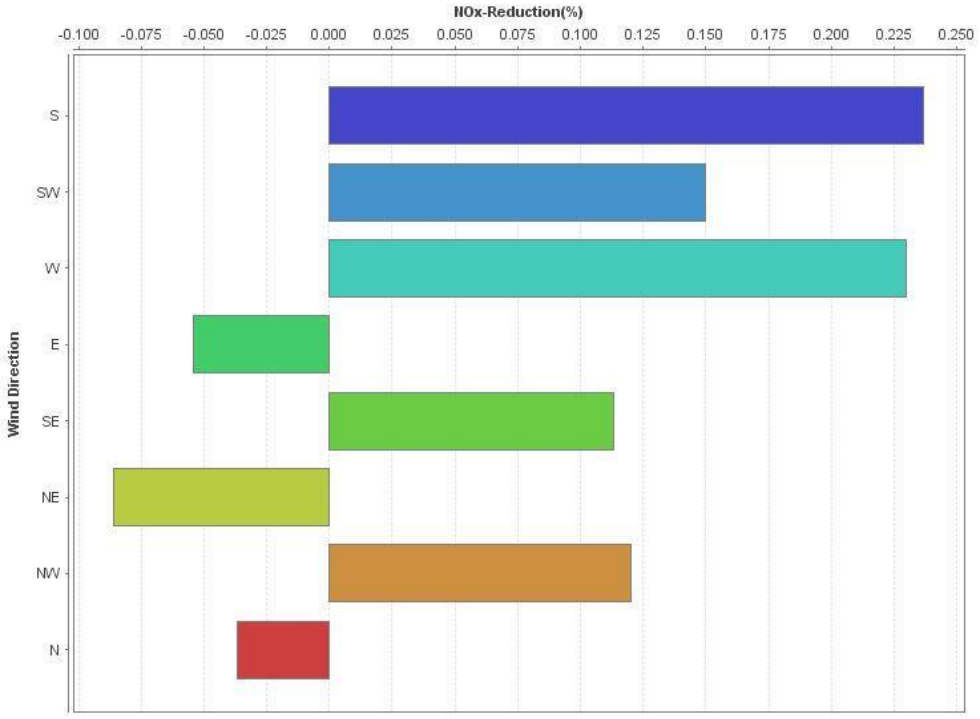

Figure 47: Median NO_x (ppb) reduction behind LBW.

Figure 48 provides the standard deviations of the reduction in the NO_x concentrations per wind direction categories: as can be observed, standard deviation percentages are greater than 5% in

most of the cases except under the north-east direction, which has a negative impact on NO_x concentrations and for which the LBW effect is reversed. In particular, as for the North direction, the absence of a clear impact of LBW clearly depends from the fact that this direction was seldom observed, which contributes to the very high variations linked to this direction which can be noticed in Figure 48.

The outlooks from the presented preliminary results can be outlined as follows: LBWs act as a baffle at street level and increase the distance between the pollutant source and human receptor.

LBWs can provide a solution to enhance localized dispersion and improve air pollution in distinct street canyons settings. However, depending on the wind direction, street geometry and position of the LBW, may cause air pollutant concentrations to increase behind the LBW, having the opposite effect of increasing pollutant concentrations instead of decreasing them. Since wind direction is very variable, LBW may produce both positive and adverse effects, which makes the designing process and their use in urban city planning very hard and ambitious. As a result of these preliminary observations, it is important to carefully plan and analyze where LBWs are placed so that they work in the desired direction to improve air pollution.

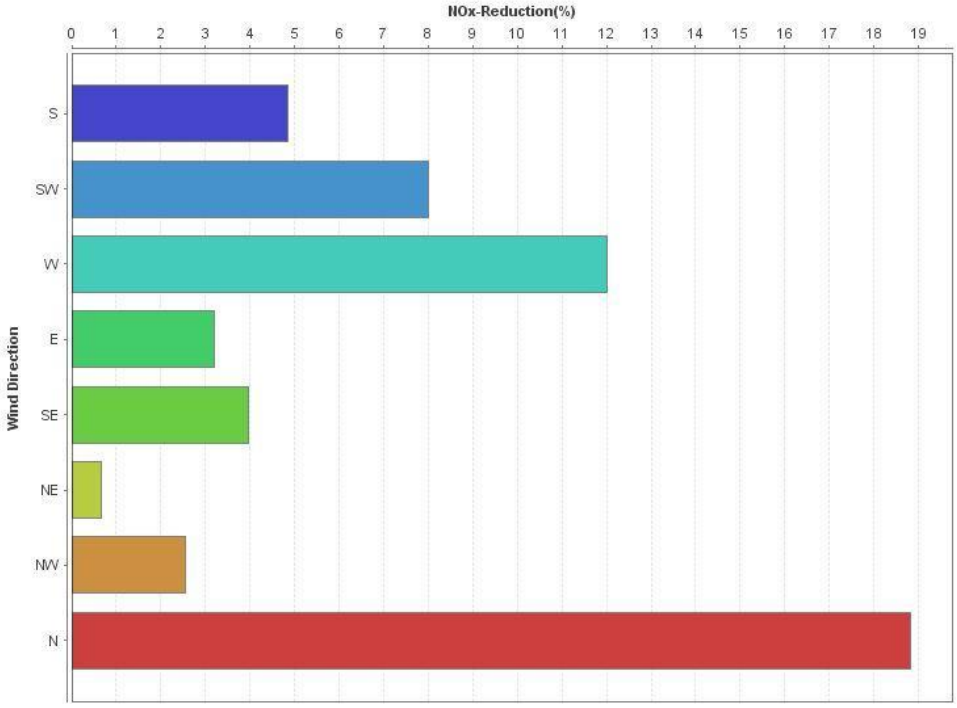

Figure 48: Standard deviation of NO_x (ppb) reduction behind LBW.

4.3 Guildford

4.3.1 Air pollution

Results from field measurements validated the air pollution modifications of vegetation barriers in open-road conditions. All collected pollutant measurements were skewed and were log transformed for computing mean and 95% confidence interval. As shown in Figure 49, in most of the cases, PNC concentrations behind the vegetation were found to be lower than clear or in front of vegetation except in the T_{CB} and TH_{CB} cases in clear vs behind site with 2% and 3% respectively.

Moreover, these concentration increases were small. The maximum improvement in PNC concentrations behind vegetation was observed with hedges (H_{IB} and H_{CB}) in both clear vs behind and in-front vs behind cases with 30% and 9%, respectively. In clear vs behind cases, BC concentrations behind the vegetation were found to be slightly higher than clear area except in TH_{CB} (4%). The H_{CB} case emerged as the worst scenario among the clear vs behind cases (-15%). On the other hand, in-front vs behind cases displayed higher BC concentration reduction of 43-63% with the lowest ones observed with H_{IB} and maximum ones in the case with TH_{IB}. BC concentration changes were relatively higher compared to the other pollutants investigated in this study.

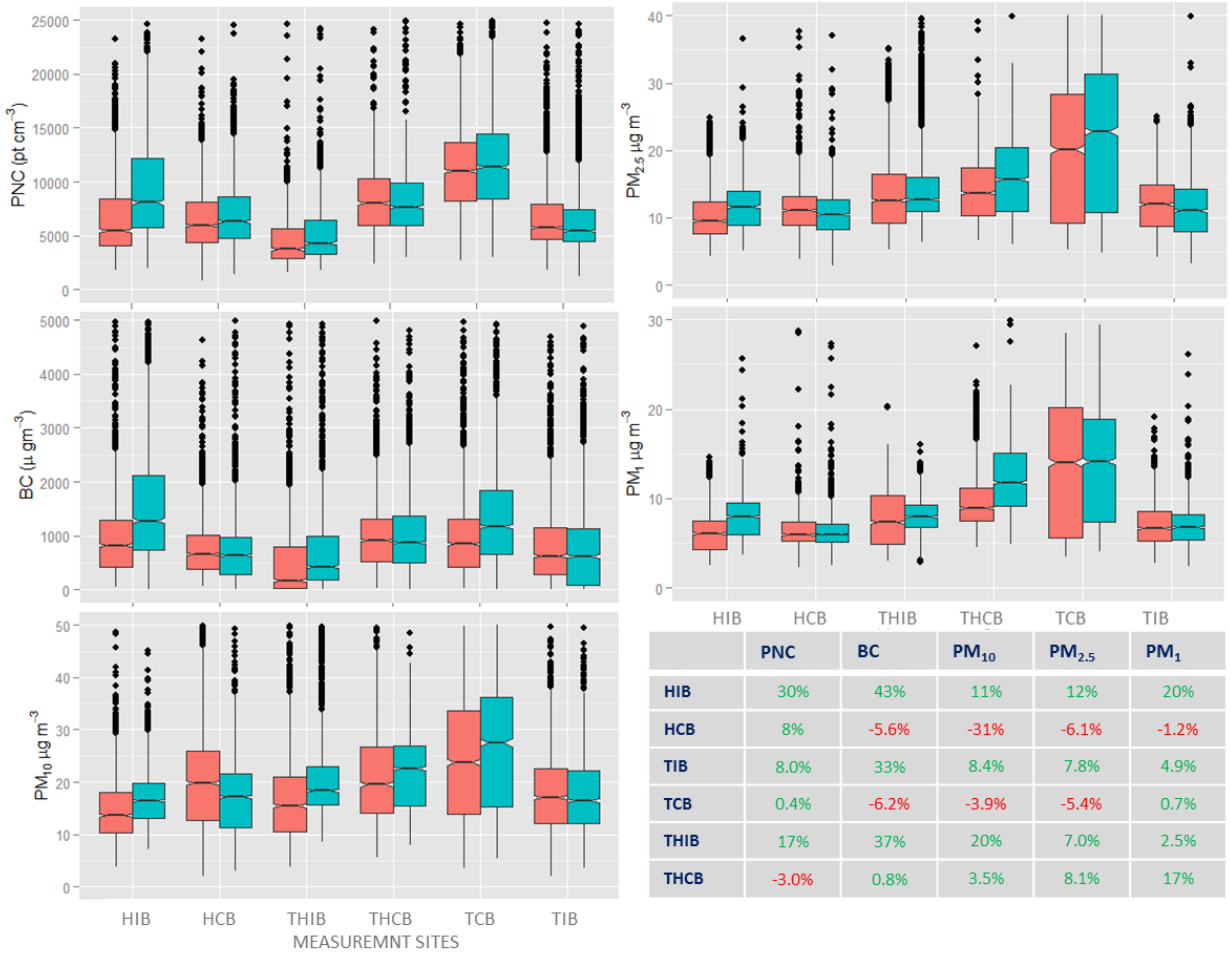

	PNC	BC	PM_{10}	$PM_{2.5}$	PM_1
HIB	30%	43%	11%	12%	20%
HCB	8%	-5.6%	-31%	-6.1%	-1.2%
TIB	8.0%	33%	8.4%	7.8%	4.9%
TCB	0.4%	-6.2%	-3.9%	-5.4%	0.7%
THIB	17%	37%	20%	7.0%	2.5%
THCB	-3.0%	0.8%	3.5%	8.1%	17%

Figure 49: Boxplots of pollutant concentration behind (red) and clear/in front (green) measurement points at the six monitoring sites in Guildford, UK: a) PNC, b) $PM_{2.5}$, c) BC, d) PM_1, e) PM_{10}. Table with percentage concentration reduction at behind location in all sites.

PM_{10} concentration changes behind vegetation exhibited a trend similar to BC concentration variations in both clear vs behind and in-front vs behind cases, but the magnitude of PM_{10} concentration changes was lower. The highest improvement in PM_{10} behind GI was observed in TH_{IB} (24%) and TH_{CB} (7%) in in-front vs behind and clear vs behind sites, respectively. The highest deterioration of 22% behind vegetation was noticed in H_{CB} scenario of clear vs behind

measurement site. $PM_{2.5}$ concentration changes were the lowest in magnitude compared to other pollutants. $PM_{2.5}$ reduction behind the vegetation followed the matching trend of concentration variations of BC and PM_{10} in clear vs behind and reversed concentration change profile of BC and PM_{10} in-front vs behind cases. Here, the highest improvement was noticed with H_{IB} and the least was reported with TH_{IB} in in-front vs behind sampling location. The maximum improvement of 8% was recorded in TH_{CB} in clear vs behind categories and an increase in $PM_{2.5}$ concentration about 22% is reported with H_{CB}. Meanwhile, maximum reduction of $PM_{2.5}$ was logged with H_{IB} (14%) and least was displayed by TH_{IB} (8%) in in-front vs behind scenarios. Improvement in PM_1 concentration behind vegetation was observed in most of the investigated scenarios leaving H_{CB} (-1%) site in clear vs behind category. PM_1 concentration variations followed that of $PM_{2.5}$. H_{IB} (25%) and TH_{CB} (19%) recorded the highest PM_1 concentration reduction behind the vegetation in in-front vs behind and clear vs behind sites respectively. Variations in PM_1 concentration behind GI (Green Infrastructure) in T_{CB} site was nominal.

Overall, the H_{IB} site presented the best improvement in air pollution behind vegetation barrier across measured pollutants, followed by TH_{IB} in in-front vs behind scenarios. In addition, the TH_{CB} displayed an improvement in air pollution in clear vs behind measurement locations. H_{CB} and T_{CB} sites resulted in deterioration of air pollution behind vegetation in clear vs behind cases. Nevertheless, all magnitudes of negative pollutant concentration changes were less than 7% excluding PM_{10} concentrations and BC concentrations in H_{CB} scenario. When comparing concentration changes among pollutants, the highest relative differences were observed with BC (gradual decay) than PNC (rapid decay) and least was witnessed in PM2.5 (no trend in decay) as expected (Karner et al., 2010; Pasquier and André, 2017). All these percentage calculations did not account for background subtraction and as such may be underestimating changes reported.

4.3.2 Influence of wind direction on air pollution

In order to understand wind direction influences of GI on concentration, three main categories were investigated in this work (Figure 50). In along-road flow conditions, the wind is blowing parallel to the road. In both cross-road and cross vegetation direction categories, flow is perpendicular to the street, but traffic emissions are at downwind in cross-vegetation and at upwind in cross-road case. There was the absence of data points for cross-road winds at measurement site TH_{IB} and for cross vegetation winds in both T_{CB} and H_{IB} sites.

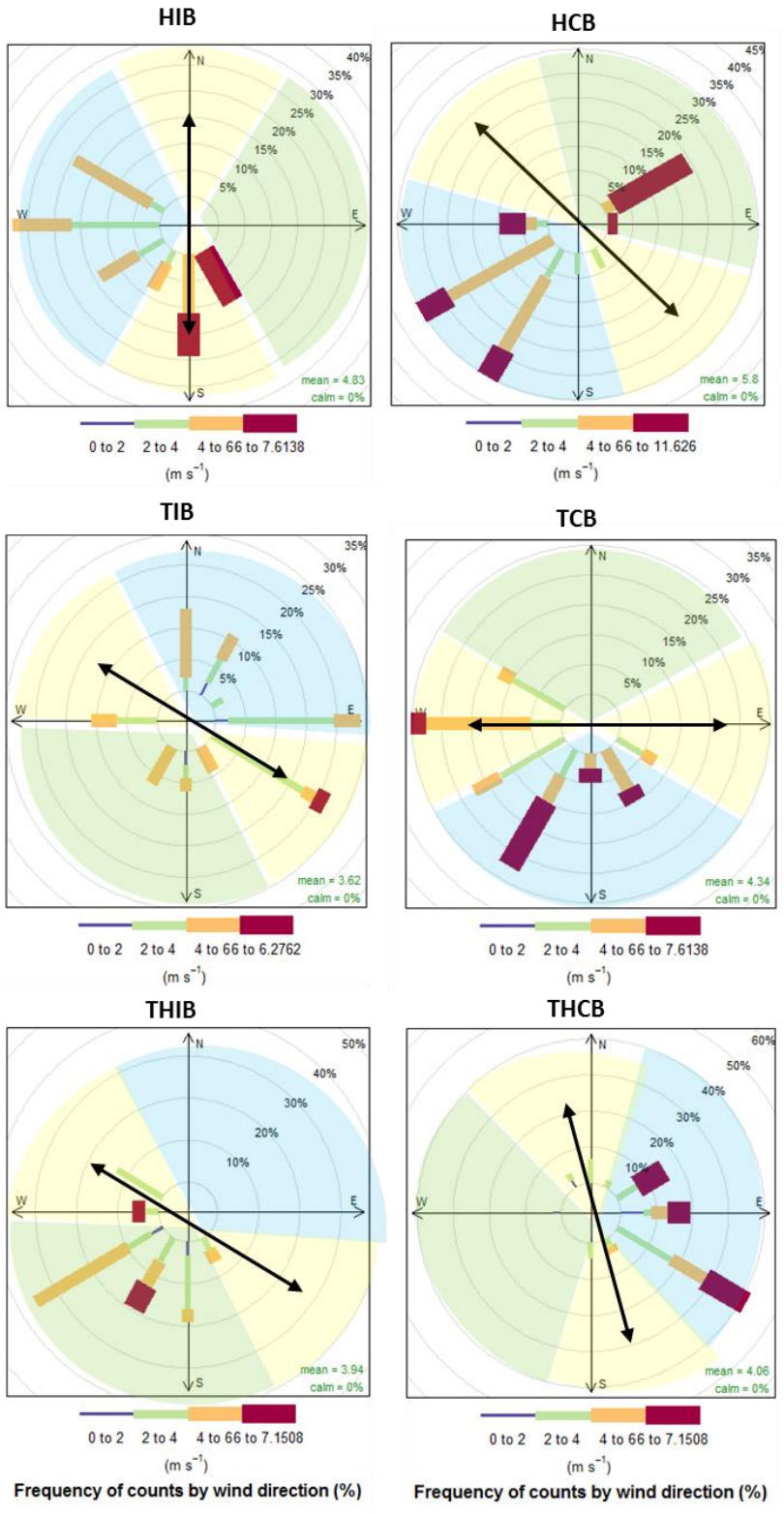

Figure 50: Wind rose diagram for each site with wind direction classification in Guildford, UK. Color codes: Blue-cross road winds, yellow- along road, and green –cross vegetation.

The percentage difference in PNC concentration under the three investigated wind direction categories was lower than that of BC and was similar to PM_1. Along-road wind conditions resulted in maximum reduction between wind categories. In addition, Hedges H_{IB} and H_{CB} in both clear vs behind and in-front vs behind cases showed the highest percentage reduction of PNC concentration of 30% and 50%, respectively. Meanwhile, in cross-road conditions, H_{IB} displayed maximum reduction (30%) followed by T_{CB} (13%) and H_{CB} (12%). The highest deterioration among all wind conditions was reported in cross-road winds even though they were less than 5% at sites T_{CB} and TH_{CB}. The lowest PNC concentration changes were observed with cross vegetation. The maximum improvement in PNC concentration was noticed with TH_{IB} (13%).

Percentage differences in BC concentrations between behind and clear/in front measurements emerged as the highest across other investigated pollutants. In addition, maximum percentage differences were similar among the different wind directions. Relatively small (< 6%) increases in BC concentrations were observed with clear vs behind in along-road wind category. On the other hand, improvement in BC concentration ranged from 49% (H_{IB}) to 65% (TH_{IB}) in in-front vs behind scenarios. In cross-road winds, all sites showed improvement behind the vegetation except H_{CB} (-23%). T_{CB} and TH_{CB} of clear vs behind cases resulted in 11% improvement and T_{IB} showed maximum BC percentage reduction of 52% among studied cases.

As for BC, being a good traffic emission tracer, no deterioration was spotted in cross vegetation wind direction. Moreover, in cross vegetation winds the percentage differences in BC concentrations ranged from 12% (T_{IB}) to 61% (TH_{IB}). The trees with hedges scenario (TH_{IB} and TH_{CB}) showed maximum reduction in BC concentration in in-front vs behind and clear vs behind, respectively.

In most of the GI scenario, PM_{10} percentage differences were consistent across wind directions except for H_{CB} and T_{CB}. In along-road winds, apart from H_{CB} (-6%) and T_{CB} (-8%) all other GI cases displayed improvements about 12-16% in PM_{10} concentration behind vegetation. The maximum reductions in PM_{10} concentrations were recorded with TH_{CB} (16%) in clear vs behind and H_{IB} (14%) in-front vs behind cases. On the contrary, in cross-road wind direction, only the H_{CB} site showed an increase in PM_{10} concentration and all other improvements in PM_{10} ranged from 2% (T_{CB}) to 15% (H_{IB}). In cross vegetation winds, H_{CB} displayed maximum deterioration of 21% in PM_{10} concentration behind the hedge and all other available sites exhibited a reduction in PM_{10}. The maximum improvement in PM_{10} concentration was observed with trees with hedges in both clear vs behind and in-front vs behind cases.

Percentage differences in average $PM_{2.5}$ concentrations were lowest than all other measured pollutants in this study. The GI scenarios H_{CB} and T_{CB} showed deterioration in $PM_{2.5}$ concentration behind vegetation in all wind directions. In along-road wind category, the maximum improvements were revealed by TH_{CB} (17%) in clear vs behind scenarios and T_{IB} (14%) in in-front vs behind cases, whereas in cross-road winds, H_{IB} (17%) recorded the maximum reduction. All clear vs behind sites exhibited negative differences in $PM_{2.5}$ from -2% to -7% in cross vegetation wind category.

In most of the wind categories, reported PM_1 percentage changes were positive. The magnitude of differences was similar to PNC and higher than PM_{10} and $PM_{2.5}$. In along-road winds, maximum improvements were noticed with TH_{CB} (29%) in clear vs behind scenarios and T_{IB} (18%) in in-front vs behind cases similar to $PM_{2.5}$ variation. Whereas with cross-road wind direction, TH_{CB} (14%) in clear vs behind scenarios and H_{IB} (31%) in in-front vs behind cases reported the highest reductions

in PM_1. No increase in PM_1 concentration behind barrier was noticed under this wind flow condition. Lastly, cross vegetation winds showed improvement in PM_1 concentrations except at the H_{CB} site.

Overall, the magnitude of the percentage differences followed the trend: $PM_{2.5}$ < PM_{10} < PM_1 < PNC < BC. In most of the investigated GI scenarios, the highest percentage changes were observed in along-road than in cross-road while the minimum ones were measured in cross vegetation wind direction categories. In general, trees and hedges TH_{CB} in clear vs behind scenarios and hedge only H_{IB} in in-front vs behind sites reported the highest reduction in pollutant concentrations behind vegetation, mainly in along-road and cross road wind conditions. In cross vegetation winds, TH_{CB} and TH_{IB} cases showed high percentage reductions among all GI. They were effective in creating a clean air zone behind vegetation with help of incoming clean air flow. The H_{CB} showed increase in all pollutants (mainly PMs) except BC in cross vegetation winds indicating upwind source of pollutants other than the road (may be from houses as traffic correlated BC is absent). Similarly, the increases in other cross vegetation pollutants simultaneously with an absence of rising BC concentrations pointed towards the emissions from background residential areas. Most of the deterioration of air pollution was found in H_{CB} and T_{CB} scenarios and had a strong correlation with their physical dimensions.

4.4 Vantaa

4.4.1 Meteorological data

At both iSCAPE - monitoring station Malminiitty and Heureka high quality meteorological data was collected with one second time resolution. This means that our data collection process was over 100-times denser than the official procedure of FMI. This can cause differences in data averaging and extreme values. To avoid this problem the near-by synoptic weather station (see Figure 16 in section 3.4.1) at the airport Helsinki-Vantaa was used as a reference station. The comparison between the datasets is shown in Figure 51. Due to the shortness of the data series no statistical test was used.

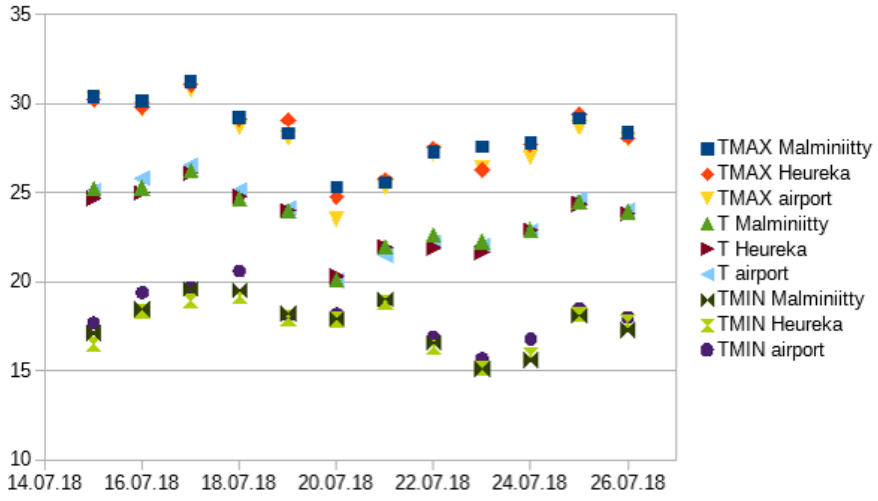

Figure 51: Comparison of daily air temperature averages (T), highest air temperatures (TMAX), and lowest air temperatures (TMIN) of the stations Malminiitty, Heureka, and Helsinki-Vantaa airport (airport) for the period July 14th - 26th 2018.

Another parameter presenting a very similar distribution to the air temperature is the incoming solar radiation. The final amount of solar radiation received depends on the exposition of the instrument, cloudiness and atmospheric composition. Normally the instrument is exposed unlimited to the sky. This is the case at Heureka, where the instrument is mounted at 10 meters height. For Malminiitty we took an intended restriction by mounting the instrument at 20 meters height facing it into the courtyard. In summertime after approximately 16:00 the instrument is shaded by the building where the monitoring station is located.

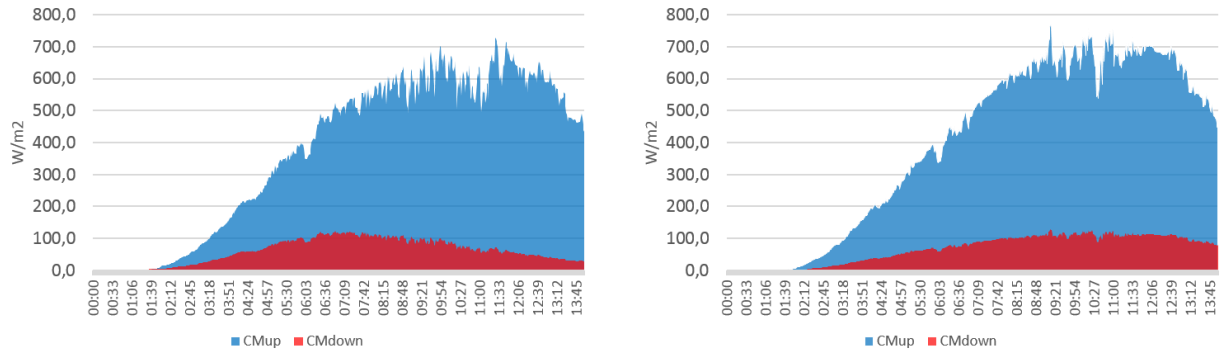

Figure 52: 1-minute average of solar incoming shortwave radiation (blue) and reflected shortwave radiation (red) at iSCAPE monitoring station Malminiitty (left) and Heureka (right) for the period July 14th - 26th 2018

The shift of the reflected shortwave radiation to an earlier maximum at Malminiitty is due the orientation of the instrument.

Another very typical phenomenon of meteorological parameters is the behavior of average wind speed and wind extremes. On one hand in build-up areas the wind speed decreases due to the roughness of the surface, on the other hand buildings force the wind through narrower street canyons.

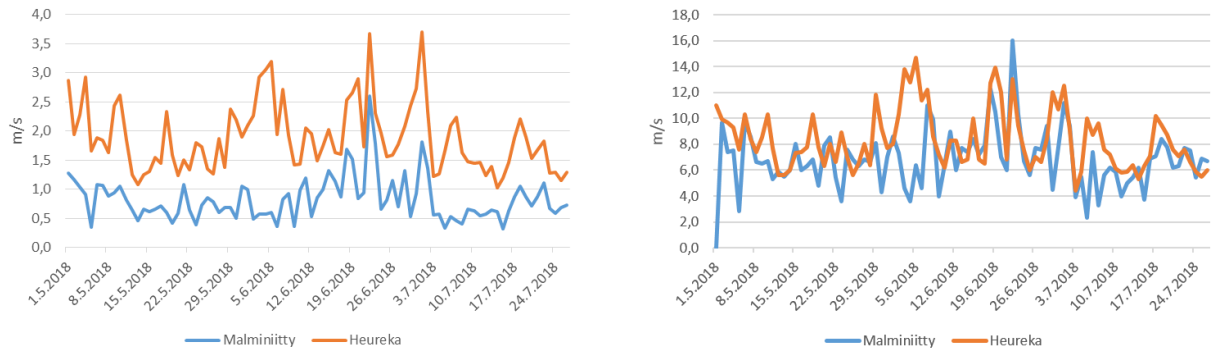

Figure 53: Mean wind speed (left) and daily maximum wind speed (right) at iSCAPE monitoring station Malminiitty (blue) and Heureka (red) for the period May 1st - July 26th 2018

4.4.2 Air pollution

During the summertime, normally, there are no air pollution issues in Finland. In the cities, the traffic emissions are reduced due to the long vacation period from June to August. Problems might occur during hot and dry summers, when forest fires, both local as well as distant, may add huge amounts of small particles into the lower atmosphere. In the worst cases, the visibility can be reduced. In the Helsinki metropolitan area, a network with seven permanent and four temporal stations is operated by HSY (see section 3.4.2). As previously reported, the stations are equipped with different sensors to monitor several traffic-related pollutants and particulate matter in different sizes. The following figures present the measurements collected during the experimental campaign.

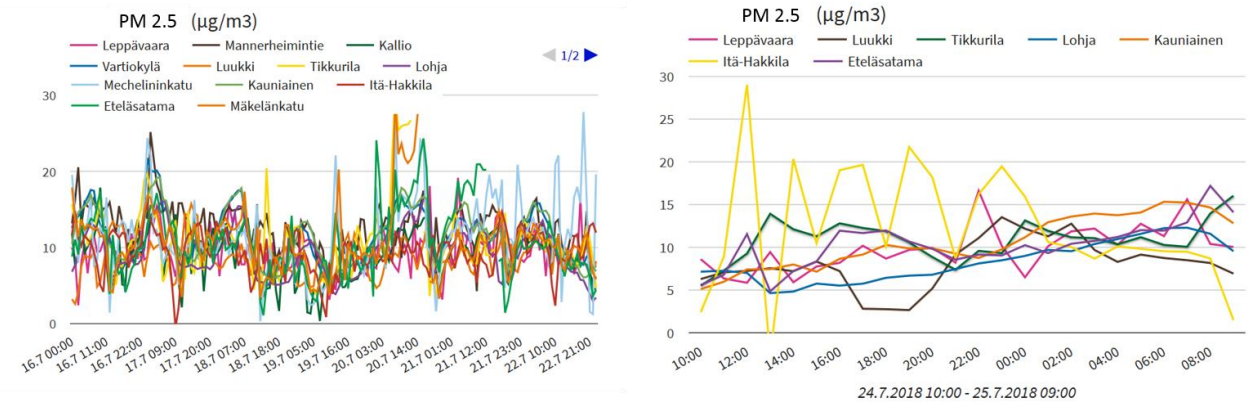

Figure 54: Results from the HSY air pollution network monitoring stations, left: weekly $PM_{2.5}$ measurements from 12 air pollution stations (HSY and Lohja), July 16th - 22nd 2018; right: detail of 24-hour $PM_{2.5}$ measurements from 7 stations in the metropolitan area, July, 25th 2018 (source: HSY, 2018)

The daily $PM_{2.5}$ concentrations show a distinguished distribution between traffic and residential areas, where in some cases the concentrations can be twice as high as in traffic areas (Figure 54). This is obvious for detached houses areas where it is common in Finland to have wood-fired saunas and furnaces.

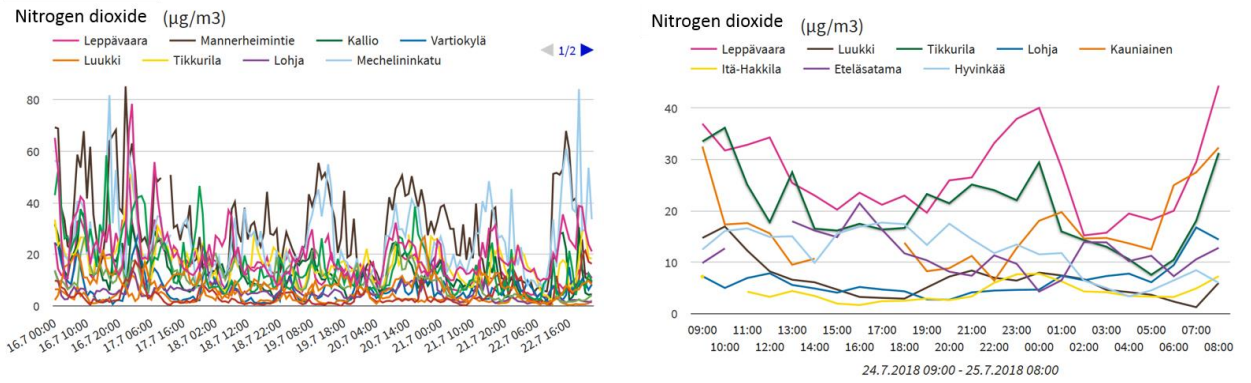

Figure 55: Results from the HSY air pollution network monitoring, left: weekly nitrogen dioxide measurements from 12 air pollution stations (HSY and Lohja), July 16th - 22nd 2018; right: detail of 24-hour nitrogen dioxide measurements from 8 stations in the larger metropolitan area, July 25th 2018 (source: HSY, 2018)

The amount for nitrogen dioxide in the air is directly related to the amount of traffic in the area. Areas with intense traffic like Mannerheimintie and Mechelininkatu in the downtown area of Helsinki measured concentrations almost always twice as high as the other measuring points (Figure 55, left). In detached houses areas like Itä-Hakkila the measured values dropped down to one third or one fourth (Figure 55, right).

5. Conclusions

Air pollution continues to pose a serious threat to human health and air pollution levels continue to exceed protection limits, also due to the continuously growing world population and the tendency to live in urban areas. Air pollution is also tightly connected to climate change: in fact, the main sources of GHG emissions are not only key drivers of climate change, but also major sources of air pollutants. Within the iSCAPE project, different monitoring campaigns have been setup for providing meteorological and air pollution levels in different target cities, for further use to validate and calibrate simulations conducted as part of other WPs, but also to evaluate the efficacy of PCSs to reduce air pollution levels and/or improving urban thermal comfort.

In Bologna, the monitoring of meteorological and air pollution levels was conducted during two intensive experimental field campaigns, one in summer 2017 and one in winter 2018. The campaigns were conducted at two urban street canyons characterized by the same orientation, but different presence of vegetation. The monitoring involved the measurement of various meteorological and turbulence parameters, measured at high time resolution, in addition to various air pollution pollutants. Two intensive thermographic campaigns were also carried out, in order to analyze and characterize the temperature distribution and the UHI effect at the city scale. The preliminary results indicate that vegetation indeed improves urban thermal comfort and reduces the UHI effect especially in the summer season (i.e., when urban thermal comfort is less). In terms of air pollution, the analysis of the differences between the two canyons and the comparison also with other fixed air pollution stations of the ARPA-ER Regional Environmental Protection Agency shows that they are produced by various factors, including the presence of vegetation, but also the different traffic volumes, geometries, packaging of the buildings and locations of the two street canyons in Bologna. In particular, the comparison showed that Marconi St. canyon, because of its geometrical and traffic characteristics, was characterized by special high levels during both campaigns. The deployment of further instrumentation for the measurement of BC concentrations and of particles size distribution during the winter campaign when the region is frequently characterized by stagnant conditions and particle pollution is more relevant highlighted other interesting differences between the two canyons. Further analyses are in progress, while the collected data is also being used to validate the CFD (Computational Fluid Dynamics) simulations conducted in the two neighborhoods, whose output will be used also to evaluate the effect of trees on fluid dynamics.

The assessment and evaluation of the Dublin LBW intervention is built upon two evaluation methods, which are being implemented as part of iSCAPE project. Firstly, a measuring study for the real-world LBW application in Dublin (which is partially presented in this report) and, secondly, a CFD modelling study of the street canyon before and after the LWB intervention, which will be presented as part of WP6. For the purpose of evaluating the potential of using LBW, changes in nitrogen oxides were monitored at two monitoring points on each side of the LBW, during two experimental campaigns, one in winter and one in summer. This report provides results related to the effects of the LBWs on the dispersion of NO_x gases based on different sets of wind directions in a street canyon geometry. Based on the results presented in this report, one can conclude that LBWs act as a baffle at street level and increase the distance between the pollutant source and

human receptor. LBWs can provide a solution to enhance localized dispersion and improve air pollution in distinct street canyons settings. However, depending on the wind direction, street geometry and position of the LBW, they may also cause air pollutant concentrations to increase behind the LBW, having the opposite effect of increasing pollutant concentrations instead of decreasing them.

Guildford field campaign investigated various pollutant concentration differences in the presences of three vegetation types such as Hedges, Trees and their combination. Changes in pollutant concentration were estimated by comparing measurements of behind vegetation with a monitoring point at a clear area or in front of vegetation. The impact of wind direction was also analyzed. The preliminary analysis identified hedge only and trees with hedges as the most effective in reducing air pollutant concentration behind the vegetation barrier. The highest concentration differences were observed with BC (gradual decay) than PNC (rapid decay) and least was witnessed in $PM_{2.5}$ (no trend in decay) as expected. The magnitude of percentage differences followed the trend: $PM_{2.5} < PM_{10} < PM_1 < PNC < BC$. Finally, the wind direction impact analysis revealed that vegetation was most effective in along the road wind condition followed by the cross road one. Further analyses are in progress.

Vantaa field campaign is investigating the effect of different PCSs such as trees and bushes. Two experimental sites were equipped with the same instrumental setup in order to collect meteorological data (wind speed and direction, rain intensity and duration, air pressure, and the four components of the energy radiation spectrum) with a high time resolution at two sites characterized by the presence of different PCSs nearby. Air pollution data are available from HSY stations located nearby. While the meteorological and air pollution data are being used as an input to the ENVI-MET simulation, the cross-comparison between the data collected at the two sites enables for studying the effect of PCSs and of mounting conditions on the measurements. Since the experimental campaign is still ongoing, here very preliminary results were presented.

Further results of the monitoring campaigns in the four cities will be presented in an update of this Deliverable, which will be delivered by the end of the project. This data collected in-situ will be further used to complement and validate the simulations conducted as part of WP4 and WP6 with the purpose to evaluate the effects of different policy scenarios and PCSs in terms of air pollution and climate change. The results of the monitoring campaigns will be used to project the in-situ knowledge to larger scales, in order to extend the impact of the interventions. Apart from the monitoring of the interventions and the information about the key parameters driving and mitigating air pollution and climate change in the various iSCAPE cities, WP5 will also involve their optimization. In particular, the interventions will be evaluated under Deliverables 5.3 and 5.4, which will report detailed evaluation of the interventions and their optimal use and impacts, also in socio-economic terms. These results will also provide input to WP7 by making available data about the costs and benefits of the interventions so as to help the development of the sustainability and exploitation strategy of iSCAPE. Finally, this WP will also ensure the continuity of the Living Labs and will assess the impact of PCSs also under the socio-economical perspective.

The evaluation of the impact of PCSs will be completed with the assessment of the effectiveness of photocatalytic coatings in contrasting air pollution, whose performance will be evaluated analyzing the results obtained during a dedicated field campaign realized by UNIBO and ARPA-ER teams and PURETI providing and applying the photocatalytic coatings at one of the University of Bologna campuses during the period 1-31 August 2018. The experimental setup and specific objective description are not part of this report, but will be discussed within WP3 (D 3.6 and 3.7).

It is worth mentioning that the experimental campaign (one of the first of this kind ever realized) was designed and realized after a careful and thoroughly review of existing literature on the subject

carried out in WP1, as well as proposing new original ideas based on the experience acquired during the previous experimental campaigns carried out in Bologna.

6. References / Bibliography

ABHIJITH, K.V., KUMAR, P., GALLAGHER, J., MCNABOLA, A., BALDAUF, R., PILLA, F., BRODERICK, B., DI SABATINO, S., & PULVIRENTI, B., 2017. Air pollution abatement performances of green infrastructure in open road and built-up street canyon experiments - A review. Atmos. Environ., 162, 71-86, doi:10.1016/j.atmosenv.2017.05.014

AL-DABBOUS, A.N. & KUMAR, P., 2014. The influence of roadside vegetation barriers on airborne nanoparticles and pedestrians exposure under varying wind conditions. Atmos. Environ. 90, 113–124. doi:10.1016/j.atmosenv.2014.03.040

BAI, X., MCPHEARSON, T., CLEUGH, H., NAGENDRA, H., TONG, X., ZHU, T., ZHU, Y.-G., 2017. Linking urbanization and the environment: conceptual and empirical advances. Annu. Rev. Env. Resour. 42, 215-240, doi:10.1146/annurev-environ-102016-061128

BIGI, A., GHERMANDI, G., HARRISON, R.M., 2012. Analysis of the air pollution climate at a background site in the Po Valley. J. Environ. Monit., 14, 552, doi:10.1039/c1em10728c

BRANTLEY, H.L., HAGLER, G.S.W., J. DESHMUKH, P., BALDAUF, R.W., 2014. Field assessment of the effects of roadside vegetation on near-road black carbon and particulate matter. Sci. Total Environ. 468–469, 120–129. doi:10.1016/j.scitotenv.2013.08.001

DALLMAN, A., MAGNUSSON, S., BRITTER, R., NORFORD, L., ENTEKHABI, D., & FERNANDO, H.J., 2014. Conditions for thermal circulation in urban street canyons. Build. Environ., 80, 184-191, doi:10.1016/j.buildenv.2014.05.014

ENVI-met, version 4. http://www.envi-met.com (last accessed on 30/07/2018)

Finnish Science Centre HEUREKA. https://www.heureka.fi/?lang=en (last accessed on 30/07/2018)

FRIEDRICH, M.J., 2018. Air pollution is greatest environmental threat to health. JAMA 319(11), 1085, doi:10.1001/jama.2018.2366

GALLAGHER, J., GILL, L. W., MCNABOLA, A., 2012. Numerical modelling of the passive control of air pollution in asymmetrical urban street canyons using refined mesh discretization schemes. Build. Environ., 56**,** 232-240, doi:10.1016/j.buildenv.2012.03.013

GALLAGHER, J., GILL, L. W., MCNABOLA, A., 2013. The passive control of air pollution exposure in Dublin, Ireland: A combined measurement and modelling case study. Sci. Tot. Environ., 458–460**,** 331-343, doi:10.1016/j.scitotenv.2013.03.079

HAGLER, G.S.W., YELVERTON, T.L.B., VEDANTHAM, R., HANSEN, A.D.A., TURNER, J.R., 2011. Post-processing method to reduce noise while preserving high time resolution in aethalometer real-time black carbon data. Aerosol Air Qual. Res. 11, 539–546, doi:10.4209/aaqr.2011.05.0055

Helsinki Region Environmental Services Authority (HSY). https://www.hsy.fi/en/residents/pages/default.aspx

HUTTNER, S. & BRUSE, M., 2009. Numerical modelling of the urban climate - A preview on ENVI-met 4.0. Presented at: The seventh International Conference on Urban Climate, 29 June

– 3 July 2009, Yokohama, Japan. Available online at: http://www.envi-met.net/documents/papers/ICUC7_ModellingV4.pdf (last accessed 30/07/2018

JANNSEN, N. A. H., GERLOFS-NIJLAND, M. E., LANKI, T., SALONEN, R. O., CASSEE, F., HOEK, G., FISCHER, P., BRUNEKREEF, B., & KRZYZANOWSKI, M., 2012. Health effects of black carbon. Edited by Rosemary Bohr. WHO Regional Office for Europe, Copenhagen, Denmark, ISBN: 97892890026653

KARNER, A.A., EISINGER, D.S., NIEMEIER, D.E.B.A., 2010. Near-Roadway Air pollution: Synthesizing the Findings from Real-World Data 44, 5334–5344. doi:10.1021/es100008x

KING, E. A., MURPHY, E. & MCNABOLA, A., 2009. Reducing pedestrian exposure to environmental pollutants: A combined noise exposure and air pollution analysis approach. Transp. Res. D Transp Environ., 14**,** 309-316, doi:10.1016/j.trd.2009.03.005

LATINI, G., GRIFONI, R.C. & PASSERINI, G., 2002. Influence of meteorological parameters on urban and suburban air pollution. WIT Trans Ecol Environ 53, doi:10.2495/AIR020751

LI, H., MEIER, F., LEE, X., CHAKRABORTY, T., LIU, J., SCHAAP, M., & SODOUDI, M., 2018. Interaction between urban heat island and urban pollution island during summer in Berlin. Sci. Tot. Environ. 636, 818-828, doi:10.1016/j.scitotenv.2018.04.254

LIN, M.Y., HAGLER, G., BALDAUF, R., ISAKOV, V., LIN, H.Y., KHLYSTOV, A., 2016. The effects of vegetation barriers on near-road ultrafine particle number and carbon monoxide concentrations. Sci. Tot. Environ. 553, 372–379. doi:10.1016/j.scitotenv.2016.02.035

MCMILLEN, R., 1988. An eddy correlation technique with extended applicability to non-simple terrain. Boun-Layer Meteorol, 43(3), 231-245.

MCNABOLA, A., BRODERICK, B. M., GILL, L. W., 2008. Reduced exposure to air pollution on the boardwalk in Dublin, Ireland. Measurement and prediction. Environ. Int., 34**,** 86-93, doi:10.1016/j.envint.2007.07.006

MCNABOLA, A., BRODERICK, B. M., GILL, L. W., 2009. A numerical investigation of the impact of low boundary walls on pedestrian exposure to air pollutants in urban street canyons. Sci. Tot. Environ., 407**,** 760-769, doi:10.1016/j.scitotenv.2008.09.036

NIU, Y., CAI, J., XIA, Y., YU, H., CHEN, R., LIN, Z., LIU, C., CHEN, C., WANG, W., PENG, L., XIA, X., FU, Q., & KAN, H., 2018. Estimation of personal ozone exposure using ambient concentrations and influencing factors. Environ. Int. 117, 237-242, doi:10.1016/j.envint.2018.05.017

PASQUIER, A. & ANDRÉ, M., 2017. Considering criteria related to spatial variabilities for the assessment of air pollution from traffic. Transp. Res. Procedia 25, 3358–3373. doi:10.1016/j.trpro.2017.05.210

RAMANATHAN, V. & CARMICHAEL, G., 2008. Global and regional climate changes due to black carbon. Nat. Geosci. 1, 221-227.

SALIZZONI, P., SOULHAC, L., MEJEAN, P., 2009. Street canyon ventilation and atmospheric turbulence. Atmos. Environ. 43(32), 5056-5067, doi:10.1016/j.atmosenv.2009.06.045

SHI, C., YUAN, R., WU, B., MENG, Y., ZHANG, H., ZHANG, H., GONG, Z., 2018. Meteorological conditions conducive to PM2.5 pollution in winter 2016/2017 in the Western Yangtze River Delta, China. Sci. Tot. Environ. 642, 1221-1232, doi:10.1016/j.scitotenv.2018.06.137

SURREY-I, 2015. Census key statistics (Key demographics, age, gender, ethnicity, religion, disability, health and carers), Guildford Local Authority in Surrey 25–27.

THUNIS, P., TRIACCHINI, G., WHITE, L., MAFFEIS, G., VOLTA, M., 2009. Air pollution and emission reductions over the Po-Valley: air pollution modeling and integrated assessment.

Proceedings of the 18th World IMACS Congress and MODSIM09 International Congress on Modeling and Simulation. ISBN: 978-0-9758400-7-8, p. 2335-2341

TITTARELLI, A., BORGINI, A., BERTOLDI, M., DE SAEGER, E., RUPRECHT, A., STEFANONI, R., TAGLIABUE, G., CONTIERO, P., & CROSIGNANI, P., 2008. Estimation of particle mass concentration in ambient air using a particle counter. Atmos. Environ. 42, 8543-8548, doi:10.1016/j.atmosenv.2008.07.056

TUCH, T., MIRME, A., TAMM, E., HEINRICH, J., HEYDER, J., BRAND, P., ROTH, C., WICHMANN, H.E., PEKKANEN, J., & KREYLING, W.G., 2000. Comparison of two particle size spectrometers from ambient aerosol measurements in environmental epidemiology. Atmos. Environ. 34, 139-149, doi:10.1016/S1352-2310(99)00248-4

VIRKKULA, A., MÄKELÄ, T., HILLAMO, R., YLI-TUOMI, T., HIRSIKKO, A., HÄMERI, K., & KOPONEN, I.K., 2007. A simple procedure for correcting loading effects of aethalometer data. J. Air & Waste Mange. Assoc. 57, 1214-1222, doi:10.3155/1047-3289.57.10.1214

YASSIN, M.F., AL-SHATTI, L.A., AL RASHIDI, M.S., 2018. Assessment of the atmospheric mixing layer height and its effect on pollutant dispersion. Environ Monit Assess 190(7), doi:10.1007/s10661-018-6737-9

WANG, J., ZHANG, X., LI, D., YANG, Y., ZHONG, J., WANG, Y., CHE, H., CHE, H., & ZHANG, Y., 2018. Interdecadal changes of summer aerosol pollution in the Yangtze River Basin of China, the relative influence of meteorological conditions and the relation to climate change. Sci. Tot. Environ. 630, 46-52, doi:10.1016/j.scitotenv.2018.01.236

WHO (World Health Organization), 2018. http://www.who.int/airpollution/en/, last accessed 19/07/2018

WICHMANN, H.E., SPIX, C., TUCH, T., WOLKE, G., PETERS, A., HEINRICH, J., KREYLING, W.G., & HEYDER, J., 2000. Daily mortality and fine and ultrafine particles in Erfurt, Germany. Part 1: role of particle number and particle mass. Res. Rep. Eff. Inst., 98, 5-86.

WITTMAACK, K., 2002. Advanced evaluation of size-differential distributions of aerosol particles. J. Aerosol Sci. 33, 1009-1025, doi:10.1016/S0021-8502(02)00052-6

Appendix Technical specifications for the instruments

In the following, we report Tables containing the main technical specifications for the Optical Particle Counter and the Microaethalometer adopted within the winter experimental field campaign in Bologna.

Met One Eight Channel Particle Counter

Specifications

Measurement principle	Optical, Light-scatter using a Laser Diode
Flow rate	1.0 LPM
Measuring range	0.3 to 10 µm (eight selectable sizes)
Concentration	0 - 9,000,000 Particles per cubic ft.
Sample flow rate	1 LPM
Sample interval	1 - 60 s
Accuracy	± 10% to calibration aerosol
Communication	RS232 output
Power	12 VDC 240 mA maximum Inlet Heater, additional 750 mA
Temperature	0 to +40°C
Weight	3 lb (1.2 kg)
Size	Diameter 4.0 in, Length 7.5 in + 12" for inlet tube

Table A1: Technical specifications of Met One Eight Channel Particle Counter.

AethLabs microAeth AE51

Specifications

Measurement principle	Real-time analysis by measuring the rate of change in absorption of transmitted light due to continuous collection of aerosol deposit on filter. Measurement at 880 nm interpreted as concentration of Black Carbon (‘BC’).
Measurement range	0-1 mg BC/m^3, filter life time dependent on concentration and flow rate setting: avg. 5 µg BC/m^3 for 24 hours @ 100 ml/min; avg. 100 µg BC/m^3 for 3 hours @ 50 ml/min; avg. 1 mg BC/m^3 for 15 minutes @ 50 ml/min
Measurement resolution	0.001 µg BC/m^3
Measurement precision	±0.1 µg BC/m^3, 1 min avg., 150 ml/min flow rate
Measurement Timebases (User setting)/	1, 10, 30, 60, or 300 seconds
Flow rate (User setting)	Internal pump provides 50, 100, 150, or 200 ml/min, monitored by mass flow meter and stabilized by closed-loop control.
Sampling	3 mm spot created on filter strip containing insert of T60 Teflon-coated borosilicate glass fiber filter material. PM2.5 size selective inlet available.

Consumables	Filter strip: 1 filter strip per sampling campaign, typically one per day. High concentration sampling may require more than one filter per day.
Data Storage	4 MB internal flash memory, providing up to 1 month data storage when operating on a 300 second timebase, and 1 week when operating on a 60 second timebase.
Communications	USB connectivity to Windows®-based PC with microAethCOM.
Data Output	Internal data files are uploaded to microAethCOM PC software and stored on local disk.
Dimensions	4.6 in (117 mm) L x 2.6 in (66 mm) W x 1.5 in (38 mm) D
Weight	Approximately 9.88 ounces (280 g).
Power	Internal rechargeable lithium-ion battery.
Operation Environment	Input: 100~240 VAC 50/60 Hz 0.2 A Output: 5VDC / 0.5A

Table A2: Technical specifications of AethLabs microAeth AE51.

FLIR T620

Specifications

Temperature range	-40°C to 650°C
Thermal sensitivity (N.E.T.D.)	<0.04°C at 30°C
Zoom	4X Continuous
Focus	Manual or Automatic (one shot)
Frame Rate	30Hz
Field of view/Minimum focus distance/FOV Match	25°x19°/0.82ft/ (0.25 m)/Field of View Match where Digital Image FOV adapts to the IR lens
Detector Type - Focal plane array (FPA) uncooled microbolometer	640x480 pixels
Spectral range	7.5 to 14 µm
Lens	25° or 45° models
Display	Built-in touch screen 4.3" color LCD (800 x 480 pixels)
Image modes	Thermal/Visual/Fused thermal image/P-i-P/MSX (Resizable and movable) and Thumbnail Gallery
Image storage	1000 radiometric JPEG images
Periodic image storage	7 seconds to 24 hours (IR) and 14 seconds to 24 hours (IR and visual)
Dimensions/Weight	143 x 196 x 94 mm/1.3 kg including battery

Table A3: Technical specifications of FLIR T620 thermal camera.

Vaisala CL31

Specifications

Performance	
Measurement range	0 … 7.6 km
Reporting cycle	programmable, 2 … 120 s
Reporting resolution	5 m/10ft., units selectable
Distance measurement accuracy against hard target	greater of ±1% or ±5 m
Laser	InGaAs diode, 910 mm
Eye safety	Class 1M IEC/EN60825-1
Electrical	
Power	100/115/230 VAC ± 10% 50 … 60 Hz max. 310 W including heating
Interfaces data	
data	RS232/RS485/Modem/LAN
maintenance	RS232
baud rate	
RS232/RS485	300 … 57,600
modem V.21, V.22	300 … 1200
Back-up battery	Internal, 2 Ah
Mechanical	
Dimensions	
total	1190 x 335 x 324 mm
measurement unit	620 x 235 x 200 mm
Weight	
total	32 kg
measurement unit	13 kg
Tilt positions	Vertical or 12° tilted
Environmental	
Temperature range	"-40 … +60°C
Humidity	0 … 100% RH
Wind	55 m/s
Housing classification	IP66
Vibration	Lloyds register/IEC60068-2-6 5 … 13.2 Hz ±1.0 mm 13.2 Hz … 100 Hz ± 0.79 mm
EMC	IEC/EN 61326
Electrical safety	IEC/EN 60950

Table A4: Technical specifications of the Vaisala CL31 ceilometer.